Eur. Phys. J. C (2025) 85:561
https://doi.org/10.1140/epjc/s10052-025-14075-3

THE EUROPEAN PHYSICAL JOURNAL C

Regular Article - Experimental Physics

Reconstruction and identification of pairs of collimated τ-leptons decaying hadronically using $\sqrt{s} = 13$ TeV pp collision data with the ATLAS detector

ATLAS Collaboration[⋆]

CERN, 1211 Geneva 23, Switzerland

Received: 15 November 2024 / Accepted: 14 March 2025

Abstract This paper describes an algorithm for reconstructing and identifying a highly collimated hadronically decaying τ-lepton pair with low transverse momentum. When two τ-leptons are highly collimated, their visible decay products might overlap, degrading the reconstruction performance for each of the τ-leptons. A dedicated treatment attempting to tag the τ-lepton pair as a single object is required. The reconstruction algorithm is based on a large radius jet and its associated two leading subjets, and the identification uses a boosted decision tree to discriminate between signatures from $\tau^+\tau^-$ systems and those arising from QCD jets. The efficiency of the identification algorithm is measured in $Z\gamma$ events using proton–proton collision data at $\sqrt{s} = 13$ TeV collected by the ATLAS experiment at the Large Hadron Collider between 2015 and 2018, corresponding to an integrated luminosity of 139 fb^{-1}. The resulting data-to-simulation scale factors are close to unity with uncertainties ranging from 26 to 37%.

Contents

1 Introduction

The τ-lepton has a mass of 1.77 GeV and a lifetime of about 2.9×10^{-13} s [1]. It is the heaviest lepton in the Standard Model (SM), and the only lepton that can decay into hadrons, with a branching ratio to hadronic final states (τ_{had}) of approximately 65%, and to each of the light leptons of approximately 17%. Out of the hadronic decay modes, approximately 77% involve one charged hadron and 22% involve three charged hadrons. The visible part of τ_{had}-lepton decays, $\tau_{\text{had-vis}}$, is defined as the vectorial sum of the decay products' four-momenta, excluding neutrinos.[1] The reconstruction and identification of $\tau_{\text{had-vis}}$ is essential to many SM measurements and searches for physics beyond the SM (BSM) [2].

In the ATLAS experiment [3], the $\tau_{\text{had-vis}}$ candidates are reconstructed from anti-k_t jets [4,5] with a radius parameter of 0.4, built from locally calibrated topological clusters [6]. As a result, a problem emerges when a pair of τ_{had} candidates originates from the decay of a highly Lorentz-boosted parent particle (boosted di-τ system). In this scenario, the $\tau_{\text{had-vis}}$ pair may become too collimated to be individually resolved using standard reconstruction techniques. When the angular distance between two $\tau_{\text{had-vis}}$ is smaller than the anti-k_t radius parameter, the seed jet constituents may contain deposits from both of the $\tau_{\text{had-vis}}$ candidates resulting in a wrong grouping of these constituents by the anti-k_t algorithm

⋆ e-mail: atlas.publications@cern.ch

[1] The *vis* subscript refers to the quantities involving visible decay products.

Published online: 22 May 2025

– possibly in conjunction with mis-association of tracks to the correct jet – and manifesting as a merging of the two $\tau_{\text{had-vis}}$ signatures into a single seed jet. It can lead to a situation in which either one or both of the $\tau_{\text{had-vis}}$ candidates are not correctly reconstructed with the proper track multiplicity, making it difficult to reconstruct the di-τ system from individually resolved $\tau_{\text{had-vis}}$. Furthermore, even when the two $\tau_{\text{had-vis}}$ are reconstructed, a partial overlap of the jets can introduce problems in the identification step, possibly leading to signatures that bear more resemblance to background. These challenges require dedicated reconstruction and identification algorithms targeting boosted di-τ systems, referred to as the di-τ tagger, to recover the sensitivity to this topology.

Generally, in a two body decay, the angular distance between the decay products is approximately proportional to the ratio of the parent mass to its transverse momentum (p_{T}). A high-p_{T} $\tau_{\text{had-vis}}$ pair tagger has already been developed by the ATLAS Collaboration [7]. It was used for a heavy, narrow, scalar resonance search in the high mass regime of 1–3 TeV, decaying into a pair of Higgs bosons, where one Higgs boson decays into a $b\bar{b}$ pair and the other one into a $\tau^{+}_{\text{had}}\tau^{-}_{\text{had}}$ pair.

However, the case of lower-p_{T} collimated di-τ objects, relevant to BSM searches in the low-mass regime, has not yet been investigated [8]. Several models predict the existence of light resonances [9,10] with masses smaller than half of the Higgs boson mass, produced either directly or through decays of SM particles – most commonly via the decay of the SM Higgs boson into a pair of (pseudo)scalars [11–19]. The di-τ tagging method for such final states is hence crucial for increasing the sensitivities to these signatures.

The method presented in Ref. [7] is not directly applicable to the decays of light parent particles, as it targets a scenario in which the boosted regime corresponds to parent p_{T} values above approximately 300 GeV. It uses seed jets with relatively high p_{T} thresholds, does not involve a dedicated energy-scale correction, and includes an identification algorithm trained to discriminate against high-p_{T} jet backgrounds. This method is thus unsuitable for the case of low-mass BSM searches and must be adapted to target signatures from the decay of light resonances with p_{T} smaller than 300 GeV.

In this paper, the reconstruction and the identification of hadronically decaying collimated di-τ systems at low p_{T} are described and their expected performance is assessed in simulation. The measurement of the di-τ tagger efficiency in data is presented, entailing the extraction of scale factors (SF), which account for differences in the identification efficiency between simulation and data. The SFs are derived in a region enriched in properly identified di-τ objects, using the SM process $Z\gamma$, where the Z boson decays into a boosted di-τ. The reconstruction efficiency measurement in data is beyond the scope of this paper. Additionally, the techniques presented in this paper are not applicable to semi-leptonic decays of di-τ systems, which are handled by other dedicated algorithms [20].

After describing the ATLAS detector in Sect. 2 and the data and Monte Carlo simulated samples in Sect. 3, Sect. 4 presents the reconstruction of standard physics objects. Section 5 introduces the reconstruction, energy-scale calibration and identification of the boosted di-τ, and Sect. 6 presents the SF measurement in $Z\gamma$ events. Finally, conclusions are given in Sect. 7.

2 The ATLAS detector

The ATLAS detector at the LHC covers nearly the entire solid angle around the collision point.[2] It consists of an inner tracking detector surrounded by a thin superconducting solenoid, electromagnetic and hadronic calorimeters, and a muon spectrometer incorporating three large superconducting air-core toroidal magnets.

The inner-detector system is immersed in a 2 T axial magnetic field and provides charged-particle tracking in the range $|\eta| < 2.5$. The high-granularity silicon pixel detector covers the vertex region and typically provides four measurements per track, the first hit generally being in the insertable B-layer (IBL) installed before Run 2 [21,22]. It is followed by the SemiConductor Tracker (SCT), which usually provides eight measurements per track. These silicon detectors are complemented by the transition radiation tracker (TRT), which enables radially extended track reconstruction up to $|\eta| = 2.0$. The TRT also provides electron identification information based on the fraction of hits (typically 30 in total) above a higher energy-deposit threshold corresponding to transition radiation.

The calorimeter system covers the pseudorapidity range $|\eta| < 4.9$. Within the region $|\eta| < 3.2$, electromagnetic calorimetry is provided by barrel and endcap high-granularity lead/liquid-argon (LAr) calorimeters, with an additional thin LAr presampler covering $|\eta| < 1.8$ to correct for energy loss in material upstream of the calorimeters. Hadronic calorimetry is provided by the steel/scintillator-tile calorimeter, segmented into three barrel structures within $|\eta| < 1.7$, and two copper/LAr hadronic endcap calorime-

[2] ATLAS uses a right-handed coordinate system with its origin at the nominal interaction point (IP) in the centre of the detector and the z-axis along the beam pipe. The x-axis points from the IP to the centre of the LHC ring, and the y-axis points upwards. Polar coordinates (r, ϕ) are used in the transverse plane, ϕ being the azimuthal angle around the z-axis. The pseudorapidity is defined in terms of the polar angle θ as $\eta = -\ln\tan(\theta/2)$ and is equal to the rapidity $y = \frac{1}{2}\ln\left(\frac{E+p_z}{E-p_z}\right)$ in the relativistic limit. Angular distance is measured in units of $\Delta R \equiv \sqrt{(\Delta y)^2 + (\Delta\phi)^2}$.

ters. The solid angle coverage is completed with forward copper/LAr and tungsten/LAr calorimeter modules optimised for electromagnetic and hadronic energy measurements respectively.

The muon spectrometer (MS) comprises separate trigger and high-precision tracking chambers measuring the deflection of muons in a magnetic field generated by the superconducting air-core toroidal magnets. The field integral of the toroids ranges between 2.0 and 6.0 Tm across most of the detector. Three layers of precision chambers, each consisting of layers of monitored drift tubes, cover the region $|\eta| < 2.7$, complemented by cathode-strip chambers in the forward region, where the background is highest. The muon trigger system covers the range $|\eta| < 2.4$ with resistive-plate chambers in the barrel, and thin-gap chambers in the endcap regions.

The luminosity is measured mainly by the LUCID–2 [23] detector that records Cherenkov light produced in the quartz windows of photomultipliers located close to the beampipe.

Events are selected by the first-level trigger system implemented in custom hardware, followed by selections made by algorithms implemented in software in the high-level trigger [24]. The first-level trigger accepts events from the 40 MHz bunch crossings at a rate below 100 kHz, which the high-level trigger further reduces in order to record complete events to disk at about 1 kHz.

A software suite [25] is used in data simulation, in the reconstruction and analysis of real and simulated data, in detector operations, and in the trigger and data acquisition systems of the experiment.

3 Data and simulated event samples

The data sample used in this paper were collected by the ATLAS experiment during the 2015 to 2018 LHC proton–proton runs at $\sqrt{s} = 13$ TeV, and corresponds to an integrated luminosity of 139 fb^{-1} [26]. Data-quality requirements are applied to ensure that all elements of the detectors were operational during data-taking [27]. Simulated Monte Carlo (MC) samples are used to study the di-τ reconstruction and to train the di-τ identification algorithm, while for the SF measurement, data samples are used as well. Table 1 shows the summary of the MC generators.

For the studies of di-τ reconstruction, calibration and the training of the di-τ classifier, simulated samples of a two-Higgs-doublet-model [28] pseudoscalar boson production (denoted by X) in association with a top-antitop-quark pair ($t\bar{t}X$) are used as the signal. Two representative X masses (m_X) are used in the classifier training, $m_X = 20$ and 60 GeV. The pseudoscalar X was set to decay into two τ-leptons, which were later set to decay hadronically. The $t\bar{t}$ pair was set to either a semileptonic or dileptonic decay (with only electrons and muons considered). The $t\bar{t}X$ samples were simulated at leading order (LO) with MadGraph5_aMC@NLO [29] using the NNPDF2.3LO set of parton distribution functions (PDF) [30], interfaced with PYTHIA 8.212 [31] to model the parton shower, hadronisation, and underlying event, with parameters set according to the A14 tune [32] and NNPDF2.3LO PDF set.

Misreconstructed (fake) di-τ objects from simulated $t\bar{t}$ production (and subsequent fully hadronic decay) events are used as the background source for training the identification algorithm and SF measurement. This background is characterised by large jet multiplicities, originating from both the light- and b-quarks. Additionally, production of high-p_{T} hadronically decaying W bosons as part of the top-quark decays can itself result in a pair of collimated jets. The choice of the $t\bar{t}$ process as a source of fakes is further motivated by its similarity to $t\bar{t}X$. The production of $t\bar{t}$ events was modelled using the POWHEGBOX v2 [33–36] generator at next-to-leading-order (NLO) in QCD with the NNPDF3.0NLO PDF set [37] and the h_{damp} parameter[3] set to 1.5 m_{top} [38]. The events were interfaced to PYTHIA 8.230 to model the parton shower, hadronisation, and underlying event, with parameters set according to the A14 tune and used the NNPDF2.3LO set of PDFs. The decays of bottom and charm hadrons were performed by EVTGEN 1.6.0 [39].

For the SF measurement, the signal samples are Z+jets, $Z\gamma$, and $Z\gamma\gamma$ where the Z boson decays into two τ-leptons. The Z+jets process was simulated with SHERPA 2.2.14 [40], with up to two jets at NLO and up to five jets at LO. The $Z\gamma$ process was simulated with SHERPA 2.2.11, with up to one jet at NLO and up to four jets at LO. The $Z\gamma\gamma$ process was simulated with SHERPA 2.2.10, with zero jets at NLO and up to two jets at LO. The matrix elements were calculated with the Comix [41] and OpenLoops [42–44] libraries, and merged with the Sherpa parton shower [45] following the MEPS@NLO prescription [46–49] and using the set of tuned parameters developed by the Sherpa authors. The Z+jets, $Z\gamma$ and $Z\gamma\gamma$ events were simulated using the NNPDF3.0NNLO PDF set [37]. Since both the Z+jets and $Z\gamma$ MC samples are used, event overlap removal was performed to avoid double counting, based on the following particle-level criteria: events from Z+jets were discarded if they contained a photon with $p_{\mathrm{T}} > 140$ GeV and if the angular distance between one of the τ-leptons and the photon was greater than 0.1.

Several SM backgrounds are used for the SF studies. The dominant SM background is due to prompt single-photon production, which was simulated with SHERPA 2.2.2. In

[3] The h_{damp} parameter is a resummation damping factor and one of the parameters that controls the matching of Powheg matrix elements to the parton shower and thus effectively regulates the high-p_{T} radiation against which the $t\bar{t}$ system recoils.

Table 1 Summary of all MC simulated samples used for the di-τ tagger development, the scale factor measurement and the estimates of the generator uncertainty assigned to the scale factor. Information about the matrix element generator, QCD perturbative order, parton distribution function set and the parton shower is provided

Process	Matrix element generator	QCD order	PDF	Parton shower
For di-τ tagger studies				
$t\bar{t}X$	MadGraph5_aMC@NLO	NLO	NNPDF2.3nnlo	PYTHIA 8.212
$t\bar{t}$	POWHEGBOX v2	NLO	NNPDF3.0nlo	PYTHIA 8.230
For scale factor measurement				
Z+jets	SHERPA 2.2.14	NLO	NNPDF3.0nnlo	Sherpa
$Z\gamma$	SHERPA 2.2.11	NLO	NNPDF3.0nnlo	Sherpa
$Z\gamma\gamma$	SHERPA 2.2.10	NLO	NNPDF3.0nnlo	Sherpa
γ+jets	SHERPA 2.2.2	NLO	NNPDF3.0nnlo	Sherpa
$W/Z(\rightarrow q\bar{q})\gamma$	SHERPA 2.1.1	LO	CT10	Sherpa
Multijet	POWHEGBOX v2	NLO	NNPDF3.0nlo	PYTHIA 8.245
$t\bar{t}$	POWHEGBOX v2	NLO	NNPDF3.0nlo	PYTHIA 8.230
$W(\rightarrow \tau\nu)$+jets	SHERPA 2.2.1	NLO	NNPDF3.0nnlo	Sherpa
For generator uncertainty estimates				
γ+jets	PYTHIA 8.244+ EVTGEN 1.7.0	LO	NNPDF2.3lo	PYTHIA 8.244
Multijet	POWHEGBOX v2	NLO	NNPDF3.0nlo	Herwig 7

this framework, NLO matrix elements for up to two partons, and LO matrix elements for up to four partons were calculated with the Comix and OpenLoops libraries. They were matched with the Sherpa parton shower using the MEPS@NLO prescription with a dynamic merging selection [50] of 20 GeV. Photons are required to be isolated according to a smooth-cone isolation criterion [51]. The samples were simulated using the NNPDF3.0nnlo PDF set, along with the dedicated set of tuned parton-shower parameters developed by the Sherpa authors. To estimate generator systematic uncertainties, an alternative γ+jets sample was used, with events produced at LO via PYTHIA 8.244, using the NNPDF2.3lo PDF set and the A14 tune.

The other subdominant SM backgrounds include QCD multijets with jets misreconstructed as photons or di-τ objects, a prompt photon produced in association with a hadronically decaying W/Z-boson, $t\bar{t}$, and W+jets production with the W boson decaying leptonically.

Samples for QCD multijets production were generated with POWHEGBOX v2 at NLO using the dijet process, and interfaced to PYTHIA 8.245 with the A14 tune and the NNPDF2.3lo PDF set. The p_{T} of the underlying Born configuration was taken as the renormalisation and factorisation scales and the NNPDF3.0nlo PDF was used. To estimate generator systematic uncertainties, an alternative multijets sample was used, with events produced at NLO with the POWHEGBOX v2 generator interfaced with Herwig 7.1 [52], using the NNPDF3.0nlo PDF set and the default Herwig 7.1 tune.

The production of $W/Z(\rightarrow q\bar{q})\gamma$ was modelled by SHERPA 2.1.1 at LO, and the parton distributions were modelled with the CT10 PDF set [53]. The $t\bar{t}$ sample is the same as the one previously described.

The production of $W(\rightarrow \tau\nu)$+jets was simulated with the SHERPA 2.2.1 generator using NLO matrix elements for up to two partons, and LO matrix elements for up to four partons calculated with the Comix and OpenLoops libraries. They were matched with the Sherpa parton shower using the MEPS@NLO prescription using the set of tuned parameters developed by the Sherpa authors. The NNPDF3.0nnlo set of PDFs was used and the samples were normalised to a next-to-next-to-leading-order cross-section prediction [54].

The effects of multiple proton–proton interactions in the same bunch crossing as the hard scatter and in neighbouring ones (pile-up) were included using simulated events generated with PYTHIA 8.186 using the NNPDF2.3lo PDF set and the A3 tune [55]. Simulated events were weighted to reproduce the distribution of the average number of interactions per bunch crossing $\langle\mu\rangle$ observed in data.

4 Event reconstruction

The following procedures are used to reconstruct photons, electrons, muons, jets, large-radius (large-R) jets, and the missing transverse momentum.

Photons and electrons are reconstructed from clusters of energy deposits in the EM calorimeter, together with tracks reconstructed in the inner tracking detector [56–58]. Pho-

ton candidates are required to have $p_{\mathrm{T}} > 150$ GeV and $|\eta| < 2.37$. The identification (ID) of photons is performed by requiring the photon to satisfy a set of identification criteria [56] based on shower shapes measured in the first two longitudinal layers of the electromagnetic calorimeter, where the first layer has high granularity and provides large discrimination between prompt photons and photons from decays of hadrons inside jets, and the leakage into the hadronic calorimeter. Two isolation (ISO) working points (WP) of photons, *Tight* and *Loose* [56], are defined based on the amount of transverse energy deposited in clusters of calorimeter cells within a cone of radius $R = 0.4$ and $R = 0.2$, respectively, around the photon, excluding the photon cluster itself, and the track isolation within a cone of radius $R = 0.2$ around the photon.

Electron candidates are identified using the likelihood identification criteria described in Ref. [56]. The *VeryLoose* identification criteria are applied to electrons. Candidates are required to have $p_{\mathrm{T}} > 10$ GeV and $|\eta| < 2.47$.

Muon candidates are reconstructed from tracks in the muon spectrometer that are matched to a corresponding track in the inner tracking detector [59]. Candidates are required to have $p_{\mathrm{T}} > 10$ GeV, $|\eta| < 2.7$, and satisfy the *Loose* identification criteria.

Jets are reconstructed from particle-flow objects [60] using the anti-k_t jet algorithm with a radius parameter of $R = 0.4$. The jets are calibrated following the procedure described in Ref. [61] and are required to have $p_{\mathrm{T}} > 30$ GeV and $|\eta| < 2.5$. Pile-up jets with $p_{\mathrm{T}} < 120$ GeV are rejected using the *Medium* working point of the jet vertex tagger [62].

Large-R jets are reconstructed using the anti-k_t jet algorithm with a radius parameter of $R = 1.0$ from particle-flow objects. Candidates are required to have $p_{\mathrm{T}} > 50$ GeV and $|\eta| < 2.5$, to ensure good overlap with the tracking volume of the ATLAS detector and reduce pile-up jet contamination.

The missing transverse momentum (with magnitude $E_{\mathrm{T}}^{\mathrm{miss}}$) is reconstructed as the negative vector sum of the transverse momenta of all the reconstructed and calibrated objects in the event, including a soft term that accounts for all tracks associated with the primary vertex but not matched to any reconstructed object [63].

A standard overlap-removal procedure is applied to resolve ambiguities where multiple physical objects are reconstructed from the same detector signature. Additionally, in the SF measurement, an overlap removal between photon and di-τ objects is performed, prioritizing the photons within $\Delta R = 1.0$ of the di-τ candidate. In a more general context, the di-τ object's priority in the object overlap removal hierarchy would place it below light leptons and photons, and above jets.

5 Di-τ reconstruction, energy-scale calibration, and identification

One of the major challenges facing light resonance searches [64–66] is the tagging of the resonance decay products. Due to the low mass of the X resonance, a significant fraction of the X resonances will be produced with transverse momenta sizeable enough to result in decay products that are highly collimated. This is demonstrated in Fig. 1a, showing the distributions of ΔR_{vis}, the particle-level visible angular distance between the two $\tau_{\text{had-vis}}$, in simulated $t\bar{t}X$ ($X \to \tau_{\mathrm{had}}\tau_{\mathrm{had}}$) events for m_X values of 20 and 60 GeV. In the following, the notations of *leading* and *subleading* refer to their ordering in p_{T}.

5.1 Reconstruction

The tagging of a nearby $\tau_{\text{had-vis}}$ pair relies on the reconstruction of a large-R jet (seed jet) and its substructure. The reconstruction algorithm was initially developed for boosted $h \to \tau_{\mathrm{had}}\tau_{\mathrm{had}}$ decays, in the context of a search for resonant di-Higgs boson production in the $b\bar{b}\tau^+\tau^-$ channel [7]. In that case, the $\tau_{\text{had-vis}}$ were expected to be produced with large individual transverse momenta, and the reconstruction was only performed for seed jets with $p_{\mathrm{T}} > 300$ GeV. However, when a *light* resonance decays into a boosted di-τ, the $\tau_{\text{had-vis}}$ p_{T} spectrum is rather soft, as demonstrated in Fig. 1b, c. In accordance, the seed jet p_{T} threshold is reduced down to 50 GeV, and the di-τ objects reconstructed from those low-p_{T} seeds are later studied.

During Run 1 and early Run 2 of the LHC, $\tau_{\text{had-vis}}$ candidates reconstructed from $R = 0.4$ anti-k_t jets in the ATLAS experiment utilised the definitions of an inner cone of radius $R = 0.2$ (core cone) and its surrounding annulus $0.2 < R < 0.4$ (isolation annulus) [67]. Once a seed jet is reconstructed, its constituents are grouped into subjets (with $p_{\mathrm{T}} > 10$ GeV) using the anti-k_t algorithm with $R = 0.2$. Thus, a consistent definition with the single $\tau_{\text{had-vis}}$ core cone, where the signature from its decay products is expected, is maintained. The seed jet area not included within the radius of any subjet (containing tracks and energy deposits not associated with any subjet) is considered as the isolation region, analogous to the isolation annulus of a $\tau_{\text{had-vis}}$ candidate. A core region is also defined for each subjet as the cone of radius $R = 0.1$ around its axis. An illustration of the reconstructed di-τ object topology is given in Fig. 2. A hadronic di-τ candidate is required to have at least two subjets, each with at least one associated track. A di-τ vertex calculation is performed to find the most likely di-τ production vertex, and subjet kinematics are calculated relative to this vertex. The track selection and track-to-vertex matching criteria are identical to those used in Ref. [68]. Impact parameter requirements used in associating tracks to subjets are calculated relative

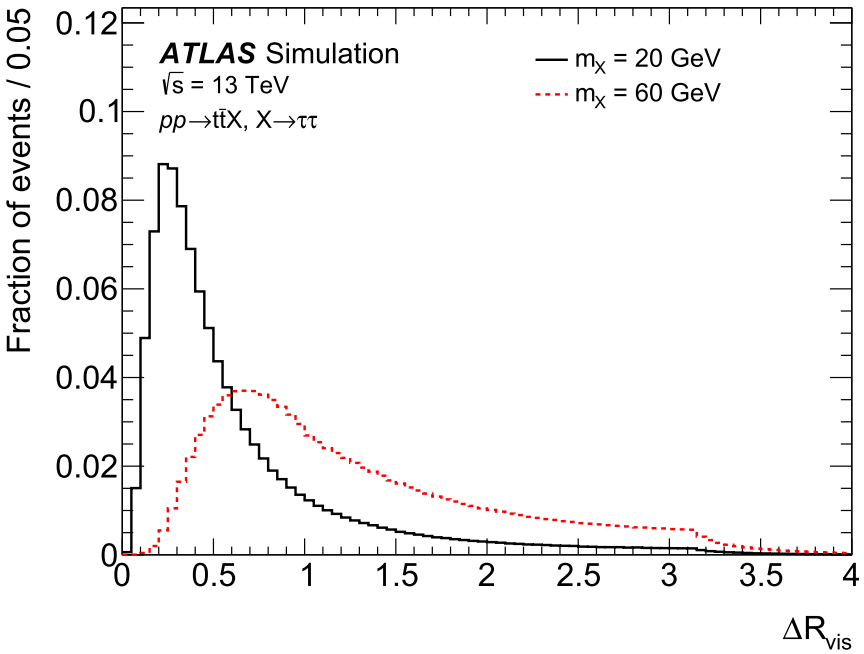

(a)

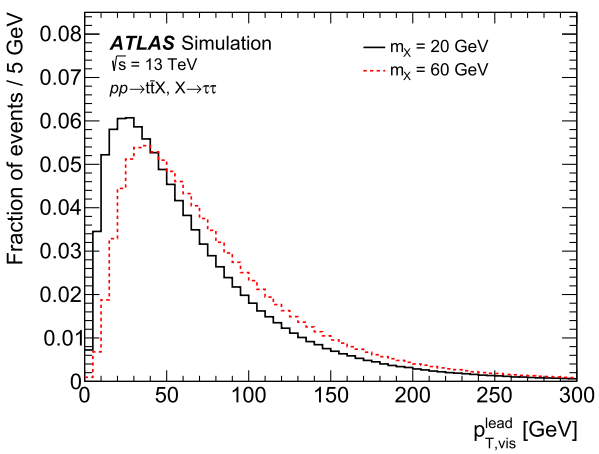

(b)

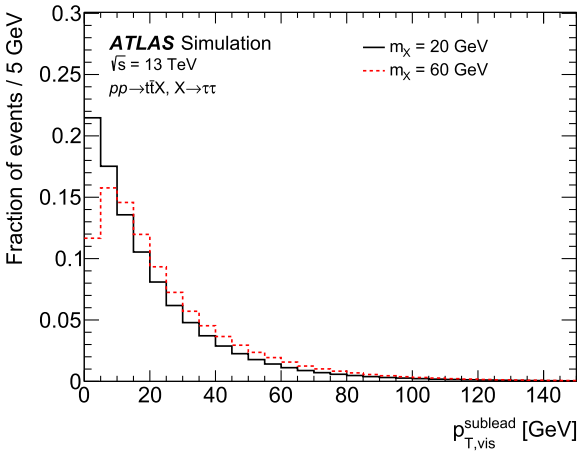

(c)

Fig. 1 Distributions of **a** visible angular distance ΔR_{vis}, **b** leading $\tau_{\text{had-vis}}$ p_{T} and **c** subleading $\tau_{\text{had-vis}}$ p_{T} in $X \to \tau_{\text{had}}\tau_{\text{had}}$ decays from $t\bar{t}X$ events, normalised to unit area, for two different m_X values

to the di-τ vertex, while for isolation region tracks the vertex with the highest $\sum(p_{\text{T}}^{\text{trk}})^2$ is used. In the following, it is assumed that the two leading subjets hold the $\tau_{\text{had-vis}}$ signatures and the sum of their four-momentum defines that of the τ_{had} pair. This assumption is valid in approximately 90% of cases for the considered $t\bar{t}X$ samples where the particle-level $\tau_{\text{had-vis}}$ are both captured by any two unique subjets of a reconstructed di-τ object.

A truth-matched di-τ is defined as a reconstructed di-τ object in which the leading and subleading subjets are each geometrically-matched to particle-level $\tau_{\text{had-vis}}$ within $\Delta R = 0.2$. The di-τ reconstruction efficiency is then defined as the fraction of events containing a truth-matched di-τ object out of all events satisfying a baseline selection applied at particle-level.

To satisfy the baseline selection, an event is required to have a single particle-level hadronically decaying $\tau^+\tau^-$ pair originating from the X resonance (discarding τ_{had} leptons from heavy-flavour hadron decays), with an angular distance $0.2 \leq \Delta R_{\text{vis}} \leq 1.0$ between the two $\tau_{\text{had-vis}}$, each of which is required to have $p_{\text{T,vis}} \geq 10$ GeV. These criteria are selected to reflect the phase-space defined by the previously described subjet reconstruction step.

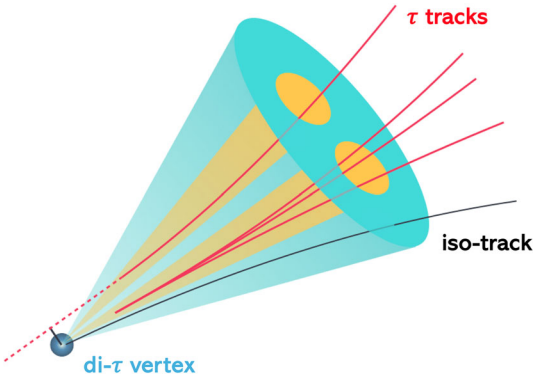

Fig. 2 Schematic illustration of the reconstructed di-τ object topology [7] for one seed jet with $R = 1.0$ and two subjets with $R = 0.2$

The reconstruction efficiencies for the boosted di-τ tagger and for two standard (resolved) $\tau_{\text{had-vis}}$ are calculated in $t\bar{t}X$ events, and are given in Fig. 3. It is evident from the figure that the di-τ reconstruction is indeed most efficient in the highly collimated $\Delta R_{\text{vis}} \leq 0.45$ regime, where resolved $\tau_{\text{had-vis}}$ reconstruction fails, and an overall larger fraction of events may be successfully reconstructed. However, its performance is clearly less resilient to increasing pile-up conditions, degrading by about 20% over the examined range. This is mainly due to the soft spectrum of the subleading $\tau_{\text{had-vis}}$ making it increasingly probable – as conditions become more severe – that pile-up contributions cause significant shifts in reconstructed seed jet and subjet axes, such that both the particle-level $\tau_{\text{had-vis}}$ are not successfully captured inside the two leading subjets of a single seed jet. Similarly, as the $p_{\text{T,vis}}$ distribution becomes softer and the angular separation between the two $\tau_{\text{had-vis}}$ increases, a single $R = 1.0$ seed jet and its subjets are less likely to capture both the $\tau_{\text{had-vis}}$ and the reconstruction efficiency correspondingly declines. Additionally, as the individual $\tau_{\text{had-vis}}$ charged-hadron multiplicities increase, the di-τ reconstruction efficiency increases by approximately 10%, while having an alleviated dependence on pile-up conditions.

5.2 Energy scale calibration

Truth-matched di-τ objects from the two generated m_X points, with either one or three charged tracks associated with each of the two leading subjets, are later used to compare reconstructed and particle-level p_{T} values; from this comparison, corrections are derived to calibrate the reconstructed momentum to the particle-level $\tau_{\text{had-vis}}$ scale. The calibration is conducted individually for each subjet, binned in reconstructed $|\eta|$ ($|\eta_{\text{reco}}|$) and associated track multiplicity (N_{prong}), in a two-step procedure similar to the one described in Ref. [68]. In the first step, the contribution to the subjet momentum due to pile-up interactions is estimated and subtracted. In the second step, a detector response correction is applied, aiming to provide the best estimate of the true $\tau_{\text{had-vis}}$ momentum.

As demonstrated in Fig. 4a, the subjet p_{T} is found to increase linearly with the number of reconstructed primary vertices (N_{PV}) in all $|\eta_{\text{reco}}|$ regions, with each vertex adding around 60 MeV to the measured p_{T}. The pile-up corrected momentum is thus given by: $p_{\text{T}}^{\text{corr}} = p_{\text{T}}^{\text{reco}} - A(|\eta_{\text{reco}}|) \times N_{\text{PV}}$. The pile-up-correction coefficients $A(|\eta_{\text{reco}}|)$ are summarised in Fig. 4b. In the second step, a detector response function is derived from the ratio of corrected and generated visible momentum in each $|\eta_{\text{reco}}|$ and N_{prong} region. This function is denoted $R(p_{\text{T}}^{\text{corr}}, |\eta_{\text{reco}}|, N_{\text{prong}})$, and is used to derive the calibrated momentum as: $p_{\text{T}}^{\text{calib}} = \frac{p_{\text{T}}^{\text{corr}}}{R(p_{\text{T}}^{\text{corr}}, |\eta_{\text{reco}}|, N_{\text{prong}})}$. Figure 5 shows the detector response functions. For p_{T} values greater or lower than the measured points, the response function is set to a constant value (its value at the measured limit). Response function values are mostly below unity due to the underlying EM scale calibration of constituent particle flow objects. The response generally displays lower values as $|\eta_{\text{reco}}|$ increases, except the $1.3 < |\eta_{\text{reco}}| \leq 1.6$ region, where the transition between barrel and end-cap calorimeters occurs and even lower response values are observed. The subjet p_{T} threshold implemented in the reconstruction induces a bias in the response distribution of very low-p_{T} $\tau_{\text{had-vis}}$, favouring candidates reconstructed with a high response and leading to a larger average response at $\langle p_{\text{T}}^{\text{corr}} \rangle \lesssim 20$ GeV. As larger associated track multiplicities provide better momentum estimations at low $p_{\text{T}}^{\text{corr}}$, the response values for 3-prong subjets are closer to unity than for 1-prong subjets across a larger $\langle p_{\text{T}}^{\text{corr}} \rangle$ range.

5.3 Identification

The di-τ reconstruction method does not provide background separation power. Limited rejection can be obtained from the introduction of selection criteria, for example on the number of subjets and their associated track multiplicities and charges. To further discriminate genuine boosted $\tau_{\text{had-vis}}$ pairs from misreconstructed di-τ candidates (originating from jets), a dedicated identification step is introduced. Identification variables are calculated for each di-τ candidate, using tracking and calorimeter information from the subjets and the isolation region. These variables are later used as inputs to train a boosted decision tree (BDT) [69–71] classifier. The signal for the classifier consists of truth-matched di-τ objects from the previously mentioned $t\bar{t}X$ events using the two generated m_X points, chosen as the upper and lower limits of the m_X range. When combined, these mass points provide a di-τ $p_{\text{T,vis}}$ phase space coverage between approximately 50–250 GeV at the most relevant $0.2 \leq \Delta R_{\text{vis}} \leq 0.6$ range, where the reconstruction effi-

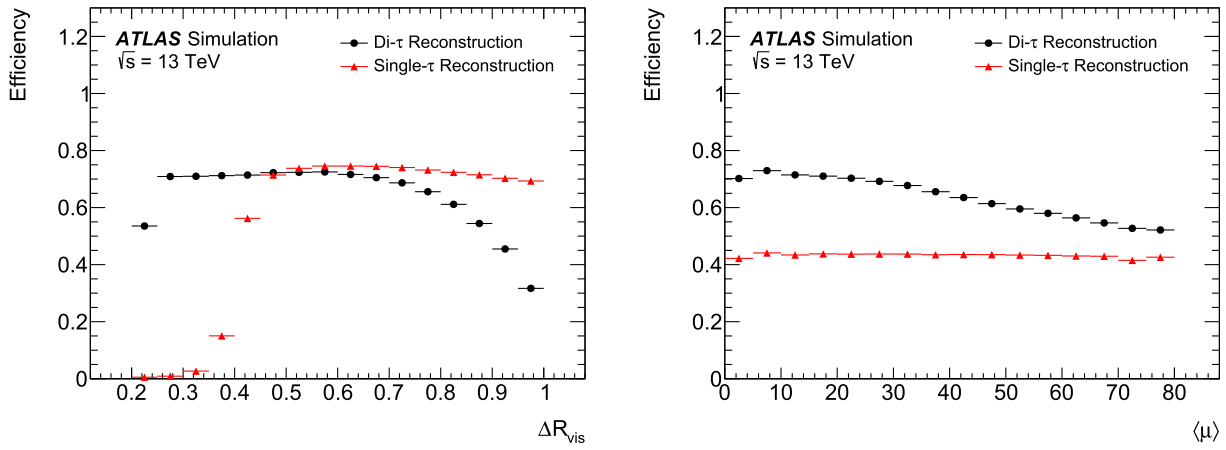

(a) (b)

Fig. 3 Di-τ reconstruction efficiency (dots) and two resolved $\tau_{\text{had-vis}}$ reconstruction efficiency (triangles) as a function of **a** the visible angular separation ΔR_{vis} between the two particle-level $\tau_{\text{had-vis}}$ and **b** the average number of interactions $\langle\mu\rangle$, measured in simulated $t\bar{t}X$ events. The $t\bar{t}X$ sample includes events with $m_X = 20$ GeV and $m_X = 60$ GeV in equal proportions. The plateau value in **b** for the two resolved $\tau_{\text{had-vis}}$ case depends strongly on the fraction of events with angular distance smaller than 0.4, which limits the reconstruction efficiency achievable using the resolved $\tau_{\text{had-vis}}$ method, and hence represents an averaged efficiency between the two m_X values. The error bars account for the statistical uncertainty in simulation

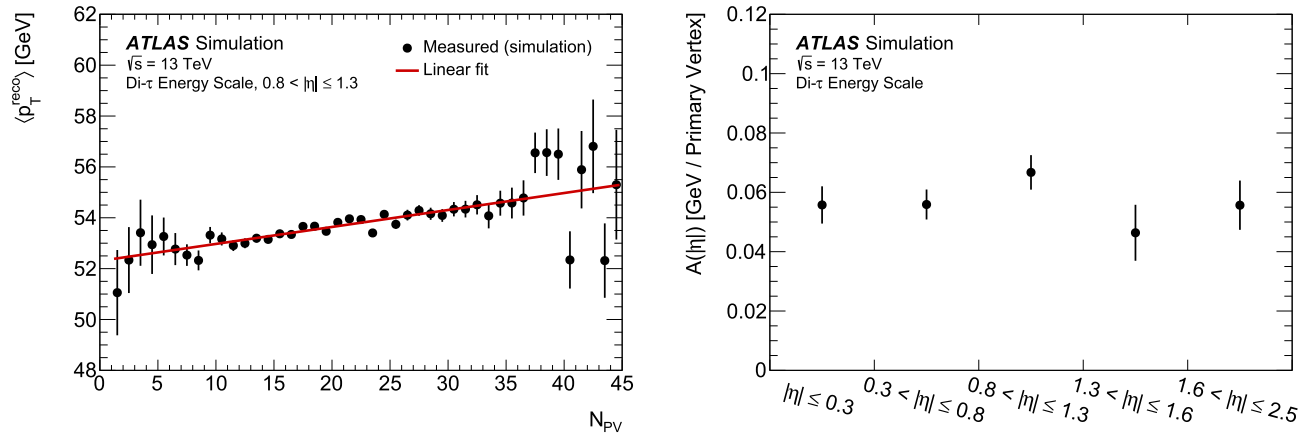

(a) (b)

Fig. 4 **a** Mean subjet $p_{\text{T}}^{\text{reco}}$ as a function of the number of reconstructed primary vertices for $0.8 < |\eta_{\text{reco}}| \leq 1.3$, where the line is the linear fit from which correction coefficients are derived. **b** Measured linear pileup-correction coefficients $A(|\eta_{\text{reco}}|)$. These are obtained for $\tau_{\text{had-vis}}$ originating from X decays in $t\bar{t}X$ events, using the two generated m_X values. The error bars in **a** account for the statistical uncertainty in simulation, while the error bars in **b** represent the uncertainty on the linear fit slope parameter

ciency is greatest. The background is composed of fake di-τ objects originating from jets in all-hadronic $t\bar{t}$ decay events. Di-τ objects entering the training are required to have either one or three charged-particle tracks associated with each of the two leading subjets.

The particular set of BDT input variables was chosen by reducing a larger set of calculated variables in steps, with consideration taken to include variables that contain information from all regions of a reconstructed di-τ: the core cone of both of the subjets, the full area of both of the subjets, the isolation region and the entire seed jet. The bulk of signal di-τ objects have p_{T} values in the range of approximately 70 to 150 GeV, while the background p_{T} spectrum is softer, ranging from approximately 20 to 80 GeV. To mitigate the dependence of the BDT output score on the transverse momentum, input events are reweighted such that the resulting di-τ p_{T} spectrum (separately for signal and background) is flattened up to 250 GeV, and exponentially decreasing beyond.

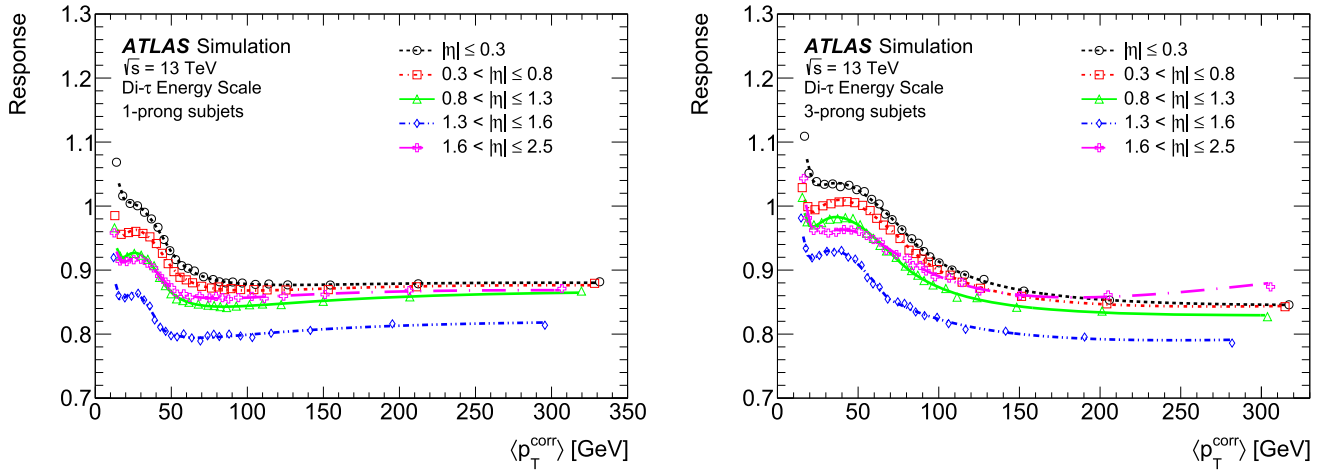

Fig. 5 Detector response function for **a** 1-prong and **b** 3-prong subjets as a function of $\langle p_{\mathrm{T}}^{\mathrm{corr}} \rangle$ in various $|\eta_{\mathrm{reco}}|$ regions, for $\tau_{\text{had-vis}}$ originating from X decays in $t\bar{t}X$ events, generated with m_X values of 20 and 60 GeV

The 16 variables used as input to the classifier are:[4]

- $n_{\text{isotracks}}$: the number of tracks associated with the isolation region.
- Subjet p_{T} fraction $f_{\text{subjet}}^{\text{(sub)lead}}$: the ratio between the transverse momenta of the subjet and the seed jet,

$$f_{\text{subjet}}^{\text{(sub)lead}} \equiv \frac{p_{\mathrm{T}}^{\text{(sub)lead}}}{p_{\mathrm{T}}^{\text{seed}}}.$$

- R_{isotrack}: the p_{T}-weighted sum of track distances from the subjet axis, for isolation-region tracks inside a cone of $\Delta R < 0.4$ around the subjets,

$$R_{\text{isotrack}} \equiv \frac{\sum_{\text{(sub)lead}} \sum_i^{\Delta R_i < 0.4} p_{\mathrm{T},i}^{\text{isotrk}} \Delta R_i}{\sum_{\text{(sub)lead}} \sum_i^{\Delta R_i < 0.4} p_{\mathrm{T},i}^{\text{isotrk}}}.$$

  This definition means the variable considers only tracks not associated with any subjet, that are within an isolation annulus similar to that of a single reconstructed $\tau_{\text{had-vis}}$. A value of zero is assigned if no tracks are found.
- $R_{\text{max}}^{\text{(sub)lead}}$: the maximal ΔR of an associated track to the subjet axis.
- Weighted core track distance $R_{\text{core}}^{\text{(sub)lead}}$: defined for a given subjet, this is the p_{T}-weighted sum of track distances from the subjet axis, for tracks found inside the core cone of the subjet,

$$R_{\text{core}}^{\text{(sub)lead}} \equiv \frac{\sum_i^{\Delta R_i < 0.1} p_{\mathrm{T},i}^{\text{trk}} \Delta R_i}{\sum_i^{\Delta R_i < 0.1} p_{\mathrm{T},i}^{\text{trk}}}.$$

  A value of zero is assigned if no tracks are found inside the core cone.
- R_{track}: p_{T}-weighted sum of track distances from the subjet axis, for $\tau_{\text{had-vis}}$ tracks inside a cone of $\Delta R < 0.2$ around the subjets,

$$R_{\text{track}} \equiv \frac{\sum_{\text{(sub)lead}} \sum_i^{\Delta R_i < 0.2} p_{\mathrm{T},i}^{\text{trk}} \Delta R_i}{\sum_{\text{(sub)lead}} \sum_i^{\Delta R_i < 0.2} p_{\mathrm{T},i}^{\text{trk}}}.$$

- $f_{\text{track}}^{\text{(sub)lead}}$: the ratio between the highest-p_{T} track inside a subjet, and the respective subjet p_{T}.
- $\log(m_{\text{tracks}}^{\text{(sub)lead}})$: logarithm of the invariant mass calculated from the four-momenta of tracks associated with the given subjet.
- $\log(|d_{0,\text{lead-track}}^{\text{(sub)lead}}|)$: logarithm of the closest distance in the transverse plane between the primary vertex and the leading track associated with the appropriate subjet.
- ΔR(lead, sublead): angular separation between the two leading subjets.

The resulting BDT distributions for training and testing events (for both signal and background) are presented in Fig. 6a, showing two well-separated peaks for the signal and background with no evidence of classifier overtraining. The resulting separation power is better illustrated through the Receiver Operating Characteristic (ROC) curve, which is defined here as the inverse background efficiency (background rejection) as a function of signal efficiency. The ROC

[4] The notation (sub)lead refers to the (sub)leading p_{T} subjet within the seed jet.

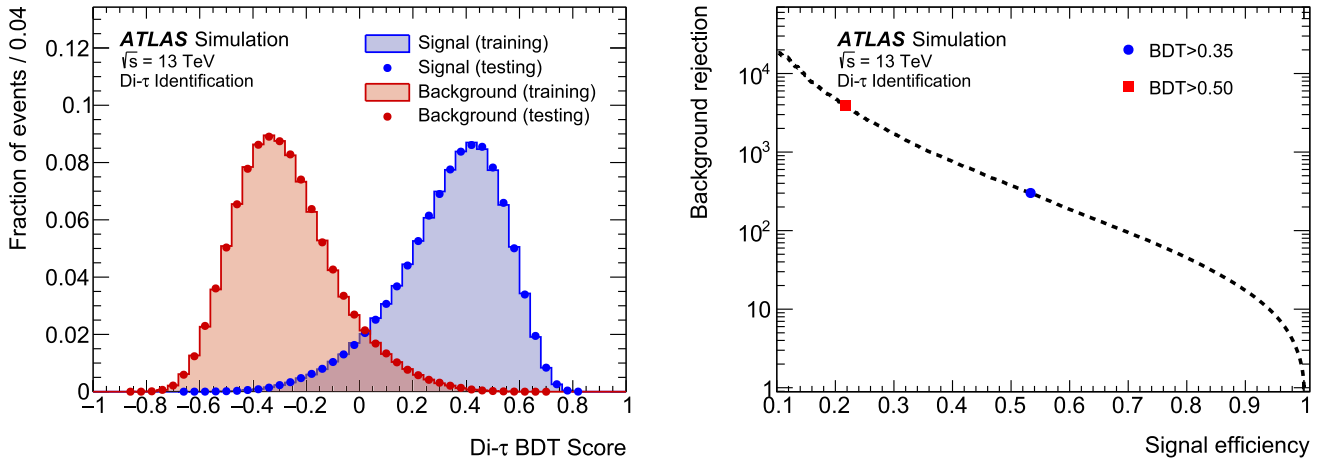

Fig. 6 Results of the classifier training, showing the **a** BDT score distributions for signal and background events and **b** background rejection factor versus signal identification efficiency, corresponding to the trained BDT score distributions. The two markers represent the *Medium* and *Tight* WPs. Signal (real) di-τ objects originate from X decays in $t\bar{t}X$ events, generated with m_X values of 20 and 60 GeV in equal proportions, while background (fake) di-τ objects originate from jets in fully-hadronic $t\bar{t}$ events

curve for the trained BDT is given in Fig. 6b, corresponding to an area under curve of 0.976, and showing that for background rejection about ∼50, the signal efficiency is ∼75%. Naturally, lower signal efficiency results in even better background rejection; for example, further increase of the background rejection by a factor of ∼100 will result in a signal efficiency reduction by a factor close to three.

Two benchmark WPs, labelled as *Medium* and *Tight*, are defined using constant selections on the classifier scores of 0.35 and 0.5, respectively. The corresponding signal efficiencies are approximately 53 and 22% for rejection factors of 300 and 4000, respectively. The dependence of the signal and background identification efficiencies for these WPs on several kinematic variables are illustrated in Figs. 7 and 8, respectively. The identification efficiency is approximately constant relative to the di-τ pseudorapidity η_{reco}, but clearly decreases as the average number of interactions $\langle\mu\rangle$ grows, a dependency which becomes more severe as the WP tightness increases. However, a similar behaviour is also observed for the background, such that the background rejection power increases as $\langle\mu\rangle$ increases. In terms of the angular separation between the two leading subjets, used as one of the input variables to the classifier, a decline in the identification efficiency as ΔR increases should be expected and is observed, with the classifier achieving its peak performance in the highly-boosted regime where the reconstruction is also most efficient. As the angular separation is inversely proportional to the transverse momentum at fixed m_X, the identification efficiency increases as the transverse momentum of the di-τ seed jet increases.

Signal and background BDT distributions are found to shift to lower values as the number of prongs in a subjet increases from one to three, leading to a decrease in both the signal and background efficiencies for a constant BDT score selection. This effect results in approximately 20% efficiency loss per subjet in signal, and approximately a tenfold increase in rejection per subjet in background. As the shift is more significant for background than for signal, the overall performance of the identification improves with increasing subjet prongness – in accordance with the performance observed for the resolved $\tau_{\text{had-vis}}$ identification [2]. Each three-pronged subjet improves the rejection by approximately a factor of two over its one-pronged counterpart, for a given constant signal efficiency.

6 Identification efficiency measurement in $Z(\rightarrow \tau\tau)+\gamma$ events

A dedicated tag-and-probe measurement is performed to measure the di-τ identification efficiency using $Z(\rightarrow \tau\tau)+\gamma$ signal events. The identification efficiencies are obtained from data and simulated events, and their ratio is defined as the SF, computed for the previously noted *Medium* and *Tight* BDT-based identification WPs. Few SM processes can be used to assess the performance of the di-τ identification algorithm in data. The $Z\gamma$ process was chosen due to its sizeable production cross-section, the limited SM background contribution in the $\tau\tau\gamma$ final state, and the Z boson p_{T} regime that can be accessed with a photon trigger. However, as the Z boson mass is larger than the considered m_X values, the

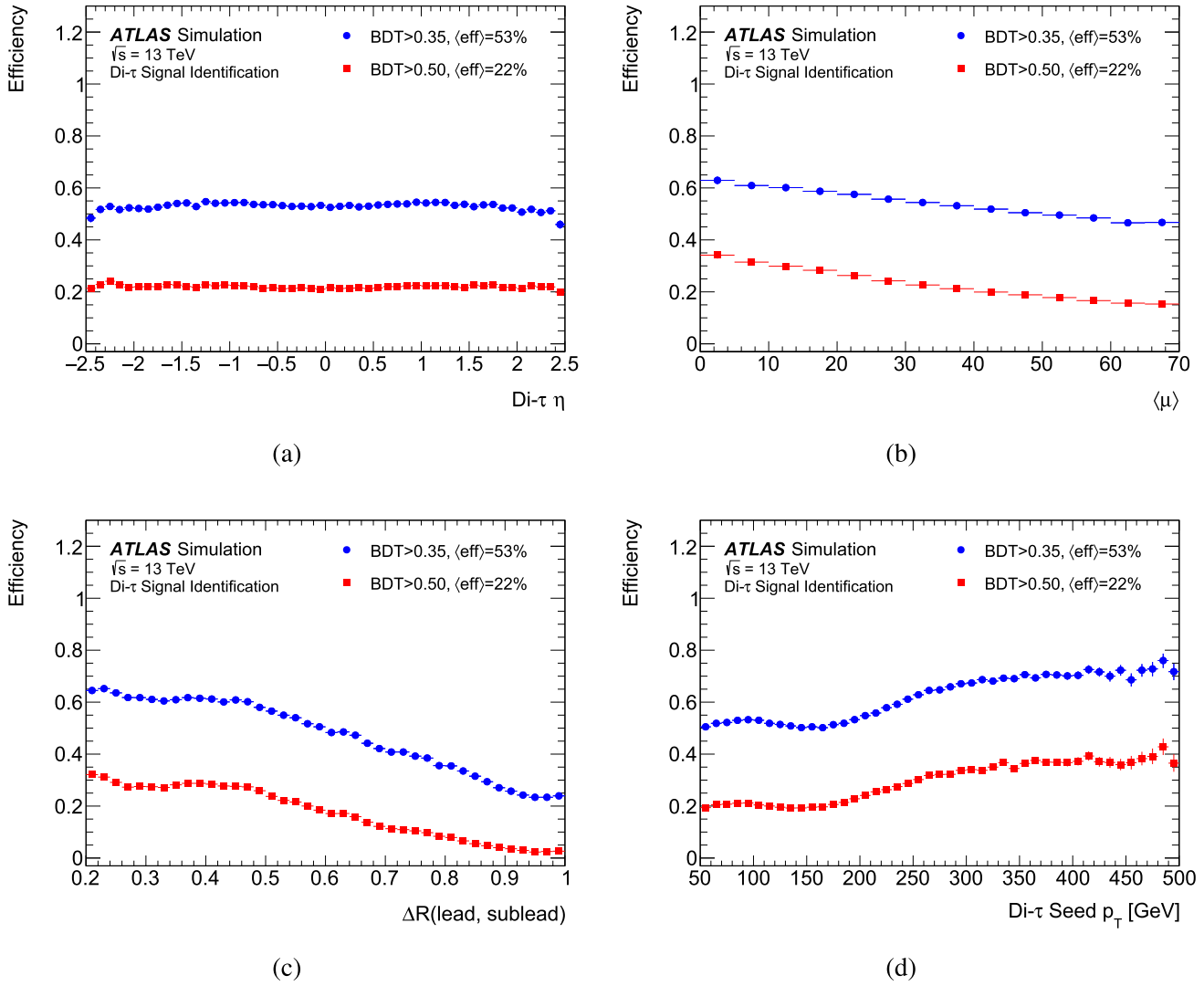

Fig. 7 Signal identification efficiency at constant BDT selections, measured in $t\bar{t}X$ events, as functions of **a** the di-τ pseudorapidity η_{reco}, **b** the average number of interactions $\langle\mu\rangle$, **c** the angular distance ΔR between the two leading di-τ subjets and **d** the transverse momentum of the di-τ seed jet. The error bars account for the statistical uncertainty in simulation. The $t\bar{t}X$ sample includes events with $m_X = 20$ GeV and $m_X = 60$ GeV in equal proportions

phase space probed in the tag-and-probe measurement is not expected to match that of $t\bar{t}X$ processes. This measurement is statistically limited and hence performed inclusively in all di-τ kinematic properties.

6.1 Event selection and categorisation

Events are selected using the lowest unprescaled trigger requiring the presence of a photon with $E_{\text{T}} > 140$ GeV [72]. The photon trigger-matching algorithm, which confirms the association between the reconstructed photon and the triggering signal, is applied. Events containing electrons or muons are vetoed.

At preselection level, events are required to contain at least one photon passing the *Tight* identification and isolation working points [56] with $p_{\text{T}} > 150$ GeV and $|\eta| < 2.37$. Events with one or more photon candidates passing looser identification and isolation requirements are also kept for estimate of the backgrounds. Additionally, events are required to contain at least one di-τ object, which must satisfy the following requirements:

- The number of subjets is at least two.
- The invariant mass of the di-τ object is within the range $40 < m_{\tau\tau} < 130$ GeV.
- Each of the two leading subjets contains either one track (1-prong) or three tracks (3-prong).

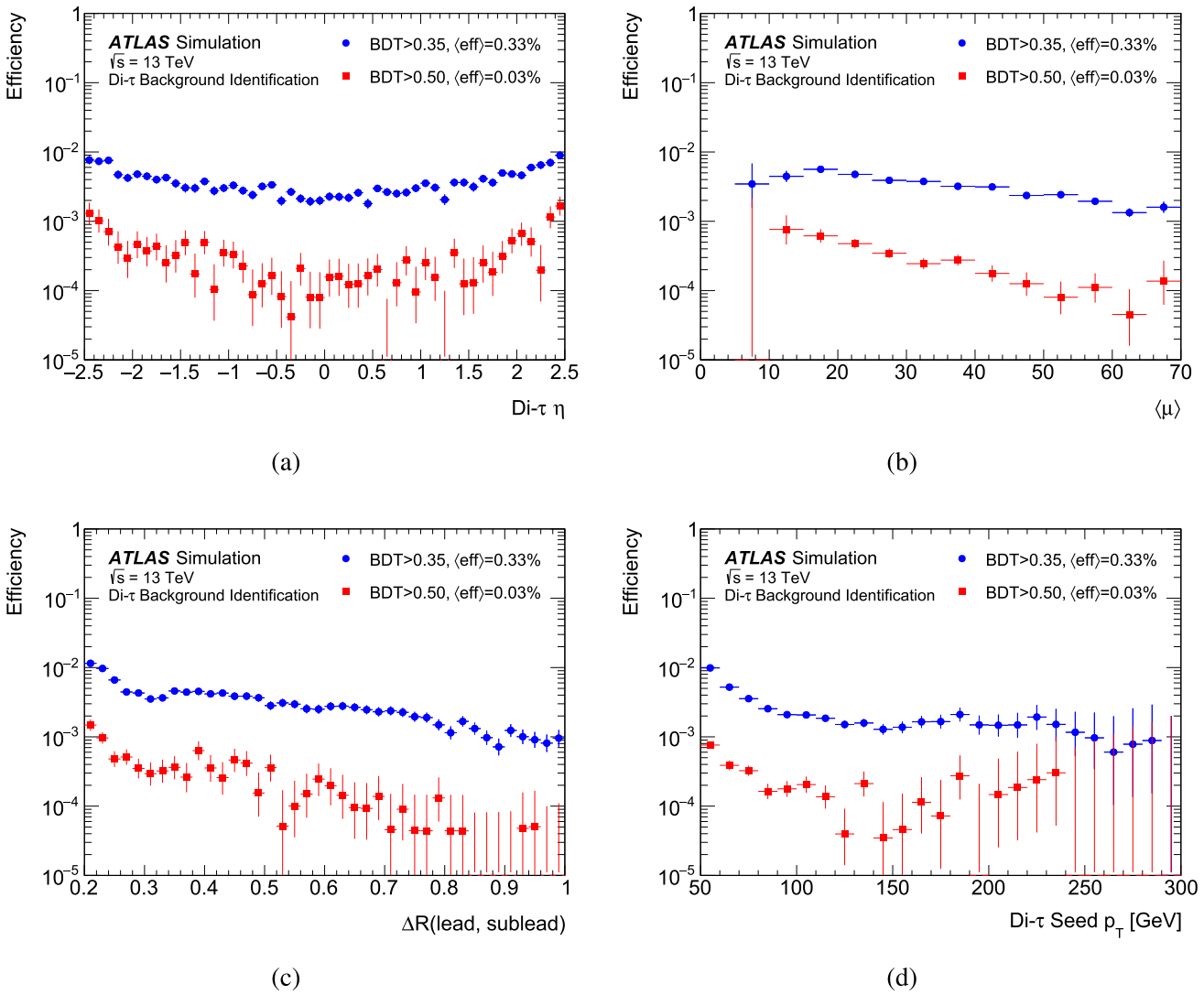

Fig. 8 Background identification efficiency at constant BDT selections, measured in $t\bar{t}$ events, as functions of **a** the di-τ pseudorapidity η_{reco}, **b** the average number of interactions $\langle\mu\rangle$, **c** the angular distance ΔR between the two leading di-τ subjets and **d** the transverse momentum of the di-τ seed jet. The error bars account for the statistical uncertainty in simulation

- The charge product of the two leading subjets is $Q \equiv q_{\text{lead}} \times q_{\text{sublead}} = \pm 1$, where q_{lead} (q_{sublead}) is the charge of the (sub)leading subjet, defined as the sum of the charges of the associated tracks.
- The transverse momentum of the seed jet selection is optimised to $90 < p_{\text{T}}^{\text{seed}} < 360$ GeV for achieving further background rejection.

The leading p_{T} photon and the leading BDT di-τ candidate are selected, and their angular separation is required to satisfy $\Delta R\,(\text{di-}\tau, \gamma) > 1.0$, selecting events where the di-τ object is well separated from the photon. This requirement enhances the contribution of events with photons originating from initial-state radiation.

Events are further divided into control region (CR), validation region (VR) and signal region (SR), according to the charge product Q of the two leading di-τ subjets, and the azimuthal angle separation between the di-τ and $E_{\text{T}}^{\text{miss}}$:

- CR: $Q = +1$, same-sign charges (SS).
- VR: $Q = -1$, opposite-sign charges (OS); and $\Delta\phi\left(\text{di-}\tau, E_{\text{T}}^{\text{miss}}\right) > 2.2$.
- SR: $Q = -1$, opposite-sign charges (OS); and $\Delta\phi\left(\text{di-}\tau, E_{\text{T}}^{\text{miss}}\right) < 2.2$.

In every region, if more than a single di-τ object fulfills the requirements, the one with the highest BDT score is selected.

Events from $Z\gamma$, $Z\gamma\gamma$ and Z+jets simulated samples, where the Z boson decays into a $\tau^+\tau^-$ pair, are classified as signal or background events based on whether the reconstructed boosted di-τ object passes the truth-matching requirement (indicating a real di-τ, as defined in Sect. 5.1) or not (indicating a misidentification), accordingly. Events from all other samples are classified as background.

6.2 Background estimation

The dominant backgrounds arise from processes containing a real photon that satisfies the trigger requirement, together with a quark- or gluon-initiated jet that is misidentified as a di-τ object. Another source is processes containing multiple energetic jets, one being misidentified as a photon and another as a di-τ object. These two sources correspond to γ+jets and multijet events respectively, and as QCD processes they are challenging to simulate. The γ+jets sample has as large as 20% theory uncertainty in its cross-section [73], compared with only 5% for the other samples [74]. Therefore, a data-driven method is used to estimate their contribution, extrapolating the amount of background in the signal region from the yields observed in control regions.

The general strategy is as follows. A data-driven background estimate method is used to obtain the γ+jets and multijet normalisations, while distribution shapes are obtained from simulation. To correct for the mismodelling of the BDT score distribution shape, events from γ+jets and multijet samples are reweighted to match the data according to a function that is obtained from the CR and tested in the VR. The contribution of all other background components is taken from simulation, and normalised to their respective theoretical predictions.

Background normalisation

The contribution from the γ+jets and multijet processes is estimated by using a sideband counting method [75], also referred to as the ABCD method. This method relies on counting events with photon candidates in four regions of a two-dimensional plane, defined by the photon isolation and identification criteria. A prompt photon region (region A) is defined by photon candidates that are isolated and satisfy the *Tight* identification, as explained in Sect. 4. Three fake-photon regions are defined in the isolation-identification plane, consisting of photon candidates that are non-*Tight* and isolated (region B), *Tight* and non-isolated (region C), or non-*Tight* and non-isolated (region D). A non-isolated photon candidate is defined by inverting the isolation requirement. A photon candidate is classified as non-*Tight* if it fails at least one of four selections associated with the shower-shape variables but passes all the other selections of the *Tight* identification [56].

Assuming negligible correlation between the photon identification and isolation would imply that the number of events with non-prompt photon candidates in the four regions (N_A, N_B, N_C and N_D) satisfy the condition $N_A/N_B = N_C/N_D$, particularly considering the multijet sample. The residual correlation between the photon isolation and identification is accounted for using the correlation factors defined as $R_c \equiv (N_A/N_B)\,/\,(N_C/N_D)$, and estimated from the multijet MC simulation. A further correction is included to take into account the contamination from real photons in the three regions (B, C, or D) that are supposed to be dominated by fake photons. This contribution is evaluated using the γ+jets MC simulation and is parameterised through the *leakage coefficients*, representing the number of real photons in each of the aforementioned regions relative to the number of real photons in region A, i.e. $f_\alpha \equiv N_\alpha^\gamma / N_A^\gamma$, with α indicating region B, C, or D. Values for these two corrections are provided in Table 2. While MC simulations are used to estimate the leakage coefficients and correlation factor, different generator combinations for both the γ+jets and multijet samples are considered and corresponding uncertainties on these quantities are assigned.

In the ABCD method, the total SM prediction is normalised to data in each of the four regions, with the contribution from real photons and jets misidentified as photons, the γ+jets and multijets samples respectively, being unknown. By assumption, the ABCD normalisation preserves the ratio represented by the leakage coefficients. Therefore, the γ+jets contribution in regions B, C, and D can be expressed via its normalised contribution in region A.

The method determines the contribution of real photons N_A^γ in region A using the relation $N_A^{\mathrm{MJ}}/N_B^{\mathrm{MJ}} = R_c \cdot N_C^{\mathrm{MJ}}/N_D^{\mathrm{MJ}}$, with N_α^{MJ} being the estimated multijet contribution in region α. Along with the previously mentioned constraints, a single equation is obtained,

$$\frac{N_{\mathrm{A}}^{\mathrm{data}} - N_{\mathrm{A}}^{\mathrm{MC}} - N_{\mathrm{A}}^{\gamma}}{N_{\mathrm{B}}^{\mathrm{data}} - N_{\mathrm{B}}^{\mathrm{MC}} - f_{\mathrm{B}} N_{\mathrm{A}}^{\gamma}} = R_c \cdot \frac{N_{\mathrm{C}}^{\mathrm{data}} - N_{\mathrm{C}}^{\mathrm{MC}} - f_{\mathrm{C}} N_{\mathrm{A}}^{\gamma}}{N_{\mathrm{D}}^{\mathrm{data}} - N_{\mathrm{D}}^{\mathrm{MC}} - f_{\mathrm{D}} N_{\mathrm{A}}^{\gamma}}$$

where N_α^{data} and N_α^{MC} refer to the number of events in data and all signal and background MC samples excluding γ+jets and multijets events, respectively, in region α.

Due to lack of statistical precision, the ABCD method is performed inclusively in each of the analysis regions, resulting in total yields predictions for γ+jets and multijet background samples in region A. The fractions relative to data are summarised in Table 3, according to which in the SR, 0.1% of data consists of multijet background, and nearly 96% corresponds to prompt single photon production. Similar fractions for the real photons component are obtained for the CR and VR. This composition is indeed expected, as region A requires photons to satisfy the *Tight* requirements for both identification and isolation, aiming to ensure the presence of

Table 2 Input to the ABCD method in the form of the leakage coefficients f_B, f_C, f_D given in percentages and the correlation factor R_c, obtained from γ+jets and multijet MC samples, respectively, for the CR, VR, and SR. Statistical uncertainties are given

		CR	VR	SR
Leakage coefficients [%]	f_B	3.96 ± 0.32	2.83 ± 0.54	3.42 ± 0.27
	f_C	11.52 ± 0.52	9.3 ± 1.1	13.56 ± 0.61
	f_D	0.61 ± 0.13	0.67 ± 0.37	0.60 ± 0.10
Correlation factor R_c		1.18 ± 0.89	$4.3^{+5.1}_{-4.3}$	0.57 ± 0.38

Table 3 Background estimate results in the form of ABCD-estimated γ+jets and multijet contributions relative to data, for the CR, VR and SR. Statistical uncertainties are given

	CR	VR	SR
γ+jets fraction [%]	94.8 ± 1.6	91 ± 10	96.0 ± 1.2
Multijet fraction [%]	1.2 ± 1.1	$4.3^{+9.7}_{-4.3}$	$0.09^{+0.29}_{-0.09}$

prompt photons; those naturally exist at particle-level in the γ+jets sample, but are suppressed in the multijet sample.

Furthermore, the multijet sample shows significant statistical loss upon the application of the preselection criteria. To ensure a smooth distribution of the di-τ BDT score, all photon selections are omitted in this simulated sample, retaining only the di-τ p_{T} selection, while the expected multijet background yield is estimated from data events and not directly obtained from the MC sample. The di-τ BDT score distribution was compared for different photon selections applied, and found to only weakly depend on selections associated with the photon.

The ABCD-normalised di-τ BDT score distribution for the CR is shown in Fig. 9. A trend can be seen in the data-to-total prediction ratio, implying a mismodelling of the di-τ BDT in the γ+jets sample. Since the ABCD method does not have any impact on the shape, a reweighting approach was developed to correct for this mismodelling.

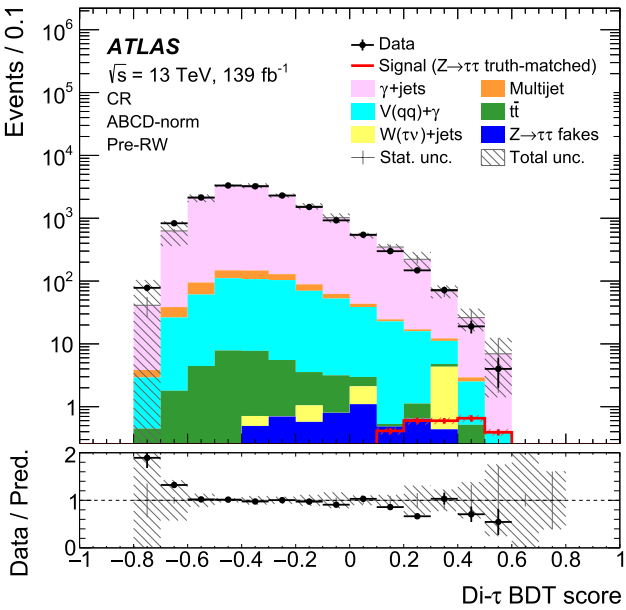

Fig. 9 Di-τ BDT score distribution with γ+jets and multijet yields ABCD-normalised in the CR, before event reweighting. Simulated events from $Z\gamma$, $Z\gamma\gamma$ and Z+jets, where $Z \to \tau\tau$, containing a reconstructed di-τ object geometrically matched to a particle-level $\tau^+\tau^-$ pair are referred to as Signal (red open histogram). The lower panel shows a bin-by-bin comparison of the data with the total predicted background and signal, in terms of event yield ratios. The uncertainty band corresponds to both the statistical and systematic uncertainties in the total SM prediction, detailed in Sect. 6.3. Error bars on the markers represent the statistical uncertainty in data

Event reweighting

The dominant background in the analysis is γ+jets, accounting for over 95% of pre-selected data events, and therefore is expected to resemble the distribution for data. However, as seen in Fig. 9, the di-τ BDT score distribution shape for γ+jets shows a discrepancy as compared with the data, and applying event reweighting can result in improved modelling. To mitigate a bias in the SF measurement arising from signal contribution in the reweighting process, a reweighting factor is derived from the BDT score distribution in the CR. The signal significance in the CR compared with the SR is smaller by factors of 22, 29, and 51 for the full BDT range, BDT $>$ 0.35 and BDT $>$ 0.5, respectively, such that biases due to signal contamination are not expected.

Furthermore, since the primary distinction between multijet and γ+jets processes is due to the presence of a prompt photon, and since both contain an energetic jet misidentified as a di-τ object, the event reweighting is applied to both of the samples. The reweighting factor, binned in BDT score values, is hence defined as $\left(N_{\mathrm{data}} - N_{\mathrm{MC\,bkg}}\right) / \left(N_\gamma + N_{\mathrm{MJ}}\right)$, where N_{data} is the number of events in the observed data, $N_{\mathrm{MC\,bkg}}$ refers to number of events in all MC background processes except for γ+jets and multijet, and N_γ, N_{MJ} refer to the ABCD-estimated yield for the γ+jets and multijet processes, respectively.

The reweighting function that is eventually employed is an analytical function that is fitted to the reweighting factor, and as such is applied as a BDT score-dependent event weight. Two criteria are considered for selecting the optimal function: the χ^2 test, evaluating the goodness of the fit in the CR, and the agreement between the data and the total prediction after reweighting in the VR. Various functions were tested on the VR, of which a fifth-order polynomial is chosen as the nominal reweighting function, while other functional forms are used to derive an associated uncertainty on the reweighting process. The pre-reweighting di-τ BDT score distribution in the VR is shown in Fig. 10a, with the corresponding post-reweighting distribution given in Fig. 10b. The latter shows the reweighting procedure impact on the VR – with the reweighting uncertainty included in the uncertainty band – increasing the total contribution from γ+jets and multijets samples by about 10% for the BDT > 0.2 domain.

The reweighting is then applied to events from γ+jets and multijet samples in the SR, modifying their contributions by about $+12$ and -1%, respectively, for the BDT > 0.2 domain. The pre- and post-reweighting BDT score distributions are shown in Fig. 10c-d, with ABCD-estimated yields given in Table 3. The event reweighting primarily affects the shape, showing negligible impact on the total normalisation of the background samples obtained through the ABCD method before reweighting, with a difference of less than 0.5%. Although designed to achieve better modelling for the background in the CR and VR, where the signal contribution is negligible, upon comparing the data-to-total prediction ratio in the SR, the declining trend vanishes with event reweighting. This correction effectively resolves the observed discrepancy, such that the total prediction and data are now within the full uncertainty band.

The reweighted di-τ BDT score distribution is used for computing the SF, as described in Sect. 6.4.

6.3 Systematic uncertainties

The systematic uncertainties that affect the SF measurements are divided into four categories: experimental uncertainties affecting the simulated background and signal processes, uncertainties derived from using different generators for γ+jets and multijet samples, uncertainties in the modelling of the reweighting factor, and theoretical uncertainties of the simulated background and signal samples. All systematic uncertainties are propagated through all the analysis chain, including the ABCD method (and particularly the leakage coefficients and correlation factor), being reprocessed independently for each systematic variation. Furthermore, fixing R_c to one to assess the impact of correlations in the ABCD method, results with background fractions differing by less than 0.1% in the SR, and hence a negligible effect on the SF. Uncertainties are added up in quadrature to express the total systematic uncertainty that corresponds to the SF, with the dominant sources listed in Table 4.

Experimental uncertainties address the luminosity determination and modelling of detector effects. The leading effects come from those associated with the modelling of pile-up interactions in simulation, photon energy scale and resolution, muon and $E_{\mathrm{T}}^{\mathrm{miss}}$ modelling, and di-τ detector modelling and energy-scale calibration. The largest contribution for the *Medium* WP stems from the pile-up reweighting due to the low statistical precision in the γ+jet sample in the corresponding BDT region.

The estimate of di-τ detector modelling and energy-scale calibration uncertainties uses four systematically varied $t\bar{t}X$ MC simulations. The di-τ reconstruction efficiency is parameterised in the particle-level di-τ p_{T} and ΔR_{vis}. The differences in efficiency of each of the varied samples to the nominal sample are summed in quadrature and are assigned as the di-τ detector modelling uncertainty, which are applied to truth-matched di-τ objects. The di-τ energy-scale uncertainty is parameterised in the calibrated di-τ p_{T}, ΔR(lead, sublead) and the subjet prongness. The calibrated subjet p_{T} distribution from the nominal sample is compared with the varied ones via a scaling parameter using a χ^2 test, and the relative uncertainty is taken as the value of the scaling parameter that minimises the χ^2 distribution. The contributions from the four different varied simulations are summed in quadrature to obtain the total uncertainty, which is applied as up and down variations on subjets p_{T} of truth-matched di-τ objects.

Different generators for the γ+jets and multijet samples are used to estimate the parton-shower and hadronisation uncertainties. The choice for the nominal generators is SHERPA 2.2.2 for γ+jets and POWHEG+PYTHIA for multijet. Two varied combinations are obtained using the nominal generator for one of the samples together with either PYTHIA for γ+jets or POWHEG+HERWIG for multijet. These variations are particularly important in the determination of uncertainties in the simulation-derived correlation factor and leakage coefficients, used to obtain the background normalisation. In both of the combinations, background events are reweighted using a dedicated fifth-order polynomial function obtained from the di-τ BDT distribution in their CR. The uncertainty considers the largest deviation from the nominal value.

To account for small variations in the SF derived from different choices of the fitting function, a corresponding uncertainty is introduced. This uncertainty considers alternative reweighting functions, chosen for their similarity to the nominal function in terms of the reduced χ^2 goodness-of-fit parameter. Specifically, a quartic polynomial and a sum of two tangent functions are selected. The uncertainty is determined as the largest deviation from the nominal value.

Uncertainties in the calculation of the cross-sections for the different processes are considered. Following the rec-

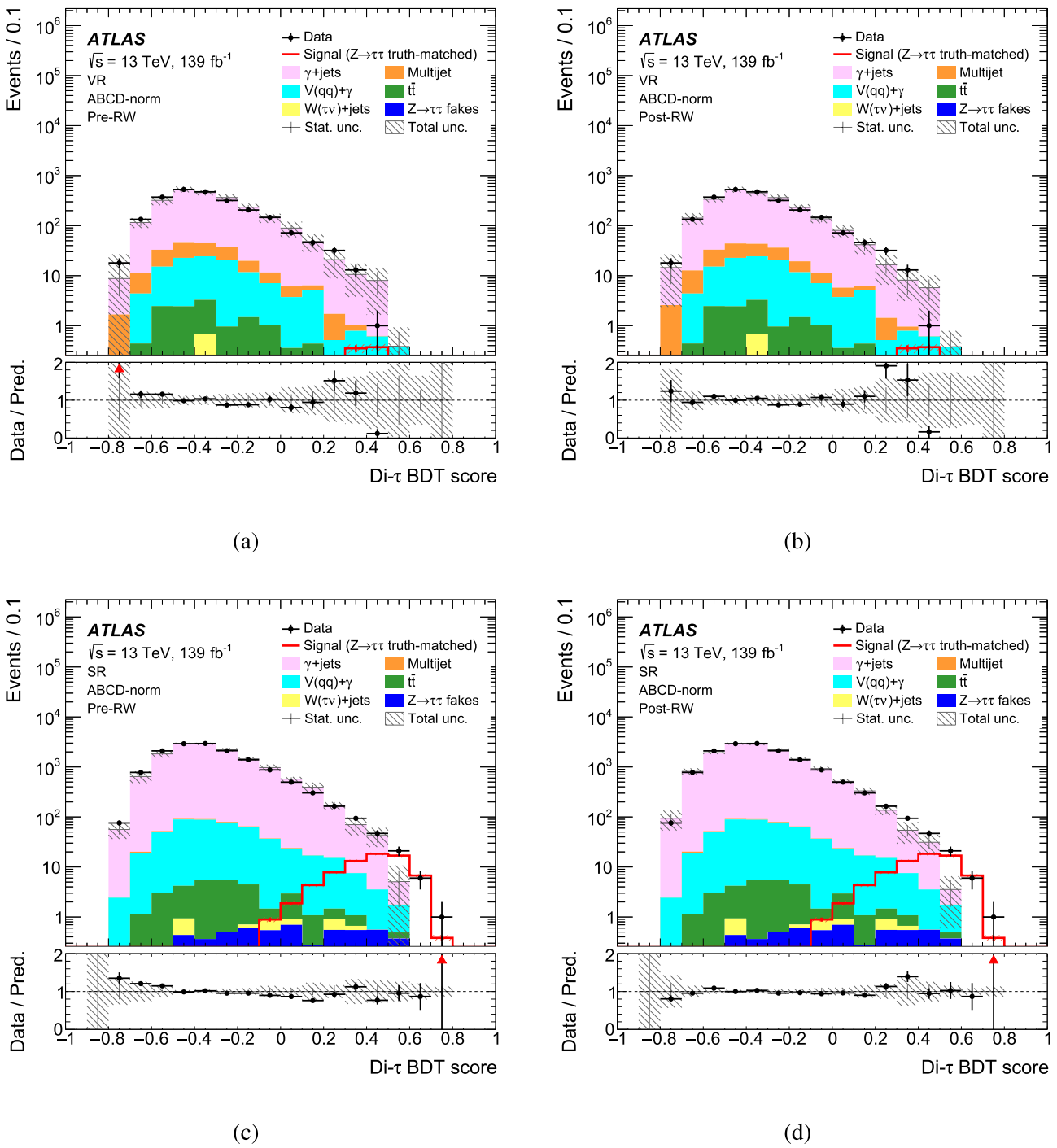

Fig. 10 Di-τ BDT score distributions with γ+jets and multijet yields ABCD-normalised in the VR **a** before and **b** after event reweighting, and in the SR **c** before and **d** after event reweighting. Simulated events from $Z\gamma$, $Z\gamma\gamma$ and Z+jets, where $Z \to \tau\tau$, containing a reconstructed di-τ object geometrically matched to a particle-level $\tau^+\tau^-$ pair are referred to as Signal (red open histogram). The lower panel shows a bin-by-bin comparison of the data with the total predicted background and signal, in terms of event yield ratios. Vertical arrows indicate points that lie outside the displayed axis range. The uncertainty band corresponds to both the statistical and systematic uncertainties in the total SM prediction, detailed in Sect. 6.3. Error bars on the markers represent the statistical uncertainty in data

Table 4 Summary of the dominant systematic uncertainties in the SF. The uncertainties are expressed as percentages relative to the nominal SF. Only uncertainties exceeding 1% are shown

Category	Source	Relative uncertainty [%]	
		Medium	Tight
Statistical	Data	21	22
	MC	28	8.3
	Total	35	23
Modelling	Theory	6.4	5.6
	Reweighting	3.7	4.1
	Generators	3.1	9.3
	Total	8.0	12
Experimental	Integrated luminosity	1.6	1.6
	Photon energy scale	4.0	–
	Photon energy resolution	2.8	–
	$E_{\mathrm{T}}^{\mathrm{miss}}$ resolution	1.0	–
	Muon sagitta evaluation	–	1.1
	Pile-up reweighting	8.7	2.0
	Di-τ detector modelling	1.9	1.2
	Di-τ calibration	1.9	1.7
	Total	9.9	3.6
Total uncertainty		37	26

Table 5 Total yields for all relevant samples that are required for the SF calculation: BDT inclusive yields, followed by *Medium* (BDT $>$ 0.35) and *Tight* (BDT $>$ 0.5) WP yields with the corresponding BDT efficiencies. 'MC background' refers to background events from all MC samples excluding γ+jets and multijet samples. 'MC signal' refers to simulated events from $Z\gamma$, $Z\gamma\gamma$ and Z+jets, where $Z \to \tau\tau$, containing a truth-matched reconstructed di-τ object. Events from both the γ+jets and multijet samples are ABCD-normalised and reweighted. Total uncertainties are given

Sample	BDT inclusive	Medium		Tight	
		Yield	Efficiency [%]	Yield	Efficiency [%]
MC signal	71.0 ± 3.3	49.7 ± 3.0	70.0 ± 4.2	24.0 ± 1.4	33.8 ± 2.0
MC background	496 ± 23	7.8 ± 1.2	1.57 ± 0.24	1.94 ± 0.63	0.39 ± 0.13
γ+jets	13750 ± 370	52 ± 15	0.38 ± 0.11	1.8 ± 3.2	0.01 ± 0.02
Multijet	13^{+130}_{-13}	$0.03^{+0.38}_{-0.03}$	$0.3^{+3.0}_{-0.3}$	< 0.01	< 0.01
Total predicted	14330 ± 390	110 ± 15	0.77 ± 0.11	27.8 ± 3.6	0.19 ± 0.02
Data	14330	110	0.77	28	0.20

ommendations given in Ref. [74], a 5% total theoretical uncertainty for the estimate of the expected event yields is assigned for all MC samples from which the normalisation is utilised, which accounts for the uncertainties arising from the choice of renormalisation and factorisation scales and the PDF choice. For the γ+jets sample, scale uncertainties are used instead, and evaluated by varying the renormalisation and factorisation scales, μ_{R} and μ_{F}, independently by factors of two and one-half, removing combinations where the variations differ by a factor of four.

6.4 Results

The di-τ identification efficiency SF is computed in the SR as the ratio of observed to expected signal efficiencies, for a specified di-τ BDT score selection. As the ABCD method fixes the total expected yield to data, the definition is reduced to a ratio of event yields. Since the predicted BDT inclusive signal purity is less than 1%, its impact on the ABCD-estimated background normalisation and therefore on the SF is negligible. The measured signal yield is obtained after subtracting the backgrounds with a misidentified di-τ object from the data:

$$\mathrm{SF} = \frac{N_{\mathrm{data}} - N_{\text{non-di-}\tau}}{N_{\text{true di}-\tau}}. \quad (1)$$

The yields for data, background and signal samples are obtained by applying the desired di-τ BDT score selection in the corresponding distribution (Fig. 10), and are given in Table 5. The resultant signal identification efficiency is

approximately 70% (34%) at background rejection rate of approximately 240 (3600) for the *Medium* (*Tight*) WP. These efficiencies differ from those estimated using the BDT training samples, shown in Fig. 7, indicating that the identification efficiency depends on the kinematic phase space in which the measurement is performed.

The SF is calculated for *Medium* and *Tight* BDT-based di-τ identification requirements, for which BDT score > 0.35 and > 0.5 selections are chosen, respectively. Being a statistically-limited study, an inclusive SF is obtained. From Eq. (1), using the total yields given in Table 5, the SFs are finally obtained:

$$\begin{aligned}\text{SF}\,(\text{BDT} > 0.35) &= 1.00 \pm 0.35\,(\text{stat.}) \pm 0.13\,(\text{syst.}) \\ &= 1.00 \pm 0.37\,(\text{tot.})\,,\end{aligned}$$

and

$$\begin{aligned}\text{SF}\,(\text{BDT} > 0.5) &= 1.01 \pm 0.24\,(\text{stat.}) \pm 0.12\,(\text{syst.}) \\ &= 1.01 \pm 0.27\,(\text{tot.})\,.\end{aligned}$$

The total relative uncertainty is about 37% (26%) for the *Medium* (*Tight*) WP. The SFs are found to be compatible with 1, well within the associated uncertainties. Notably, the statistical uncertainty for the *Medium* WP is larger than for the *Tight* WP. This counterintuitive behaviour is due to the larger absolute uncertainty of the background component relative to the difference between the number of data events and background events in the *Medium* WP, which is roughly three times larger than in the *Tight* WP.

The corresponding SF will be applied as an event weight to simulated events containing a di-τ object geometrically matched to a $\tau^{+}_{\text{had}}\tau^{-}_{\text{had}}$ pair at particle-level, in future ATLAS studies utilising this tagger. In analyses targeting a different phase space compared with this measurement, additional uncertainties may be required – likely in the form of an extrapolation uncertainty in one or more kinematic features of the di-τ object.

7 Conclusions

A tagging algorithm for hadronically decaying Lorentz-boosted di-τ systems originating from decays of low-mass particles with p_{T} smaller than 300 GeV is presented. The identification algorithm applies a BDT using features of the di-τ object reconstructed based on tracking and calorimeter information from the ATLAS detector at the Large Hadron Collider. A measurement of the identification efficiency was performed with $Z\gamma$ events using proton–proton collision data at $\sqrt{s} = 13$ TeV recorded with the ATLAS detector between 2015 and 2018, corresponding to an integrated luminosity of 139 fb^{-1}. Two BDT-based di-τ identification criteria, *Medium* and *Tight*, were defined, corresponding to estimated signal efficiencies of approximately 70 and 34%, with measured background rejection rates of approximately 240 and 3600, respectively. The measured identification scale factors are 1.00 ± 0.37 (tot.) and 1.01 ± 0.27 (tot.), respectively, demonstrating good data-to-simulation agreement for the di-τ object modelling. This novel measurement allows using the tagger as an alternative to the standard ATLAS $\tau_{\text{had-vis}}$ reconstruction. Physics analyses may combine both methods to reject fake di-τ background, improving search sensitivities at p_{T} values characteristic of the kinematic phase space relevant to light resonance searches.

Acknowledgements We thank CERN for the very successful operation of the LHC and its injectors, as well as the support staff at CERN and at our institutions worldwide without whom ATLAS could not be operated efficiently. The crucial computing support from all WLCG partners is acknowledged gratefully, in particular from CERN, the ATLAS Tier-1 facilities at TRIUMF/SFU (Canada), NDGF (Denmark, Norway, Sweden), CC-IN2P3 (France), KIT/GridKA (Germany), INFN-CNAF (Italy), NL-T1 (Netherlands), PIC (Spain), RAL (UK) and BNL (USA), the Tier-2 facilities worldwide and large non-WLCG resource providers. Major contributors of computing resources are listed in Ref. [76]. We gratefully acknowledge the support of ANPCyT, Argentina; YerPhI, Armenia; ARC, Australia; BMWFW and FWF, Austria; ANAS, Azerbaijan; CNPq and FAPESP, Brazil; NSERC, NRC and CFI, Canada; CERN; ANID, Chile; CAS, MOST and NSFC, China; Minciencias, Colombia; MEYS CR, Czech Republic; DNRF and DNSRC, Denmark; IN2P3-CNRS and CEA-DRF/IRFU, France; SRNSFG, Georgia; BMBF, HGF and MPG, Germany; GSRI, Greece; RGC and Hong Kong SAR, China; ISF and Benoziyo Center, Israel; INFN, Italy; MEXT and JSPS, Japan; CNRST, Morocco; NWO, Netherlands; RCN, Norway; MNiSW, Poland; FCT, Portugal; MNE/IFA, Romania; MSTDI, Serbia; MSSR, Slovakia; ARIS and MVZI, Slovenia; DSI/NRF, South Africa; MICIU/AEI, Spain; SRC and Wallenberg Foundation, Sweden; SERI, SNSF and Cantons of Bern and Geneva, Switzerland; NSTC, Taipei; TENMAK, Türkiye; STFC/UKRI, United Kingdom; DOE and NSF, United States of America. Individual groups and members have received support from BCKDF, CANARIE, CRC and DRAC, Canada; CERN-CZ, FORTE and PRIMUS, Czech Republic; COST, ERC, ERDF, Horizon 2020, ICSC-NextGenerationEU and Marie Skłodowska-Curie Actions, European Union; Investissements d'Avenir Labex, Investissements d'Avenir Idex and ANR, France; DFG and AvH Foundation, Germany; Herakleitos, Thales and Aristeia programmes co-financed by EU-ESF and the Greek NSRF, Greece; BSF-NSF and MINERVA, Israel; NCN and NAWA, Poland; La Caixa Banking Foundation, CERCA Programme Generalitat de Catalunya and PROMETEO and GenT Programmes Generalitat Valenciana, Spain; Göran Gustafssons Stiftelse, Sweden; The Royal Society and Leverhulme Trust, United Kingdom. In addition, individual members wish to acknowledge support from Armenia: Yerevan Physics Institute (FAPERJ); CERN: European Organization for Nuclear Research (CERN PJAS); Chile: Agencia Nacional de Investigación y Desarrollo (FONDECYT 1230812, FONDECYT 1230987, FONDECYT 1240864); China: Chinese Ministry of Science and Technology (MOST-2023YFA1605700, MOST-2023YFA1609300), National Natural Science Foundation of China (NSFC - 12175119, NSFC 12275265, NSFC-12075060); Czech Republic: Czech Science Foundation (GACR - 24-11373 S), Ministry of Education Youth and Sports (FORTE CZ.02.01.01/00/22_008/0004632), PRIMUS Research Programme (PRIMUS/21/SCI/017); EU: H2020 European Research Council (ERC - 101002463); European Union: European Research Council (ERC - 948254, ERC 101089007), Horizon 2020 Framework Programme (MUCCA - CHIST-ERA-19-XAI-00), European Union, Future Artificial Intelligence Research (FAIR-

NextGenerationEU PE00000013), Italian Center for High Performance Computing, Big Data and Quantum Computing (ICSC, NextGenerationEU); France: Agence Nationale de la Recherche (ANR-20-CE31-0013, ANR-21-CE31-0013, ANR-21-CE31-0022, ANR-22-EDIR-0002), Investissements d'Avenir Labex (ANR-11-LABX-0012); Germany: Baden-Württemberg Stiftung (BW Stiftung-Postdoc Eliteprogramme), Deutsche Forschungsgemeinschaft (DFG - 469666862, DFG - CR 312/5-2); Italy: Istituto Nazionale di Fisica Nucleare (ICSC, NextGenerationEU), Ministero dell'Università e della Ricerca (PRIN - 20223N7F8K - PNRR M4.C2.1.1); Japan: Japan Society for the Promotion of Science (JSPS KAKENHI JP22H01227, JSPS KAKENHI JP22H04944, JSPS KAKENHI JP22KK0227, JSPS KAKENHI JP23KK0245); Netherlands: Netherlands Organisation for Scientific Research (NWO Veni 2020 - VI.Veni.202.179); Norway: Research Council of Norway (RCN-314472); Poland: Ministry of Science and Higher Education (IDUB AGH, POB8, D4 no 9722), Polish National Agency for Academic Exchange (PPN/PPO/2020/1/00002/U/00001), Polish National Science Centre (NCN 2021/42/E/ST2/00350, NCN OPUS 2023/51/B/ST2/02507, NCN OPUS nr 2022/47/B/ST2/03059, NCN UMO-2019/34/E/ST2/00393, NCN & H2020 MSCA 945339, UMO-2020/37/B/ST2/01043, UMO-2021/40/C/ST2/00187, UMO-2022/47/O/ST2/00148, UMO-2023/49/B/ST2/04085, UMO-2023/51/B/ST2/00920); Slovenia: Slovenian Research Agency (ARIS grant J1-3010); Spain: Generalitat Valenciana (Artemisa, FEDER, IDIFEDER/2018/048), Ministry of Science and Innovation (MCIN & NextGenEU PCI2022-135018-2, MICIN & FEDER PID2021-125273NB, RYC2019-028510-I, RYC2020-030254-I, RYC2021-031273-I, RYC2022-038164-I); Sweden: Carl Trygger Foundation (Carl Trygger Foundation CTS 22:2312), Swedish Research Council (Swedish Research Council 2023-04654, VR 2018-00482, VR 2021-03651, VR 2022-03845, VR 2022-04683, VR 2023-03403), Knut and Alice Wallenberg Foundation (KAW 2018.0458, KAW 2019.0447, KAW 2022.0358); Switzerland: Swiss National Science Foundation (SNSF - PCEFP2_194658); United Kingdom: Leverhulme Trust (Leverhulme Trust RPG-2020-004), Royal Society (NIF-R1-231091); United States of America: U.S. Department of Energy (ECA DE-AC02-76SF00515), Neubauer Family Foundation.

Data Availability Statement This manuscript has no associated data. [Authors' comment: Data sharing not applicable to this article as no datasets were generated or analysed during the current study.]

Code Availability Statement This manuscript has no associated code/software. [Authors' comment: Code/Software sharing not applicable to this article as no code/software was generated or analysed during the current study.]

Funded by SCOAP[3].

References

1. Particle Data Group, S. Navas et al., Review of particle physics. Phys. Rev. D **110**, 030001 (2024)
2. ATLAS Collaboration, Reconstruction, identification, and calibration of hadronically decaying tau leptons with the ATLAS detector for the LHC Run 3 and reprocessed Run 2 data. ATL-PHYS-PUB-2022-044, 2022. https://cds.cern.ch/record/2827111
3. ATLAS Collaboration, The ATLAS Experiment at the CERN large hadron collider. JINST **3**, S08003 (2008)
4. M. Cacciari, G.P. Salam, G. Soyez, The anti-k_t jet clustering algorithm. JHEP **04**, 063 (2008). arXiv:0802.1189 [hep-ph]
5. M. Cacciari, G.P. Salam, G. Soyez, FastJet user manual. Eur. Phys. J. C **72**, 1896 (2012). arXiv:1111.6097 [hep-ph]
6. ATLAS Collaboration, Topological cell clustering in the ATLAS calorimeters and its performance in LHC Run 1. Eur. Phys. J. C **77**, 490 (2017). arXiv:1603.02934 [hep-ex]
7. ATLAS Collaboration, Reconstruction and identification of boosted di-τ systems in a search for Higgs boson pairs using 13 TeV proton.proton collision data in ATLAS. JHEP **11**, 163 (2020). arXiv:2007.14811 [hep-ex]
8. M. Mühlleitner, M.O.P. Sampaio, R. Santos, J. Wittbrodt, Phenomenological comparison of models with extended Higgs sectors. JHEP **08**, 132 (2017). arXiv:1703.07750 [hep-ph]
9. M. Casolino, T. Farooque, A. Juste, T. Liu, M. Spannowsky, Probing a light CP-odd scalar in di-top-associated production at the LHC. Eur. Phys. J. C **75**, 498 (2015). arXiv:1507.07004 [hep-ph]
10. W.-F. Chang, T. Modak, J.N. Ng, Signal for a light singlet scalar at the LHC. Phys. Rev. D **97**, 055020 (2018). arXiv:1711.05722 [hep-ph]
11. S. Chang, R. Dermisek, J.F. Gunion, N. Weiner, Nonstandard Higgs boson decays. Annu. Rev. Nucl. Part. Sci. **58**, 75 (2008). arXiv:0801.4554 [hep-ph]
12. V. Silveira, A. Zee, Scalar phantoms. Phys. Lett. B **161**, 136 (1985)
13. S. Profumo, M.J. Ramsey-Musolf, G. Shaughnessy, Singlet Higgs phenomenology and the electroweak phase transition. JHEP **08**, 010 (2007). arXiv:0705.2425 [hep-ph]
14. S. Ipek, D. McKeen, A.E. Nelson, Renormalizable model for the galactic center gamma-ray excess from dark matter annihilation. Phys. Rev. D **90**, 055021 (2014). arXiv:1404.3716 [hep-ph]
15. N. Blinov, J. Kozaczuk, D.E. Morrissey, C. Tamarit, Electroweak baryogenesis from exotic electroweak symmetry breaking. Phys. Rev. D **92**, 035012 (2015). arXiv:1504.05195 [hep-ph]
16. N. Craig, A. Katz, M. Strassler, R. Sundrum, Naturalness in the dark at the LHC. JHEP **07**, 105 (2015). arXiv:1501.05310 [hep-ph]
17. M. Bauer, M. Neubert, A. Thamm, Collider probes of axion-like particles. JHEP **12**, 044 (2017). arXiv:1708.00443 [hep-ph]
18. R. Dermíšek, J.F. Gunion, Escaping the large fine-tuning and little hierarchy problems in the next to minimal supersymmetric model and $h \to aa$ decays. Phys. Rev. Lett. 95 (2005). arXiv:hep-ph/0502105
19. D. Curtin, C.B. Verhaaren, Discovering uncolored naturalness in exotic Higgs decays. JHEP **12**, 072 (2015). arXiv:1506.06141 [hep-ph]
20. ATLAS Collaboration, Improved reconstruction of highly boosted τ-lepton pairs in the $\tau\tau \to (\mu\nu_\mu\nu_\tau)(\text{hadrons} + \nu_\tau)$ decay channels with the ATLAS detector. (2024). arXiv:2412.14937 [hep-ex]
21. ATLAS Collaboration, ATLAS insertable b-layer: technical design report. ATLAS-TDR-19; CERN-LHCC-2010-013, 2010. https://cds.cern.ch/record/1291633. Addendum: ATLAS-TDR-19-ADD-1; CERN-LHCC-2012-009, 2012. https://cds.cern.ch/record/1451888
22. B. Abbott et al., Production and integration of the ATLAS insertable B-layer. JINST **13**, T05008 (2018). arXiv:1803.00844 [physics.ins-det]

23. G. Avoni et al., The new LUCID-2 detector for luminosity measurement and monitoring in ATLAS. JINST **13**, P07017 (2018)
24. ATLAS Collaboration, Performance of the ATLAS trigger system in 2015. Eur. Phys. J. C **77**, 317 (2017). arXiv:1611.09661 [hep-ex]
25. ATLAS Collaboration, Software and computing for Run 3 of the ATLAS experiment at the LHC. (2024). arXiv:2404.06335 [hep-ex]
26. ATLAS Collaboration, Luminosity determination in pp collisions at $\sqrt{s} = 13$ TeV using the ATLAS detector at the LHC. ATLAS-CONF-2019-021, 2019. https://cds.cern.ch/record/2677054
27. ATLAS Collaboration, ATLAS data quality operations and performance for 2015–2018 data-taking. JINST **15**, P04003 (2020). arXiv:1911.04632 [physics.ins-det]
28. G.C. Branco et al., Theory and phenomenology of two-Higgs-doublet models. Phys. Rep. **516**, 1 (2012). arXiv:1106.0034 [hep-ph]
29. J. Alwall et al., The automated computation of tree-level and next-to-leading order differential cross sections, and their matching to parton shower simulations. JHEP **07**, 079 (2014). arXiv:1405.0301 [hep-ph]
30. NNPDF Collaboration, R.D. Ball et al., Parton distributions with LHC data. Nucl. Phys. B **867**, 244 (2013). arXiv:1207.1303 [hep-ph]
31. T. Sjöstrand et al., An introduction to PYTHIA 8.2. Comput. Phys. Commun. **191**, 159 (2015). arXiv:1410.3012 [hep-ph]
32. ATLAS Collaboration, ATLAS Pythia 8 tunes to 7 TeV data. ATL-PHYS-PUB-2014-021, 2014. https://cds.cern.ch/record/1966419
33. S. Frixione, G. Ridolfi, P. Nason, A positive-weight next-to-leading-order Monte Carlo for heavy flavour hadroproduction. JHEP **09**, 126 (2007). arXiv:0707.3088 [hep-ph]
34. P. Nason, A new method for combining NLO QCD with shower Monte Carlo algorithms. JHEP **11**, 040 (2004). arXiv:hep-ph/0409146
35. S. Frixione, P. Nason, C. Oleari, Matching NLO QCD computations with parton shower simulations: the POWHEG method. JHEP **11**, 070 (2007). arXiv:0709.2092 [hep-ph]
36. S. Alioli, P. Nason, C. Oleari, E. Re, A general framework for implementing NLO calculations in shower Monte Carlo programs: the POWHEG BOX. JHEP **06**, 043 (2010). arXiv:1002.2581 [hep-ph]
37. NNPDF Collaboration, R.D. Ball et al., Parton distributions for the LHC run II. JHEP **04**, 040 (2015). arXiv:1410.8849 [hep-ph]
38. ATLAS Collaboration, Studies on top-quark Monte Carlo modelling for Top2016. ATL-PHYS-PUB-2016-020, 2016. https://cds.cern.ch/record/2216168
39. D.J. Lange, The EvtGen particle decay simulation package. Nucl. Instrum. Methods A **462**, 152 (2001)
40. E. Bothmann et al., Event generation with Sherpa 2.2. SciPost Phys. **7**, 034 (2019). arXiv:1905.09127 [hep-ph]
41. T. Gleisberg, S. Höche, Comix, a new matrix element generator. JHEP **12**, 039 (2008). arXiv:0808.3674 [hep-ph]
42. F. Buccioni et al., OpenLoops 2. Eur. Phys. J. C **79**, 866 (2019). arXiv:1907.13071 [hep-ph]
43. F. Cascioli, P. Maierhöfer, S. Pozzorini, Scattering amplitudes with open loops. Phys. Rev. Lett. **108**, 111601 (2012). arXiv:1111.5206 [hep-ph]
44. A. Denner, S. Dittmaier, L. Hofer, Collier: a Fortran-based complex one-loop library in extended regularizations. Comput. Phys. Commun. **212**, 220 (2017). arXiv:1604.06792 [hep-ph]
45. S. Schumann, F. Krauss, A parton shower algorithm based on Catani–Seymour dipole factorisation. JHEP **03**, 038 (2008). arXiv:0709.1027 [hep-ph]
46. S. Höche, F. Krauss, M. Schönherr, F. Siegert, A critical appraisal of NLO+PS matching methods. JHEP **09**, 049 (2012). arXiv:1111.1220 [hep-ph]
47. S. Höche, F. Krauss, M. Schönherr, F. Siegert, QCD matrix elements + parton showers. The NLO case. JHEP **04**, 027 (2013). arXiv:1207.5030 [hep-ph]
48. S. Catani, F. Krauss, B.R. Webber, R. Kuhn, QCD matrix elements + parton showers. JHEP **11**, 063 (2001). arXiv:hep-ph/0109231
49. S. Höche, F. Krauss, S. Schumann, F. Siegert, QCD matrix elements and truncated showers. JHEP **05**, 053 (2009). arXiv:0903.1219 [hep-ph]
50. F. Siegert, A practical guide to event generation for prompt photon production with Sherpa. J. Phys. G **44**, 044007 (2017). arXiv:1611.07226 [hep-ph]
51. S. Frixione, Isolated photons in perturbative QCD. Phys. Lett. B **429**, 369 (1998). arXiv:hep-ph/9801442
52. J. Bellm et al., Herwig 7.0/Herwig++ 3.0 release note. Eur. Phys. J. C **76**, 196 (2016). arXiv:1512.01178 [hep-ph]
53. H.-L. Lai et al., New parton distributions for collider physics. Phys. Rev. D **82**, 074024 (2010). arXiv:1007.2241 [hep-ph]
54. C. Anastasiou, L. Dixon, K. Melnikov, F. Petriello, High-precision QCD at hadron colliders: electroweak gauge boson rapidity distributions at next-to-next-to leading order. Phys. Rev. D **69**, 094008 (2004). arXiv:hep-ph/0312266
55. ATLAS Collaboration, The Pythia 8 A3 tune description of ATLAS minimum bias and inelastic measurements incorporating the Donnachie–Landshoff diffractive model. ATL-PHYS-PUB-2016-017, 2016. https://cds.cern.ch/record/2206965
56. ATLAS Collaboration, Electron and photon performance measurements with the ATLAS detector using the 2015–2017 LHC proton–proton collision data. JINST **14**, P12006 (2019). arXiv:1908.00005 [hep-ex]
57. ATLAS Collaboration, Electron and photon efficiencies in LHC Run 2 with the ATLAS experiment. JHEP **05**, 162 (2024). arXiv:2308.13362 [hep-ex]
58. ATLAS Collaboration, Electron and photon energy calibration with the ATLAS detector using LHC Run 2 data. JINST **19**, P02009 (2024). arXiv:2309.05471 [hep-ex]
59. ATLAS Collaboration, Muon reconstruction and identification efficiency in ATLAS using the full Run 2 pp collision data set at $\sqrt{s} = 13$ TeV. Eur. Phys. J. C **81**, 578 (2021). arXiv:2012.00578 [hep-ex]
60. ATLAS Collaboration, Jet reconstruction and performance using particle flow with the ATLAS detector. Eur. Phys. J. C **77**, 466 (2017). arXiv:1703.10485 [hep-ex]
61. ATLAS Collaboration, Jet energy scale and resolution measured in proton–proton collisions at $\sqrt{s} = 13$ TeV with the ATLAS detector. Eur. Phys. J. C **81**, 689 (2021). arXiv:2007.02645 [hep-ex]
62. ATLAS Collaboration, Performance of pile-up mitigation techniques for jets in pp collisions at $\sqrt{s} = 8$ TeV using the ATLAS detector. Eur. Phys. J. C **76**, 581 (2016). arXiv:1510.03823 [hep-ex]
63. ATLAS Collaboration, The performance of missing transverse momentum reconstruction and its significance with the ATLAS detector using 140 fb^{-1} of $\sqrt{s} = 13$ TeV pp collisions. (2024). arXiv:2402.05858 [hep-ex]
64. ATLAS Collaboration, Search for Higgs boson decays into two new low-mass spin-0 particles in the $4b$ channel with the ATLAS detector using pp collisions at $\sqrt{s} = 13$ TeV. Phys. Rev. D **102**, 112006 (2020). arXiv:2005.12236 [hep-ex]
65. C.M.S. Collaboration, Search for a light pseudoscalar Higgs boson in the boosted $\mu\mu\tau\tau$ final state in proton–proton collisions at $\sqrt{s} = 13$ TeV. JHEP **08**, 139 (2020). arXiv:2005.08694 [hep-ex]
66. ATLAS Collaboration, Search for Higgs boson decays into a pair of pseudoscalar particles in the $bb\mu\mu$ final state with the ATLAS detector in pp collisions at $\sqrt{s}$=13 TeV. Phys. Rev. D **105**, 012006 (2022). arXiv:2110.00313 [hep-ex]

67. ATLAS Collaboration, Identification and energy calibration of hadronically decaying tau leptons with the ATLAS experiment in pp collisions at $\sqrt{s} = 8$ TeV. Eur. Phys. J. C **75**, 303 (2015). arXiv:1412.7086 [hep-ex]
68. ATLAS Collaboration, Reconstruction, energy calibration, and identification of hadronically decaying tau leptons in the ATLAS Experiment for Run-2 of the LHC. ATL-PHYS-PUB-2015-045, 2015. https://cds.cern.ch/record/2064383
69. L. Breiman, J. Friedman, R.A. Olshen, C.J. Stone, Classification and Regression Trees (Chapman and Hall/CRC, 2017). isbn: 978-1-315-13947-0, 978-0-412-04841-8
70. Y. Freund, R.E. Schapire, Experiments with a new boosting algorithm. in International Conference on Machine Learning, 1996. https://api.semanticscholar.org/CorpusID:1836349
71. Y. Freund, R.E. Schapire, A decision-theoretic generalization of on-line learning and an application to boosting. J. Comput. Syst. Sci. **55**, 119 (1997)
72. ATLAS Collaboration, Performance of electron and photon triggers in ATLAS during LHC Run 2. Eur. Phys. J. C **80**, 47 (2020). arXiv:1909.00761 [hep-ex]
73. ATLAS Collaboration, Measurement of the cross section for isolated-photon plus jet production in pp collisions at $\sqrt{s} = 13$ TeV using the ATLAS detector. Phys. Lett. B **780**, 578 (2018). arXiv:1801.00112 [hep-ex]
74. ATLAS Collaboration, Measurement of $W^{\pm}$ and Z boson production cross sections in pp collisions at $\sqrt{s} = 13$ TeV with the ATLAS detector. ATLAS-CONF-2015-039, 2015. https://cds.cern.ch/record/2045487
75. ATLAS Collaboration, Measurement of the inclusive isolated prompt photons cross section in pp collisions at $\sqrt{s} = 7$ TeV with the ATLAS detector using 4.6 fb^{-1}. Phys. Rev. D **89**, 052004 (2014). arXiv:1311.1440 [hep-ex]
76. ATLAS Collaboration, ATLAS computing acknowledgements. ATL-SOFT-PUB-2025-001, 2025. https://cds.cern.ch/record/2922210

ATLAS Collaboration*

G. Aad[105], E. Aakvaag[17], B. Abbott[124], S. Abdelhameed[120a], K. Abeling[57], N. J. Abicht[51], S. H. Abidi[30], M. Aboelela[46], A. Aboulhorma[36e], H. Abramowicz[156], H. Abreu[155], Y. Abulaiti[121], B. S. Acharya[71a,71b,l], A. Ackermann[65a], C. Adam Bourdarios[4], L. Adamczyk[88a], S. V. Addepalli[148], M. J. Addison[104], J. Adelman[119], A. Adiguzel[22c], T. Adye[138], A. A. Affolder[140], Y. Afik[41], M. N. Agaras[13], A. Aggarwal[103], C. Agheorghiesei[28c], F. Ahmadov[40,aa], S. Ahuja[98], X. Ai[64e], G. Aielli[78a,78b], A. Aikot[168], M. Ait Tamlihat[36e], B. Aitbenchikh[36a], M. Akbiyik[103], T. P. A. Åkesson[101], A. V. Akimov[150], D. Akiyama[173], N. N. Akolkar[25], S. Aktas[22a], K. Al Khoury[43], G. L. Alberghi[24b], J. Albert[170], P. Albicocco[55], G. L. Albouy[62], S. Alderweireldt[54], Z. L. Alegria[125], M. Aleksa[37], I. N. Aleksandrov[40], C. Alexa[28b], T. Alexopoulos[10], F. Alfonsi[24b], M. Algren[58], M. Alhroob[172], B. Ali[136], H. M. J. Ali[94,t], S. Ali[32], S. W. Alibocus[95], M. Aliev[34c], G. Alimonti[73a], W. Alkakhi[57], C. Allaire[68], B. M. M. Allbrooke[151], J. S. Allen[104], J. F. Allen[54], C. A. Allendes Flores[141f], P. P. Allport[21], A. Aloisio[74a,74b], F. Alonso[93], C. Alpigiani[143], Z. M. K. Alsolami[94], M. Alvarez Estevez[102], A. Alvarez Fernandez[103], M. Alves Cardoso[58], M. G. Alviggi[74a,74b], M. Aly[104], Y. Amaral Coutinho[85b], A. Ambler[107], C. Amelung[37], M. Amerl[104], C. G. Ames[112], D. Amidei[109], B. Amini[56], K. Amirie[159], S. P. Amor Dos Santos[134a], K. R. Amos[168], D. Amperiadou[157], S. An[86], V. Ananiev[129], C. Anastopoulos[144], T. Andeen[11], J. K. Anders[37], A. C. Anderson[61], S. Y. Andrean[49a,49b], A. Andreazza[73a,73b], S. Angelidakis[9], A. Angerami[43], A. V. Anisenkov[38], A. Annovi[76a], C. Antel[58], E. Antipov[150], M. Antonelli[55], F. Anulli[77a], M. Aoki[86], T. Aoki[158], M. A. Aparo[151], L. Aperio Bella[50], C. Appelt[156], A. Apyan[27], S. J. Arbiol Val[89], C. Arcangeletti[55], A. T. H. Arce[53], J.-F. Arguin[111], S. Argyropoulos[157], J.-H. Arling[50], O. Arnaez[4], H. Arnold[150], G. Artoni[77a,77b], H. Asada[114], K. Asai[122], S. Asai[158], N. A. Asbah[37], R. A. Ashby Pickering[172], K. Assamagan[30], R. Astalos[29a], K. S. V. Astrand[101], S. Atashi[163], R. J. Atkin[34a], H. Atmani[36f], P. A. Atmasiddha[132], K. Augsten[136], A. D. Auriol[21], V. A. Austrup[104], G. Avolio[37], K. Axiotis[58], G. Azuelos[111,ae], D. Babal[29b], H. Bachacou[139], K. Bachas[157,p], A. Bachiu[35], E. Bachmann[52], A. Badea[41], T. M. Baer[109], P. Bagnaia[77a,77b], M. Bahmani[19], D. Bahner[56], K. Bai[127], J. T. Baines[138], L. Baines[97], O. K. Baker[177], E. Bakos[16], D. Bakshi Gupta[8], L. E. Balabram Filho[85b], V. Balakrishnan[124], R. Balasubramanian[4], E. M. Baldin[38], P. Balek[88a], E. Ballabene[24a,24b], F. Balli[139], L. M. Baltes[65a], W. K. Balunas[33], J. Balz[103], I. Bamwidhi[120b], E. Banas[89], M. Bandieramonte[133], A. Bandyopadhyay[25], S. Bansal[25], L. Barak[156], M. Barakat[50], E. L. Barberio[108], D. Barberis[59a,59b], M. Barbero[105], M. Z. Barel[118], T. Barillari[113], M.-S. Barisits[37], T. Barklow[148], P. Baron[126], D. A. Baron Moreno[104], A. Baroncelli[64a], A. J. Barr[130], J. D. Barr[99], F. Barreiro[102], J. Barreiro Guimarães da Costa[14], M. G. Barros Teixeira[134a], S. Barsov[38], F. Bartels[65a], R. Bartoldus[148], A. E. Barton[94], P. Bartos[29a], A. Basan[103], M. Baselga[51], A. Bassalat[68,b], M. J. Basso[160a], S. Bataju[46], R. Bate[169], R. L. Bates[61],

S. Batlamous[102], B. Batool[146], M. Battaglia[140], D. Battulga[19], M. Bauce[77a,77b], M. Bauer[81], P. Bauer[25], L. T. Bazzano Hurrell[31], J. B. Beacham[53], T. Beau[131], J. Y. Beaucamp[93], P. H. Beauchemin[162], P. Bechtle[25], H. P. Beck[20,o], K. Becker[172], A. J. Beddall[84], V. A. Bednyakov[40], C. P. Bee[150], L. J. Beemster[16], T. A. Beermann[37], M. Begalli[85d], M. Begel[30], A. Behera[150], J. K. Behr[50], J. F. Beirer[37], F. Beisiegel[25], M. Belfkir[120b], G. Bella[156], L. Bellagamba[24b], A. Bellerive[35], P. Bellos[21], K. Beloborodov[38], D. Benchekroun[36a], F. Bendebba[36a], Y. Benhammou[156], K. C. Benkendorfer[63], L. Beresford[50], M. Beretta[55], E. Bergeaas Kuutmann[166], N. Berger[4], B. Bergmann[136], J. Beringer[18a], G. Bernardi[5], C. Bernius[148], F. U. Bernlochner[25], F. Bernon[37], A. Berrocal Guardia[13], T. Berry[98], P. Berta[137], A. Berthold[52], S. Bethke[113], A. Betti[77a,77b], A. J. Bevan[97], N. K. Bhalla[56], S. Bhatta[150], D. S. Bhattacharya[171], P. Bhattarai[148], Z. M. Bhatti[121], K. D. Bhide[56], V. S. Bhopatkar[125], R. M. Bianchi[133], G. Bianco[24a,24b], O. Biebel[112], M. Biglietti[79a], C. S. Billingsley[46], Y. Bimgdi[36f], M. Bindi[57], A. Bingham[176], A. Bingul[22b], C. Bini[77a,77b], G. A. Bird[33], M. Birman[174], M. Biros[137], S. Biryukov[151], T. Bisanz[51], E. Bisceglie[45a,45b], J. P. Biswal[138], D. Biswas[146], I. Bloch[50], A. Blue[61], U. Blumenschein[97], J. Blumenthal[103], V. S. Bobrovnikov[38], M. Boehler[56], B. Boehm[171], D. Bogavac[37], A. G. Bogdanchikov[38], L. S. Boggia[131], C. Bohm[49a], V. Boisvert[98], P. Bokan[37], T. Bold[88a], M. Bomben[5], M. Bona[97], M. Boonekamp[139], A. G. Borbély[61], I. S. Bordulev[38], G. Borissov[94], D. Bortoletto[130], D. Boscherini[24b], M. Bosman[13], K. Bouaouda[36a], N. Bouchhar[168], L. Boudet[4], J. Boudreau[133], E. V. Bouhova-Thacker[94], D. Boumediene[42], R. Bouquet[59a,59b], A. Boveia[123], J. Boyd[37], D. Boye[30], I. R. Boyko[40], L. Bozianu[58], J. Bracinik[21], N. Brahimi[4], G. Brandt[176], O. Brandt[33], F. Braren[50], B. Brau[106], J. E. Brau[127], R. Brener[174], L. Brenner[118], R. Brenner[166], S. Bressler[174], G. Brianti[80a,80b], D. Britton[61], D. Britzger[113], I. Brock[25], R. Brock[110], G. Brooijmans[43], A. J. Brooks[70], E. M. Brooks[160b], E. Brost[30], L. M. Brown[170], L. E. Bruce[63], T. L. Bruckler[130], P. A. Bruckman de Renstrom[89], B. Brüers[50], A. Bruni[24b], G. Bruni[24b], D. Brunner[49a,49b], M. Bruschi[24b], N. Bruscino[77a,77b], T. Buanes[17], Q. Buat[143], D. Buchin[113], A. G. Buckley[61], O. Bulekov[38], B. A. Bullard[148], S. Burdin[95], C. D. Burgard[51], A. M. Burger[37], B. Burghgrave[8], O. Burlayenko[56], J. Burleson[167], J. T. P. Burr[33], J. C. Burzynski[147], E. L. Busch[43], V. Büscher[103], P. J. Bussey[61], J. M. Butler[26], C. M. Buttar[61], J. M. Butterworth[99], W. Buttinger[138], C. J. Buxo Vazquez[110], A. R. Buzykaev[38], S. Cabrera Urbán[168], L. Cadamuro[68], D. Caforio[60], H. Cai[133], Y. Cai[14,115c], Y. Cai[115a], V. M. M. Cairo[37], O. Cakir[3a], N. Calace[37], P. Calafiura[18a], G. Calderini[131], P. Calfayan[35], G. Callea[61], L. P. Caloba[85b], D. Calvet[42], S. Calvet[42], M. Calvetti[76a,76b], R. Camacho Toro[131], S. Camarda[37], D. Camarero Munoz[27], P. Camarri[78a,78b], M. T. Camerlingo[74a,74b], D. Cameron[37], C. Camincher[170], M. Campanelli[99], A. Camplani[44], V. Canale[74a,74b], A. C. Canbay[3a], E. Canonero[98], J. Cantero[168], Y. Cao[167], F. Capocasa[27], M. Capua[45a,45b], A. Carbone[73a,73b], R. Cardarelli[78a], J. C. J. Cardenas[8], M. P. Cardiff[27], G. Carducci[45a,45b], T. Carli[37], G. Carlino[74a], J. I. Carlotto[13], B. T. Carlson[133,q], E. M. Carlson[160a,170], J. Carmignani[95], L. Carminati[73a,73b], A. Carnelli[139], M. Carnesale[37], S. Caron[117], E. Carquin[141f], I. B. Carr[108], S. Carrá[73a], G. Carratta[24a,24b], A. M. Carroll[127], M. P. Casado[13,i], M. Caspar[50], F. L. Castillo[4], L. Castillo Garcia[13], V. Castillo Gimenez[168], N. F. Castro[134a,134e], A. Catinaccio[37], J. R. Catmore[129], T. Cavaliere[4], V. Cavaliere[30], L. J. Caviedes Betancourt[23b], Y. C. Cekmecelioglu[50], E. Celebi[84], S. Cella[37], V. Cepaitis[58], K. Cerny[126], A. S. Cerqueira[85a], A. Cerri[151], L. Cerrito[78a,78b], F. Cerutti[18a], B. Cervato[146], A. Cervelli[24b], G. Cesarini[55], S. A. Cetin[84], P. M. Chabrillat[131], D. Chakraborty[119], J. Chan[18a], W. Y. Chan[158], J. D. Chapman[33], E. Chapon[139], B. Chargeishvili[154b], D. G. Charlton[21], M. Chatterjee[20], C. Chauhan[137], Y. Che[115a], S. Chekanov[6], S. V. Chekulaev[160a], G. A. Chelkov[40,a], A. Chen[109], B. Chen[156], B. Chen[170], H. Chen[115a], H. Chen[30], J. Chen[64c], J. Chen[147], M. Chen[130], S. Chen[90], S. J. Chen[115a], X. Chen[64c], X. Chen[15,ad], Y. Chen[64a], C. L. Cheng[175], H. C. Cheng[66a], S. Cheong[148], A. Cheplakov[40], E. Cheremushkina[50], E. Cherepanova[118], R. Cherkaoui El Moursli[36e], E. Cheu[7], K. Cheung[67], L. Chevalier[139], V. Chiarella[55], G. Chiarelli[76a], N. Chiedde[105], G. Chiodini[72a], A. S. Chisholm[21], A. Chitan[28b], M. Chitishvili[168], M. V. Chizhov[40,r], K. Choi[11], Y. Chou[143], E. Y. S. Chow[117], K. L. Chu[174], M. C. Chu[66a], X. Chu[14,115c], Z. Chubinidze[55], J. Chudoba[135], J. J. Chwastowski[89], D. Cieri[113], K. M. Ciesla[88a], V. Cindro[96], A. Ciocio[18a], F. Cirotto[74a,74b], Z. H. Citron[174], M. Citterio[73a], D. A. Ciubotaru[28b], A. Clark[58], P. J. Clark[54], N. Clarke Hall[99], C. Clarry[159], J. M. Clavijo Columbie[50], S. E. Clawson[50], C. Clement[49a,49b], Y. Coadou[105], M. Cobal[71a,71c], A. Coccaro[59b], R. F. Coelho Barrue[134a], R. Coelho Lopes De Sa[106], S. Coelli[73a], L. S. Colangeli[159], B. Cole[43], J. Collot[62], P. Conde Muiño[134a,134g], M. P. Connell[34c], S. H. Connell[34c], E. I. Conroy[130], F. Conventi[74a,af], H. G. Cooke[21], A. M. Cooper-Sarkar[130], F. A. Corchia[24a,24b], A. Cordeiro Oudot Choi[131], L. D. Corpe[42], M. Corradi[77a,77b],

F. Corriveau[107,y], A. Cortes-Gonzalez[19], M. J. Costa[168], F. Costanza[4], D. Costanzo[144], B. M. Cote[123], J. Couthures[4], G. Cowan[98], K. Cranmer[175], L. Cremer[51], D. Cremonini[24a,24b], S. Crépé-Renaudin[62], F. Crescioli[131], M. Cristinziani[146], M. Cristoforetti[80a,80b], V. Croft[118], J. E. Crosby[125], G. Crosetti[45a,45b], A. Cueto[102], H. Cui[99], Z. Cui[7], W. R. Cunningham[61], F. Curcio[168], J. R. Curran[54], P. Czodrowski[37], M. J. Da Cunha Sargedas De Sousa[59a,59b], J. V. Da Fonseca Pinto[85b], C. Da Via[104], W. Dabrowski[88a], T. Dado[37], S. Dahbi[153], T. Dai[109], D. Dal Santo[20], C. Dallapiccola[106], M. Dam[44], G. D'amen[30], V. D'Amico[112], J. Damp[103], J. R. Dandoy[35], D. Dannheim[37], M. Danninger[147], V. Dao[150], G. Darbo[59b], S. J. Das[30], F. Dattola[50], S. D'Auria[73a,73b], A. D'Avanzo[74a,74b], C. David[34a], T. Davidek[137], I. Dawson[97], H. A. Day-hall[136], K. De[8], C. De Almeida Rossi[159], R. De Asmundis[74a], N. De Biase[50], S. De Castro[24a,24b], N. De Groot[117], P. de Jong[118], H. De la Torre[119], A. De Maria[115a], A. De Salvo[77a], U. De Sanctis[78a,78b], F. De Santis[72a,72b], A. De Santo[151], J. B. De Vivie De Regie[62], J. Debevc[96], D. V. Dedovich[40], J. Degens[95], A. M. Deiana[46], F. Del Corso[24a,24b], J. Del Peso[102], L. Delagrange[131], F. Deliot[139], C. M. Delitzsch[51], M. Della Pietra[74a,74b], D. Della Volpe[58], A. Dell'Acqua[37], L. Dell'Asta[73a,73b], M. Delmastro[4], C. C. Delogu[103], P. A. Delsart[62], S. Demers[177], M. Demichev[40], S. P. Denisov[38], L. D'Eramo[42], D. Derendarz[89], F. Derue[131], P. Dervan[95], K. Desch[25], C. Deutsch[25], F. A. Di Bello[59a,59b], A. Di Ciaccio[78a,78b], L. Di Ciaccio[4], A. Di Domenico[77a,77b], C. Di Donato[74a,74b], A. Di Girolamo[37], G. Di Gregorio[37], A. Di Luca[80a,80b], B. Di Micco[79a,79b], R. Di Nardo[79a,79b], K. F. Di Petrillo[41], M. Diamantopoulou[35], F. A. Dias[118], T. Dias Do Vale[147], M. A. Diaz[141a,141b], A. R. Didenko[40], M. Didenko[168], E. B. Diehl[109], S. Díez Cornell[50], C. Diez Pardos[146], C. Dimitriadi[166], A. Dimitrievska[21], J. Dingfelder[25], T. Dingley[130], I.-M. Dinu[28b], S. J. Dittmeier[65b], F. Dittus[37], M. Divisek[137], B. Dixit[95], F. Djama[105], T. Djobava[154b], C. Doglioni[101,104], A. Dohnalova[29a], J. Dolejsi[137], Z. Dolezal[137], K. Domijan[88a], K. M. Dona[41], M. Donadelli[85d], B. Dong[110], J. Donini[42], A. D'Onofrio[74a,74b], M. D'Onofrio[95], J. Dopke[138], A. Doria[74a], N. Dos Santos Fernandes[134a], P. Dougan[104], M. T. Dova[93], A. T. Doyle[61], M. A. Draguet[130], M. P. Drescher[57], E. Dreyer[174], I. Drivas-koulouris[10], M. Drnevich[121], M. Drozdova[58], D. Du[64a], T. A. du Pree[118], F. Dubinin[38], M. Dubovsky[29a], E. Duchovni[174], G. Duckeck[112], O. A. Ducu[28b], D. Duda[54], A. Dudarev[37], E. R. Duden[27], M. D'uffizi[104], L. Duflot[68], M. Dührssen[37], I. Duminica[28g], A. E. Dumitriu[28b], M. Dunford[65a], S. Dungs[51], K. Dunne[49a,49b], A. Duperrin[105], H. Duran Yildiz[3a], M. Düren[60], A. Durglishvili[154b], D. Duvnjak[35], B. L. Dwyer[119], G. I. Dyckes[18a], M. Dyndal[88a], B. S. Dziedzic[37], Z. O. Earnshaw[151], G. H. Eberwein[130], B. Eckerova[29a], S. Eggebrecht[57], E. Egidio Purcino De Souza[85e], L. F. Ehrke[58], G. Eigen[17], K. Einsweiler[18a], T. Ekelof[166], P. A. Ekman[101], S. El Farkh[36b], Y. El Ghazali[64a], H. El Jarrari[37], A. El Moussaouy[36a], V. Ellajosyula[166], M. Ellert[166], F. Ellinghaus[176], N. Ellis[37], J. Elmsheuser[30], M. Elsawy[120a], M. Elsing[37], D. Emeliyanov[138], Y. Enari[86], I. Ene[18a], S. Epari[13], P. A. Erland[89], D. Ernani Martins Neto[89], M. Errenst[176], M. Escalier[68], C. Escobar[168], E. Etzion[156], G. Evans[134a,134b], H. Evans[70], L. S. Evans[98], A. Ezhilov[38], S. Ezzarqtouni[36a], F. Fabbri[24a,24b], L. Fabbri[24a,24b], G. Facini[99], V. Fadeyev[140], R. M. Fakhrutdinov[38], D. Fakoudis[103], S. Falciano[77a], L. F. Falda Ulhoa Coelho[37], F. Fallavollita[113], G. Falsetti[45a,45b], J. Faltova[137], C. Fan[167], K. Y. Fan[66b], Y. Fan[14], Y. Fang[14,115c], M. Fanti[73a,73b], M. Faraj[71a,71b], Z. Farazpay[100], A. Farbin[8], A. Farilla[79a], T. Farooque[110], S. M. Farrington[54,138], F. Fassi[36e], D. Fassouliotis[9], M. Faucci Giannelli[78a,78b], W. J. Fawcett[33], L. Fayard[68], P. Federic[137], P. Federicova[135], O. L. Fedin[38,a], M. Feickert[175], L. Feligioni[105], D. E. Fellers[127], C. Feng[64b], Z. Feng[118], M. J. Fenton[163], L. Ferencz[50], R. A. M. Ferguson[94], S. I. Fernandez Luengo[141f], P. Fernandez Martinez[69], M. J. V. Fernoux[105], J. Ferrando[94], A. Ferrari[166], P. Ferrari[117,118], R. Ferrari[75a], D. Ferrere[58], C. Ferretti[109], D. Fiacco[77a,77b], F. Fiedler[103], P. Fiedler[136], S. Filimonov[38], A. Filipčič[96], E. K. Filmer[160a], F. Filthaut[117], M. C. N. Fiolhais[134a,134c,c], L. Fiorini[168], W. C. Fisher[110], T. Fitschen[104], P. M. Fitzhugh[139], I. Fleck[146], P. Fleischmann[109], T. Flick[176], M. Flores[34d,ab], L. R. Flores Castillo[66a], L. Flores Sanz De Acedo[37], F. M. Follega[80a,80b], N. Fomin[33], J. H. Foo[159], A. Formica[139], A. C. Forti[104], E. Fortin[37], A. W. Fortman[18a], M. G. Foti[18a], L. Fountas[9,j], D. Fournier[68], H. Fox[94], P. Francavilla[76a,76b], S. Francescato[63], S. Franchellucci[58], M. Franchini[24a,24b], S. Franchino[65a], D. Francis[37], L. Franco[117], V. Franco Lima[37], L. Franconi[50], M. Franklin[63], G. Frattari[27], Y. Y. Frid[156], J. Friend[61], N. Fritzsche[37], A. Froch[56], D. Froidevaux[37], J. A. Frost[130], Y. Fu[64a], S. Fuenzalida Garrido[141f], M. Fujimoto[105], K. Y. Fung[66a], E. Furtado De Simas Filho[85e], M. Furukawa[158], J. Fuster[168], A. Gaa[57], A. Gabrielli[24a,24b], A. Gabrielli[159], P. Gadow[37], G. Gagliardi[59a,59b], L. G. Gagnon[18a], S. Gaid[165], S. Galantzan[156], J. Gallagher[1], E. J. Gallas[130], A. L. Gallen[166], B. J. Gallop[138], K. K. Gan[123], S. Ganguly[158], Y. Gao[54], F. M. Garay Walls[141a,141b], B. Garcia[30], C. García[168], A. Garcia Alonso[118],

A. G. Garcia Caffaro[177], J. E. García Navarro[168], M. Garcia-Sciveres[18a], G. L. Gardner[132], R. W. Gardner[41], N. Garelli[162], D. Garg[82], R. B. Garg[148], J. M. Gargan[54], C. A. Garner[159], C. M. Garvey[34a], V. K. Gassmann[162], G. Gaudio[75a], V. Gautam[13], P. Gauzzi[77a,77b], J. Gavranovic[96], I. L. Gavrilenko[38], A. Gavrilyuk[38], C. Gay[169], G. Gaycken[127], E. N. Gazis[10], A. A. Geanta[28b], C. M. Gee[140], A. Gekow[123], C. Gemme[59b], M. H. Genest[62], A. D. Gentry[116], S. George[98], W. F. George[21], T. Geralis[48], A. A. Gerwin[124], P. Gessinger-Befurt[37], M. E. Geyik[176], M. Ghani[172], K. Ghorbanian[97], A. Ghosal[146], A. Ghosh[163], A. Ghosh[7], B. Giacobbe[24b], S. Giagu[77a,77b], T. Giani[118], A. Giannini[64a], S. M. Gibson[98], M. Gignac[140], D. T. Gil[88b], A. K. Gilbert[88a], B. J. Gilbert[43], D. Gillberg[35], G. Gilles[118], L. Ginabat[131], D. M. Gingrich[2,ae], M. P. Giordani[71a,71c], P. F. Giraud[139], G. Giugliarelli[71a,71c], D. Giugni[73a], F. Giuli[78a,78b], I. Gkialas[9,j], L. K. Gladilin[38], C. Glasman[102], G. R. Gledhill[127], G. Glemža[50], M. Glisic[127], I. Gnesi[45b], Y. Go[30], M. Goblirsch-Kolb[37], B. Gocke[51], D. Godin[111], B. Gokturk[22a], S. Goldfarb[108], T. Golling[58], M. G. D. Gololo[34g], D. Golubkov[38], J. P. Gombas[110], A. Gomes[134a,134b], G. Gomes Da Silva[146], A. J. Gomez Delegido[168], R. Gonçalo[134a], L. Gonella[21], A. Gongadze[154c], F. Gonnella[21], J. L. Gonski[148], R. Y. González Andana[54], S. González de la Hoz[168], R. Gonzalez Lopez[95], C. Gonzalez Renteria[18a], M. V. Gonzalez Rodrigues[50], R. Gonzalez Suarez[166], S. Gonzalez-Sevilla[58], L. Goossens[37], B. Gorini[37], E. Gorini[72a,72b], A. Gorišek[96], T. C. Gosart[132], A. T. Goshaw[53], M. I. Gostkin[40], S. Goswami[125], C. A. Gottardo[37], S. A. Gotz[112], M. Gouighri[36b], V. Goumarre[50], A. G. Goussiou[143], N. Govender[34c], R. P. Grabarczyk[130], I. Grabowska-Bold[88a], K. Graham[35], E. Gramstad[129], S. Grancagnolo[72a,72b], C. M. Grant[1,139], P. M. Gravila[28f], F. G. Gravili[72a,72b], H. M. Gray[18a], M. Greco[72a,72b], M. J. Green[1], C. Grefe[25], A. S. Grefsrud[17], I. M. Gregor[50], K. T. Greif[163], P. Grenier[148], S. G. Grewe[113], A. A. Grillo[140], K. Grimm[32], S. Grinstein[13,u], J.-F. Grivaz[68], E. Gross[174], J. Grosse-Knetter[57], L. Guan[109], J. G. R. Guerrero Rojas[168], G. Guerrieri[37], R. Gugel[103], J. A. M. Guhit[109], A. Guida[19], E. Guilloton[172], S. Guindon[37], F. Guo[14,115c], J. Guo[64c], L. Guo[50], L. Guo[14], Y. Guo[109], A. Gupta[51], R. Gupta[133], S. Gurbuz[25], S. S. Gurdasani[56], G. Gustavino[77a,77b], P. Gutierrez[124], L. F. Gutierrez Zagazeta[132], M. Gutsche[52], C. Gutschow[99], C. Gwenlan[130], C. B. Gwilliam[95], E. S. Haaland[129], A. Haas[121], M. Habedank[61], C. Haber[18a], H. K. Hadavand[8], A. Hadef[52], A. I. Hagan[94], J. J. Hahn[146], E. H. Haines[99], M. Haleem[171], J. Haley[125], G. D. Hallewell[105], L. Halser[20], K. Hamano[170], M. Hamer[25], E. J. Hampshire[98], J. Han[64b], L. Han[115a], L. Han[64a], S. Han[18a], Y. F. Han[159], K. Hanagaki[86], M. Hance[140], D. A. Hangal[43], H. Hanif[147], M. D. Hank[132], J. B. Hansen[44], P. H. Hansen[44], D. Harada[58], T. Harenberg[176], S. Harkusha[178], M. L. Harris[106], Y. T. Harris[25], J. Harrison[13], N. M. Harrison[123], P. F. Harrison[172], N. M. Hartman[113], N. M. Hartmann[112], R. Z. Hasan[98,138], Y. Hasegawa[145], F. Haslbeck[130], S. Hassan[17], R. Hauser[110], C. M. Hawkes[21], R. J. Hawkings[37], Y. Hayashi[158], D. Hayden[110], C. Hayes[109], R. L. Hayes[118], C. P. Hays[130], J. M. Hays[97], H. S. Hayward[95], F. He[64a], M. He[14,115c], Y. He[50], Y. He[99], N. B. Heatley[97], V. Hedberg[101], A. L. Heggelund[129], N. D. Hehir[97,*], C. Heidegger[56], K. K. Heidegger[56], J. Heilman[35], S. Heim[50], T. Heim[18a], J. G. Heinlein[132], J. J. Heinrich[127], L. Heinrich[113,ac], J. Hejbal[135], A. Held[175], S. Hellesund[17], C. M. Helling[169], S. Hellman[49a,49b], R. C. W. Henderson[94], L. Henkelmann[33], A. M. Henriques Correia[37], H. Herde[101], Y. Hernández Jiménez[150], L. M. Herrmann[25], T. Herrmann[52], G. Herten[56], R. Hertenberger[112], L. Hervas[37], M. E. Hesping[103], N. P. Hessey[160a], J. Hessler[113], M. Hidaoui[36b], N. Hidic[137], E. Hill[159], S. J. Hillier[21], J. R. Hinds[110], F. Hinterkeuser[25], M. Hirose[128], S. Hirose[161], D. Hirschbuehl[176], T. G. Hitchings[104], B. Hiti[96], J. Hobbs[150], R. Hobincu[28e], N. Hod[174], M. C. Hodgkinson[144], B. H. Hodkinson[130], A. Hoecker[37], D. D. Hofer[109], J. Hofer[168], T. Holm[25], M. Holzbock[37], L. B. A. H. Hommels[33], B. P. Honan[104], J. J. Hong[70], J. Hong[64c], T. M. Hong[133], B. H. Hooberman[167], W. H. Hopkins[6], M. C. Hoppesch[167], Y. Horii[114], M. E. Horstmann[113], S. Hou[153], M. R. Housenga[167], A. S. Howard[96], J. Howarth[61], J. Hoya[6], M. Hrabovsky[126], A. Hrynevich[50], T. Hryn'ova[4], P. J. Hsu[67], S.-C. Hsu[143], T. Hsu[68], M. Hu[18a], Q. Hu[64a], S. Huang[33], X. Huang[14,115c], Y. Huang[144], Y. Huang[103], Y. Huang[14], Z. Huang[104], Z. Hubacek[136], M. Huebner[25], F. Huegging[25], T. B. Huffman[130], M. Hufnagel Maranha De Faria[85a], C. A. Hugli[50], M. Huhtinen[37], S. K. Huiberts[17], R. Hulsken[107], N. Huseynov[12,g], J. Huston[110], J. Huth[63], R. Hyneman[148], G. Iacobucci[58], G. Iakovidis[30], L. Iconomidou-Fayard[68], J. P. Iddon[37], P. Iengo[74a,74b], R. Iguchi[158], Y. Iiyama[158], T. Iizawa[130], Y. Ikegami[86], D. Iliadis[157], N. Ilic[159], H. Imam[85c], G. Inacio Goncalves[85d], T. Ingebretsen Carlson[49a,49b], J. M. Inglis[97], G. Introzzi[75a,75b], M. Iodice[79a], V. Ippolito[77a,77b], R. K. Irwin[95], M. Ishino[158], W. Islam[175], C. Issever[19], S. Istin[22a,ai], H. Ito[173], R. Iuppa[80a,80b], A. Ivina[174], J. M. Izen[47], V. Izzo[74a], P. Jacka[135], P. Jackson[1], C. S. Jagfeld[112], G. Jain[160a], P. Jain[50], K. Jakobs[56], T. Jakoubek[174], J. Jamieson[61], W. Jang[158],

M. Javurkova[106], P. Jawahar[104], L. Jeanty[127], J. Jejelava[154a], P. Jenni[56,f], C. E. Jessiman[35], C. Jia[64b], H. Jia[169], J. Jia[150], X. Jia[14,115c], Z. Jia[115a], C. Jiang[54], S. Jiggins[50], J. Jimenez Pena[13], S. Jin[115a], A. Jinaru[28b], O. Jinnouchi[142], P. Johansson[144], K. A. Johns[7], J. W. Johnson[140], F. A. Jolly[50], D. M. Jones[151], E. Jones[50], K. S. Jones[8], P. Jones[33], R. W. L. Jones[94], T. J. Jones[95], H. L. Joos[37,57], R. Joshi[123], J. Jovicevic[16], X. Ju[18a], J. J. Junggeburth[37], T. Junkermann[65a], A. Juste Rozas[13,u], M. K. Juzek[89], S. Kabana[141e], A. Kaczmarska[89], M. Kado[113], H. Kagan[123], M. Kagan[148], A. Kahn[132], C. Kahra[103], T. Kaji[158], E. Kajomovitz[155], N. Kakati[174], I. Kalaitzidou[56], C. W. Kalderon[30], N. J. Kang[140], D. Kar[34g], K. Karava[130], M. J. Kareem[160b], E. Karentzos[25], O. Karkout[118], S. N. Karpov[40], Z. M. Karpova[40], V. Kartvelishvili[94], A. N. Karyukhin[38], E. Kasimi[157], J. Katzy[50], S. Kaur[35], K. Kawade[145], M. P. Kawale[124], C. Kawamoto[90], T. Kawamoto[64a], E. F. Kay[37], F. I. Kaya[162], S. Kazakos[110], V. F. Kazanin[38], Y. Ke[150], J. M. Keaveney[34a], R. Keeler[170], G. V. Kehris[63], J. S. Keller[35], J. J. Kempster[151], O. Kepka[135], B. P. Kerridge[138], S. Kersten[176], B. P. Kerševan[96], L. Keszeghova[29a], S. Ketabchi Haghighat[159], R. A. Khan[133], A. Khanov[125], A. G. Kharlamov[38], T. Kharlamova[38], E. E. Khoda[143], M. Kholodenko[134a], T. J. Khoo[19], G. Khoriauli[171], J. Khubua[154b,*], Y. A. R. Khwaira[131], B. Kibirige[34g], D. Kim[6], D. W. Kim[49a,49b], Y. K. Kim[41], N. Kimura[99], M. K. Kingston[57], A. Kirchhoff[57], C. Kirfel[25], F. Kirfel[25], J. Kirk[138], A. E. Kiryunin[113], S. Kita[161], C. Kitsaki[10], O. Kivernyk[25], M. Klassen[162], C. Klein[35], L. Klein[171], M. H. Klein[46], S. B. Klein[58], U. Klein[95], A. Klimentov[30], T. Klioutchnikova[37], P. Kluit[118], S. Kluth[113], E. Kneringer[81], T. M. Knight[159], A. Knue[51], M. Kobel[52], D. Kobylianskii[174], S. F. Koch[130], M. Kocian[148], P. Kodyš[137], D. M. Koeck[127], P. T. Koenig[25], T. Koffas[35], O. Kolay[52], I. Koletsou[4], T. Komarek[89], K. Köneke[56], A. X. Y. Kong[1], T. Kono[122], N. Konstantinidis[99], P. Kontaxakis[58], B. Konya[101], R. Kopeliansky[43], S. Koperny[88a], K. Korcyl[89], K. Kordas[157,e], A. Korn[99], S. Korn[57], I. Korolkov[13], N. Korotkova[38], B. Kortman[118], O. Kortner[113], S. Kortner[113], W. H. Kostecka[119], V. V. Kostyukhin[146], A. Kotsokechagia[37], A. Kotwal[53], A. Koulouris[37], A. Kourkoumeli-Charalampidi[75a,75b], C. Kourkoumelis[9], E. Kourlitis[113], O. Kovanda[127], R. Kowalewski[170], W. Kozanecki[127], A. S. Kozhin[38], V. A. Kramarenko[38], G. Kramberger[96], P. Kramer[25], M. W. Krasny[131], A. Krasznahorkay[37], A. C. Kraus[119], J. W. Kraus[176], J. A. Kremer[50], T. Kresse[52], L. Kretschmann[176], J. Kretzschmar[95], K. Kreul[19], P. Krieger[159], K. Krizka[21], K. Kroeninger[51], H. Kroha[113], J. Kroll[135], J. Kroll[132], K. S. Krowpman[110], U. Kruchonak[40], H. Krüger[25], N. Krumnack[83], M. C. Kruse[53], O. Kuchinskaia[38], S. Kuday[3a], S. Kuehn[37], R. Kuesters[56], T. Kuhl[50], V. Kukhtin[40], Y. Kulchitsky[40], S. Kuleshov[141b,141d], M. Kumar[34g], N. Kumari[50], P. Kumari[160b], A. Kupco[135], T. Kupfer[51], A. Kupich[38], O. Kuprash[56], H. Kurashige[87], L. L. Kurchaninov[160a], O. Kurdysh[68], Y. A. Kurochkin[39], A. Kurova[38], M. Kuze[142], A. K. Kvam[106], J. Kvita[126], T. Kwan[107], N. G. Kyriacou[109], L. A. O. Laatu[105], C. Lacasta[168], F. Lacava[77a,77b], H. Lacker[19], D. Lacour[131], N. N. Lad[99], E. Ladygin[40], A. Lafarge[42], B. Laforge[131], T. Lagouri[177], F. Z. Lahbabi[36a], S. Lai[57], J. E. Lambert[170], S. Lammers[70], W. Lampl[7], C. Lampoudis[157,e], G. Lamprinoudis[103], A. N. Lancaster[119], E. Lançon[30], U. Landgraf[56], M. P. J. Landon[97], V. S. Lang[56], O. K. B. Langrekken[129], A. J. Lankford[163], F. Lanni[37], K. Lantzsch[25], A. Lanza[75a], M. Lanzac Berrocal[168], J. F. Laporte[139], T. Lari[73a], F. Lasagni Manghi[24b], M. Lassnig[37], V. Latonova[135], A. Laurier[155], S. D. Lawlor[144], Z. Lawrence[104], R. Lazaridou[172], M. Lazzaroni[73a,73b], B. Le[104], H. D. M. Le[110], E. M. Le Boulicaut[177], L. T. Le Pottier[18a], B. Leban[24a,24b], A. Lebedev[83], M. LeBlanc[104], F. Ledroit-Guillon[62], S. C. Lee[153], S. Lee[49a,49b], T. F. Lee[95], L. L. Leeuw[34c], M. Lefebvre[170], C. Leggett[18a], G. Lehmann Miotto[37], M. Leigh[58], W. A. Leight[106], W. Leinonen[117], A. Leisos[157,s], M. A. L. Leite[85c], C. E. Leitgeb[19], R. Leitner[137], K. J. C. Leney[46], T. Lenz[25], S. Leone[76a], C. Leonidopoulos[54], A. Leopold[149], R. Les[110], C. G. Lester[33], M. Levchenko[38], J. Levêque[4], L. J. Levinson[174], G. Levrini[24a,24b], M. P. Lewicki[89], C. Lewis[143], D. J. Lewis[4], L. Lewitt[144], A. Li[30], B. Li[64b], C. Li[64a], C.-Q. Li[113], H. Li[64a], H. Li[64b], H. Li[115a], H. Li[15], H. Li[64b], J. Li[64c], K. Li[14], L. Li[64c], M. Li[14,115c], S. Li[14,115c], S. Li[64c,64d,d], T. Li[5], X. Li[107], Z. Li[158], Z. Li[14,115c], Z. Li[64a], S. Liang[14,115c], Z. Liang[14], M. Liberatore[139], B. Liberti[78a], K. Lie[66c], J. Lieber Marin[85e], H. Lien[70], H. Lin[109], K. Lin[110], L. Linden[112], R. E. Lindley[7], J. H. Lindon[2], J. Ling[63], E. Lipeles[132], A. Lipniacka[17], A. Lister[169], J. D. Little[70], B. Liu[14], B. X. Liu[115b], D. Liu[64c,64d], E. H. L. Liu[21], J. B. Liu[64a], J. K. K. Liu[33], K. Liu[64d], K. Liu[64c,64d], M. Liu[64a], M. Y. Liu[64a], P. Liu[14], Q. Liu[64c,64d,143], X. Liu[64a], X. Liu[64b], Y. Liu[115b,115c], Y. L. Liu[64b], Y. W. Liu[64a], S. L. Lloyd[97], E. M. Lobodzinska[50], P. Loch[7], E. Lodhi[159], T. Lohse[19], K. Lohwasser[144], E. Loiacono[50], J. D. Lomas[21], J. D. Long[43], I. Longarini[163], R. Longo[167], I. Lopez Paz[69], A. Lopez Solis[50], N. A. Lopez-canelas[7], N. Lorenzo Martinez[4], A. M. Lory[112], M. Losada[120a], G. Löschcke Centeno[151], O. Loseva[38], X. Lou[49a,49b], X. Lou[14,115c], A. Lounis[68], P. A. Love[94], G. Lu[14,115c],

M. Lu[68], S. Lu[132], Y. J. Lu[67], H. J. Lubatti[143], C. Luci[77a,77b], F. L. Lucio Alves[115a], F. Luehring[70], O. Lukianchuk[68], B. S. Lunday[132], O. Lundberg[149], B. Lund-Jensen[149,*], N. A. Luongo[6], M. S. Lutz[37], A. B. Lux[26], D. Lynn[30], R. Lysak[135], E. Lytken[101], V. Lyubushkin[40], T. Lyubushkina[40], M. M. Lyukova[150], M.Firdaus M. Soberi[54], H. Ma[30], K. Ma[64a], L. L. Ma[64b], W. Ma[64a], Y. Ma[125], J. C. MacDonald[103], P. C. Machado De Abreu Farias[85e], R. Madar[42], T. Madula[99], J. Maeda[87], T. Maeno[30], P. T. Mafa[34c], H. Maguire[144], V. Maiboroda[139], A. Maio[134a,134b,134d], K. Maj[88a], O. Majersky[50], S. Majewski[127], N. Makovec[68], V. Maksimovic[16], B. Malaescu[131], Pa. Malecki[89], V. P. Maleev[38], F. Malek[62,n], M. Mali[96], D. Malito[98], U. Mallik[82,*], S. Maltezos[10], S. Malyukov[40], J. Mamuzic[13], G. Mancini[55], M. N. Mancini[27], G. Manco[75a,75b], J. P. Mandalia[97], S. S. Mandarry[151], I. Mandić[96], L. Manhaes de Andrade Filho[85a], I. M. Maniatis[174], J. Manjarres Ramos[92], D. C. Mankad[174], A. Mann[112], S. Manzoni[37], L. Mao[64c], X. Mapekula[34c], A. Marantis[157,s], G. Marchiori[5], M. Marcisovsky[135], C. Marcon[73a], M. Marinescu[21], S. Marium[50], M. Marjanovic[124], A. Markhoos[56], M. Markovitch[68], M. K. Maroun[106], E. J. Marshall[94], Z. Marshall[18a], S. Marti-Garcia[168], J. Martin[99], T. A. Martin[138], V. J. Martin[54], B. Martin dit Latour[17], L. Martinelli[77a,77b], M. Martinez[13,u], P. Martinez Agullo[168], V. I. Martinez Outschoorn[106], P. Martinez Suarez[13], S. Martin-Haugh[138], G. Martinovicova[137], V. S. Martoiu[28b], A. C. Martyniuk[99], A. Marzin[37], D. Mascione[80a,80b], L. Masetti[103], J. Masik[104], A. L. Maslennikov[38], S. L. Mason[43], P. Massarotti[74a,74b], P. Mastrandrea[76a,76b], A. Mastroberardino[45a,45b], T. Masubuchi[128], T. T. Mathew[127], T. Mathisen[166], J. Matousek[137], D. M. Mattern[51], J. Maurer[28b], T. Maurin[61], A. J. Maury[68], B. Maček[96], D. A. Maximov[38], A. E. May[104], R. Mazini[34g], I. Maznas[119], M. Mazza[110], S. M. Mazza[140], E. Mazzeo[73a,73b], J. P. Mc Gowan[170], S. P. Mc Kee[109], C. A. Mc Lean[6], C. C. McCracken[169], E. F. McDonald[108], A. E. McDougall[118], L. F. Mcelhinney[94], J. A. Mcfayden[151], R. P. McGovern[132], R. P. Mckenzie[34g], T. C. Mclachlan[50], D. J. Mclaughlin[99], S. J. McMahon[138], C. M. Mcpartland[95], R. A. McPherson[170,y], S. Mehlhase[112], A. Mehta[95], D. Melini[168], B. R. Mellado Garcia[34g], A. H. Melo[57], F. Meloni[50], A. M. Mendes Jacques Da Costa[104], H. Y. Meng[159], L. Meng[94], S. Menke[113], M. Mentink[37], E. Meoni[45a,45b], G. Mercado[119], S. Merianos[157], C. Merlassino[71a,71c], L. Merola[74a,74b], C. Meroni[73a,73b], J. Metcalfe[6], A. S. Mete[6], E. Meuser[103], C. Meyer[70], J.-P. Meyer[139], R. P. Middleton[138], L. Mijović[54], G. Mikenberg[174], M. Mikestikova[135], M. Mikuž[96], H. Mildner[103], A. Milic[37], D. W. Miller[41], E. H. Miller[148], L. S. Miller[35], A. Milov[174], D. A. Milstead[49a,49b], T. Min[115a], A. A. Minaenko[38], I. A. Minashvili[154b], A. I. Mincer[121], B. Mindur[88a], M. Mineev[40], Y. Mino[90], L. M. Mir[13], M. Miralles Lopez[61], M. Mironova[18a], M. C. Missio[117], A. Mitra[172], V. A. Mitsou[168], Y. Mitsumori[114], O. Miu[159], P. S. Miyagawa[97], T. Mkrtchyan[65a], M. Mlinarevic[99], T. Mlinarevic[99], M. Mlynarikova[37], S. Mobius[20], P. Mogg[112], M. H. Mohamed Farook[116], A. F. Mohammed[14,115c], S. Mohapatra[43], G. Mokgatitswane[34g], L. Moleri[174], B. Mondal[146], S. Mondal[136], K. Mönig[50], E. Monnier[105], L. Monsonis Romero[168], J. Montejo Berlingen[13], A. Montella[49a,49b], M. Montella[123], F. Montereali[79a,79b], F. Monticelli[93], S. Monzani[71a,71c], A. Morancho Tarda[44], N. Morange[68], A. L. Moreira De Carvalho[50], M. Moreno Llácer[168], C. Moreno Martinez[58], J. M. Moreno Perez[23b], P. Morettini[59b], S. Morgenstern[37], M. Morii[63], M. Morinaga[158], M. Moritsu[91], F. Morodei[77a,77b], P. Moschovakos[37], B. Moser[130], M. Mosidze[154b], T. Moskalets[46], P. Moskvitina[117], J. Moss[32,k], P. Moszkowicz[88a], A. Moussa[36d], Y. Moyal[174], E. J. W. Moyse[106], O. Mtintsilana[34g], S. Muanza[105], J. Mueller[133], D. Muenstermann[94], R. Müller[37], G. A. Mullier[166], A. J. Mullin[33], J. J. Mullin[132], A. E. Mulski[63], D. P. Mungo[159], D. Munoz Perez[168], F. J. Munoz Sanchez[104], M. Murin[104], W. J. Murray[138,172], M. Muškinja[96], C. Mwewa[30], A. G. Myagkov[38,a], A. J. Myers[8], G. Myers[109], M. Myska[136], B. P. Nachman[18a], K. Nagai[130], K. Nagano[86], R. Nagasaka[158], J. L. Nagle[30,ag], E. Nagy[105], A. M. Nairz[37], Y. Nakahama[86], K. Nakamura[86], K. Nakkalil[5], H. Nanjo[128], E. A. Narayanan[46], I. Naryshkin[38], L. Nasella[73a,73b], S. Nasri[120b], C. Nass[25], G. Navarro[23a], J. Navarro-Gonzalez[168], R. Nayak[156], A. Nayaz[19], P. Y. Nechaeva[38], S. Nechaeva[24a,24b], F. Nechansky[135], L. Nedic[130], T. J. Neep[21], A. Negri[75a,75b], M. Negrini[24b], C. Nellist[118], C. Nelson[107], K. Nelson[109], S. Nemecek[135], M. Nessi[37,h], M. S. Neubauer[167], F. Neuhaus[103], J. Neundorf[50], J. Newell[95], P. R. Newman[21], C. W. Ng[133], Y. W. Y. Ng[50], B. Ngair[120a], H. D. N. Nguyen[111], R. B. Nickerson[130], R. Nicolaidou[139], J. Nielsen[140], M. Niemeyer[57], J. Niermann[57], N. Nikiforou[37], V. Nikolaenko[38,a], I. Nikolic-Audit[131], K. Nikolopoulos[21], P. Nilsson[30], I. Ninca[50], G. Ninio[156], A. Nisati[77a], N. Nishu[2], R. Nisius[113], N. Nitika[71a,71c], J.-E. Nitschke[52], E. K. Nkadimeng[34g], T. Nobe[158], T. Nommensen[152], M. B. Norfolk[144], B. J. Norman[35], M. Noury[36a], J. Novak[96], T. Novak[96], L. Novotny[136], R. Novotny[116], L. Nozka[126], K. Ntekas[163], N. M. J. Nunes De Moura Junior[85b], J. Ocariz[131], A. Ochi[87], I. Ochoa[134a], S. Oerdek[50,v], J. T. Offermann[41],

A. Ogrodnik[137], A. Oh[104], C. C. Ohm[149], H. Oide[86], R. Oishi[158], M. L. Ojeda[37], Y. Okumura[158], L. F. Oleiro Seabra[134a], I. Oleksiyuk[58], S. A. Olivares Pino[141d], G. Oliveira Correa[13], D. Oliveira Damazio[30], J. L. Oliver[163], Ö. O. Öncel[56], A. P. O'Neill[20], A. Onofre[134a,134e], P. U. E. Onyisi[11], M. J. Oreglia[41], D. Orestano[79a,79b], N. Orlando[13], R. S. Orr[159], L. M. Osojnak[132], R. Ospanov[64a], Y. Osumi[114], G. Otero y Garzon[31], H. Otono[91], P. S. Ott[65a], G. J. Ottino[18a], M. Ouchrif[36d], F. Ould-Saada[129], T. Ovsiannikova[143], M. Owen[61], R. E. Owen[138], V. E. Ozcan[22a], F. Ozturk[89], N. Ozturk[8], S. Ozturk[84], H. A. Pacey[130], A. Pacheco Pages[13], C. Padilla Aranda[13], G. Padovano[77a,77b], S. Pagan Griso[18a], G. Palacino[70], A. Palazzo[72a,72b], J. Pampel[25], J. Pan[177], T. Pan[66a], D. K. Panchal[11], C. E. Pandini[118], J. G. Panduro Vazquez[138], H. D. Pandya[1], H. Pang[15], P. Pani[50], G. Panizzo[71a,71c], L. Panwar[131], L. Paolozzi[58], S. Parajuli[167], A. Paramonov[6], C. Paraskevopoulos[55], D. Paredes Hernandez[66b], A. Pareti[75a,75b], K. R. Park[43], T. H. Park[159], M. A. Parker[33], F. Parodi[59a,59b], V. A. Parrish[54], J. A. Parsons[43], U. Parzefall[56], B. Pascual Dias[111], L. Pascual Dominguez[102], E. Pasqualucci[77a], S. Passaggio[59b], F. Pastore[98], P. Patel[89], U. M. Patel[53], J. R. Pater[104], T. Pauly[37], F. Pauwels[137], C. I. Pazos[162], M. Pedersen[129], R. Pedro[134a], S. V. Peleganchuk[38], O. Penc[37], E. A. Pender[54], S. Peng[15], G. D. Penn[177], K. E. Penski[112], M. Penzin[38], B. S. Peralva[85d], A. P. Pereira Peixoto[143], L. Pereira Sanchez[148], D. V. Perepelitsa[30,ag], G. Perera[106], E. Perez Codina[160a], M. Perganti[10], H. Pernegger[37], S. Perrella[77a,77b], O. Perrin[42], K. Peters[50], R. F. Y. Peters[104], B. A. Petersen[37], T. C. Petersen[44], E. Petit[105], V. Petousis[136], C. Petridou[157,e], T. Petru[137], A. Petrukhin[146], M. Pettee[18a], A. Petukhov[84], K. Petukhova[37], R. Pezoa[141f], L. Pezzotti[37], G. Pezzullo[177], A. J. Pfleger[37], T. M. Pham[175], T. Pham[108], P. W. Phillips[138], G. Piacquadio[150], E. Pianori[18a], F. Piazza[127], R. Piegaia[31], D. Pietreanu[28b], A. D. Pilkington[104], M. Pinamonti[71a,71c], J. L. Pinfold[2], B. C. Pinheiro Pereira[134a], J. Pinol Bel[13], A. E. Pinto Pinoargote[139], L. Pintucci[71a,71c], K. M. Piper[151], A. Pirttikoski[58], D. A. Pizzi[35], L. Pizzimento[66b], A. Pizzini[118], M.-A. Pleier[30], V. Pleskot[137], E. Plotnikova[40], G. Poddar[97], R. Poettgen[101], L. Poggioli[131], S. Polacek[137], G. Polesello[75a], A. Poley[147,160a], A. Polini[24b], C. S. Pollard[172], Z. B. Pollock[123], E. Pompa Pacchi[124], N. I. Pond[99], D. Ponomarenko[70], L. Pontecorvo[37], S. Popa[28a], G. A. Popeneciu[28d], A. Poreba[37], D. M. Portillo Quintero[160a], S. Pospisil[136], M. A. Postill[144], P. Postolache[28c], K. Potamianos[172], P. A. Potepa[88a], I. N. Potrap[40], C. J. Potter[33], H. Potti[152], J. Poveda[168], M. E. Pozo Astigarraga[37], A. Prades Ibanez[78a,78b], J. Pretel[170], D. Price[104], M. Primavera[72a], L. Primomo[71a,71c], M. A. Principe Martin[102], R. Privara[126], T. Procter[61], M. L. Proffitt[143], N. Proklova[132], K. Prokofiev[66c], G. Proto[113], J. Proudfoot[6], M. Przybycien[88a], W. W. Przygoda[88b], A. Psallidas[48], J. E. Puddefoot[144], D. Pudzha[56], D. Pyatiizbyantseva[38], J. Qian[109], R. Qian[110], D. Qichen[104], Y. Qin[13], T. Qiu[54], A. Quadt[57], M. Queitsch-Maitland[104], G. Quetant[58], R. P. Quinn[169], G. Rabanal Bolanos[63], D. Rafanoharana[56], F. Raffaeli[78a,78b], F. Ragusa[73a,73b], J. L. Rainbolt[41], J. A. Raine[58], S. Rajagopalan[30], E. Ramakoti[38], L. Rambelli[59a,59b], I. A. Ramirez-Berend[35], K. Ran[50,115c], D. S. Rankin[132], N. P. Rapheeha[34g], H. Rasheed[28b], V. Raskina[131], D. F. Rassloff[65a], A. Rastogi[18a], S. Rave[103], S. Ravera[59a,59b], B. Ravina[57], I. Ravinovich[174], M. Raymond[37], A. L. Read[129], N. P. Readioff[144], D. M. Rebuzzi[75a,75b], G. Redlinger[30], A. S. Reed[113], K. Reeves[27], J. A. Reidelsturz[176], D. Reikher[127], A. Rej[51], C. Rembser[37], M. Renda[28b], F. Renner[50], A. G. Rennie[163], A. L. Rescia[50], S. Resconi[73a], M. Ressegotti[59a,59b], S. Rettie[37], J. G. Reyes Rivera[110], E. Reynolds[18a], O. L. Rezanova[38], P. Reznicek[137], H. Riani[36d], N. Ribaric[53], E. Ricci[80a,80b], R. Richter[113], S. Richter[49a,49b], E. Richter-Was[88b], M. Ridel[131], S. Ridouani[36d], P. Rieck[121], P. Riedler[37], E. M. Riefel[49a,49b], J. O. Rieger[118], M. Rijssenbeek[150], M. Rimoldi[37], L. Rinaldi[24a,24b], P. Rincke[57], T. T. Rinn[30], M. P. Rinnagel[112], G. Ripellino[166], I. Riu[13], J. C. Rivera Vergara[170], F. Rizatdinova[125], E. Rizvi[97], B. R. Roberts[18a], S. S. Roberts[140], S. H. Robertson[107,y], D. Robinson[33], M. Robles Manzano[103], A. Robson[61], A. Rocchi[78a,78b], C. Roda[76a,76b], S. Rodriguez Bosca[37], Y. Rodriguez Garcia[23a], A. M. Rodríguez Vera[119], S. Roe[37], J. T. Roemer[37], A. R. Roepe-Gier[140], O. Røhne[129], R. A. Rojas[37], C. P. A. Roland[131], J. Roloff[30], A. Romaniouk[81], E. Romano[75a,75b], M. Romano[24b], A. C. Romero Hernandez[167], N. Rompotis[95], L. Roos[131], S. Rosati[77a], B. J. Rosser[41], E. Rossi[130], E. Rossi[74a,74b], L. P. Rossi[63], L. Rossini[56], R. Rosten[123], M. Rotaru[28b], B. Rottler[56], C. Rougier[92], D. Rousseau[68], D. Rousso[50], A. Roy[167], S. Roy-Garand[159], A. Rozanov[105], Z. M. A. Rozario[61], Y. Rozen[155], A. Rubio Jimenez[168], V. H. Ruelas Rivera[19], T. A. Ruggeri[1], A. Ruggiero[130], A. Ruiz-Martinez[168], A. Rummler[37], Z. Rurikova[56], N. A. Rusakovich[40], H. L. Russell[170], G. Russo[77a,77b], J. P. Rutherfoord[7], S. Rutherford Colmenares[33], M. Rybar[137], E. B. Rye[129], A. Ryzhov[46], J. A. Sabater Iglesias[58], H.F.-W. Sadrozinski[140], F. Safai Tehrani[77a], B. Safarzadeh Samani[138], S. Saha[1], M. Sahinsoy[84], A. Saibel[168], M. Saimpert[139], M. Saito[158], T. Saito[158], A. Sala[73a,73b],

D. Salamani[37], A. Salnikov[148], J. Salt[168], A. Salvador Salas[156], D. Salvatore[45a,45b], F. Salvatore[151], A. Salzburger[37], D. Sammel[56], E. Sampson[94], D. Sampsonidis[157,e], D. Sampsonidou[127], J. Sánchez[168], V. Sanchez Sebastian[168], H. Sandaker[129], C. O. Sander[50], J. A. Sandesara[106], M. Sandhoff[176], C. Sandoval[23b], L. Sanfilippo[65a], D. P. C. Sankey[138], T. Sano[90], A. Sansoni[55], L. Santi[37,77b], C. Santoni[42], H. Santos[134a,134b], A. Santra[174], E. Sanzani[24a,24b], K. A. Saoucha[165], J. G. Saraiva[134a,134d], J. Sardain[7], O. Sasaki[86], K. Sato[161], C. Sauer[37], E. Sauvan[4], P. Savard[159,ae], R. Sawada[158], C. Sawyer[138], L. Sawyer[100], C. Sbarra[24b], A. Sbrizzi[24a,24b], T. Scanlon[99], J. Schaarschmidt[143], U. Schäfer[103], A. C. Schaffer[46,68], D. Schaile[112], R. D. Schamberger[150], C. Scharf[19], M. M. Schefer[20], V. A. Schegelsky[38], D. Scheirich[137], M. Schernau[141e], C. Scheulen[57], C. Schiavi[59a,59b], M. Schioppa[45a,45b], B. Schlag[148], S. Schlenker[37], J. Schmeing[176], M. A. Schmidt[176], K. Schmieden[103], C. Schmitt[103], N. Schmitt[103], S. Schmitt[50], L. Schoeffel[139], A. Schoening[65b], P. G. Scholer[35], E. Schopf[130], M. Schott[25], J. Schovancova[37], S. Schramm[58], T. Schroer[58], H.-C. Schultz-Coulon[65a], M. Schumacher[56], B. A. Schumm[140], Ph. Schune[139], A. J. Schuy[143], H. R. Schwartz[140], A. Schwartzman[148], T. A. Schwarz[109], Ph. Schwemling[139], R. Schwienhorst[110], F. G. Sciacca[20], A. Sciandra[30], G. Sciolla[27], F. Scuri[76a], C. D. Sebastiani[95], K. Sedlaczek[119], S. C. Seidel[116], A. Seiden[140], B. D. Seidlitz[43], C. Seitz[50], J. M. Seixas[85b], G. Sekhniaidze[74a], L. Selem[62], N. Semprini-Cesari[24a,24b], A. Semushin[38,178], D. Sengupta[58], V. Senthilkumar[168], L. Serin[68], M. Sessa[78a,78b], H. Severini[124], F. Sforza[59a,59b], A. Sfyrla[58], Q. Sha[14], E. Shabalina[57], A. H. Shah[33], R. Shaheen[149], J. D. Shahinian[132], D. Shaked Renous[174], L. Y. Shan[14], M. Shapiro[18a], A. Sharma[37], A. S. Sharma[169], P. Sharma[82], P. B. Shatalov[38], K. Shaw[151], S. M. Shaw[104], Q. Shen[64c], D. J. Sheppard[147], P. Sherwood[99], L. Shi[99], X. Shi[14], S. Shimizu[86], C. O. Shimmin[177], I. P. J. Shipsey[130,*], S. Shirabe[91], M. Shiyakova[40,w], M. J. Shochet[41], D. R. Shope[129], B. Shrestha[124], S. Shrestha[123,ah], I. Shreyber[38], M. J. Shroff[170], P. Sicho[135], A. M. Sickles[167], E. Sideras Haddad[34g,164], A. C. Sidley[118], A. Sidoti[24b], F. Siegert[52], Dj. Sijacki[16], F. Sili[93], J. M. Silva[54], I. Silva Ferreira[85b], M. V. Silva Oliveira[30], S. B. Silverstein[49a], S. Simion[68], R. Simoniello[37], E. L. Simpson[104], H. Simpson[151], L. R. Simpson[109], S. Simsek[84], S. Sindhu[57], P. Sinervo[159], S. Singh[30], S. Sinha[50], S. Sinha[104], M. Sioli[24a,24b], I. Siral[37], E. Sitnikova[50], J. Sjölin[49a,49b], A. Skaf[57], E. Skorda[21], P. Skubic[124], M. Slawinska[89], I. Slazyk[17], V. Smakhtin[174], B. H. Smart[138], S.Yu. Smirnov[38], Y. Smirnov[38], L. N. Smirnova[38,a], O. Smirnova[101], A. C. Smith[43], D. R. Smith[163], E. A. Smith[41], J. L. Smith[104], R. Smith[148], H. Smitmanns[103], M. Smizanska[94], K. Smolek[136], A. A. Snesarev[38], H. L. Snoek[118], S. Snyder[30], R. Sobie[170,y], A. Soffer[156], C. A. Solans Sanchez[37], E.Yu. Soldatov[38], U. Soldevila[168], A. A. Solodkov[38], S. Solomon[27], A. Soloshenko[40], K. Solovieva[56], O. V. Solovyanov[42], P. Sommer[52], A. Sonay[13], W. Y. Song[160b], A. Sopczak[136], A. L. Sopio[54], F. Sopkova[29b], J. D. Sorenson[116], I. R. Sotarriva Alvarez[142], V. Sothilingam[65a], O. J. Soto Sandoval[141b,141c], S. Sottocornola[70], R. Soualah[165], Z. Soumaimi[36e], D. South[50], N. Soybelman[174], S. Spagnolo[72a,72b], M. Spalla[113], D. Sperlich[56], G. Spigo[37], B. Spisso[74a,74b], D. P. Spiteri[61], M. Spousta[137], E. J. Staats[35], R. Stamen[65a], A. Stampekis[21], E. Stanecka[89], W. Stanek-Maslouska[50], M. V. Stange[52], B. Stanislaus[18a], M. M. Stanitzki[50], B. Stapf[50], E. A. Starchenko[38], G. H. Stark[140], J. Stark[92], P. Staroba[135], P. Starovoitov[65a], S. Stärz[107], R. Staszewski[89], G. Stavropoulos[48], A. Stefl[37], P. Steinberg[30], B. Stelzer[147,160a], H. J. Stelzer[133], O. Stelzer-Chilton[160a], H. Stenzel[60], T. J. Stevenson[151], G. A. Stewart[37], J. R. Stewart[125], M. C. Stockton[37], G. Stoicea[28b], M. Stolarski[134a], S. Stonjek[113], A. Straessner[52], J. Strandberg[149], S. Strandberg[49a,49b], M. Stratmann[176], M. Strauss[124], T. Strebler[105], P. Strizenec[29b], R. Ströhmer[171], D. M. Strom[127], R. Stroynowski[46], A. Strubig[49a,49b], S. A. Stucci[30], B. Stugu[17], J. Stupak[124], N. A. Styles[50], D. Su[148], S. Su[64a], W. Su[64d], X. Su[64a], D. Suchy[29a], K. Sugizaki[158], V. V. Sulin[38], M. J. Sullivan[95], D. M. S. Sultan[130], L. Sultanaliyeva[38], S. Sultansoy[3b], T. Sumida[90], S. Sun[175], W. Sun[14], O. Sunneborn Gudnadottir[166], N. Sur[105], M. R. Sutton[151], H. Suzuki[161], M. Svatos[135], M. Swiatlowski[160a], T. Swirski[171], I. Sykora[29a], M. Sykora[137], T. Sykora[137], D. Ta[103], K. Tackmann[50,v], A. Taffard[163], R. Tafirout[160a], J. S. Tafoya Vargas[68], Y. Takubo[86], M. Talby[105], A. A. Talyshev[38], K. C. Tam[66b], N. M. Tamir[156], A. Tanaka[158], J. Tanaka[158], R. Tanaka[68], M. Tanasini[150], Z. Tao[169], S. Tapia Araya[141f], S. Tapprogge[103], A. Tarek Abouelfadl Mohamed[110], S. Tarem[155], K. Tariq[14], G. Tarna[28b], G. F. Tartarelli[73a], M. J. Tartarin[92], P. Tas[137], M. Tasevsky[135], E. Tassi[45a,45b], A. C. Tate[167], G. Tateno[158], Y. Tayalati[36e,x], G. N. Taylor[108], W. Taylor[160b], P. Teixeira-Dias[98], J. J. Teoh[159], K. Terashi[158], J. Terron[102], S. Terzo[13], M. Testa[55], R. J. Teuscher[159,y], A. Thaler[81], O. Theiner[58], T. Theveneaux-Pelzer[105], O. Thielmann[176], D. W. Thomas[98], J. P. Thomas[21], E. A. Thompson[18a], P. D. Thompson[21], E. Thomson[132], R. E. Thornberry[46], C. Tian[64a], Y. Tian[58], V. Tikhomirov[38,a], Yu.A. Tikhonov[38], S. Timoshenko[38], D. Timoshyn[137], E. X. L. Ting[1], P. Tipton[177], A. Tishelman-Charny[30], S. H. Tlou[34g], K. Todome[142],

S. Todorova-Nova[137], S. Todt[52], L. Toffolin[71a,71c], M. Togawa[86], J. Tojo[91], S. Tokár[29a], K. Tokushuku[86], O. Toldaiev[70], M. Tomoto[86,114], L. Tompkins[148,m], K. W. Topolnicki[88b], E. Torrence[127], H. Torres[92], E. Torró Pastor[168], M. Toscani[31], C. Tosciri[41], M. Tost[11], D. R. Tovey[144], I. S. Trandafir[28b], T. Trefzger[171], A. Tricoli[30], I. M. Trigger[160a], S. Trincaz-Duvoid[131], D. A. Trischuk[27], B. Trocmé[62], A. Tropina[40], L. Truong[34c], M. Trzebinski[89], A. Trzupek[89], F. Tsai[150], M. Tsai[109], A. Tsiamis[157], P. V. Tsiareshka[40], S. Tsigaridas[160a], A. Tsirigotis[157,s], V. Tsiskaridze[159], E. G. Tskhadadze[154a], M. Tsopoulou[157], Y. Tsujikawa[90], I. I. Tsukerman[38], V. Tsulaia[18a], S. Tsuno[86], K. Tsuri[122], D. Tsybychev[150], Y. Tu[66b], A. Tudorache[28b], V. Tudorache[28b], A. N. Tuna[63], S. Turchikhin[59a,59b], I. Turk Cakir[3a], R. Turra[73a], T. Turtuvshin[40,z], P. M. Tuts[43], S. Tzamarias[157,e], E. Tzovara[103], F. Ukegawa[161], P. A. Ulloa Poblete[141b,141c], E. N. Umaka[30], G. Unal[37], A. Undrus[30], G. Unel[163], J. Urban[29b], P. Urrejola[141a], G. Usai[8], R. Ushioda[142], M. Usman[111], F. Ustuner[54], Z. Uysal[84], V. Vacek[136], B. Vachon[107], T. Vafeiadis[37], A. Vaitkus[99], C. Valderanis[112], E. Valdes Santurio[49a,49b], M. Valente[160a], S. Valentinetti[24a,24b], A. Valero[168], E. Valiente Moreno[168], A. Vallier[92], J. A. Valls Ferrer[168], D. R. Van Arneman[118], T. R. Van Daalen[143], A. Van Der Graaf[51], P. Van Gemmeren[6], M. Van Rijnbach[37], S. Van Stroud[99], I. Van Vulpen[118], P. Vana[137], M. Vanadia[78a,78b], U. M. Vande Voorde[149], W. Vandelli[37], E. R. Vandewall[125], D. Vannicola[156], L. Vannoli[55], R. Vari[77a], E. W. Varnes[7], C. Varni[18b], T. Varol[153], D. Varouchas[68], L. Varriale[168], K. E. Varvell[152], M. E. Vasile[28b], L. Vaslin[86], A. Vasyukov[40], L. M. Vaughan[125], R. Vavricka[103], T. Vazquez Schroeder[37], J. Veatch[32], V. Vecchio[104], M. J. Veen[106], I. Veliscek[30], L. M. Veloce[159], F. Veloso[134a,134c], S. Veneziano[77a], A. Ventura[72a,72b], S. Ventura Gonzalez[139], A. Verbytskyi[113], M. Verducci[76a,76b], C. Vergis[97], M. Verissimo De Araujo[85b], W. Verkerke[118], J. C. Vermeulen[118], C. Vernieri[148], M. Vessella[106], M. C. Vetterli[147,ae], A. Vgenopoulos[103], N. Viaux Maira[141f], T. Vickey[144], O. E. Vickey Boeriu[144], G. H. A. Viehhauser[130], L. Vigani[65b], M. Vigl[113], M. Villa[24a,24b], M. Villaplana Perez[168], E. M. Villhauer[54], E. Vilucchi[55], M. G. Vincter[35], A. Visibile[118], C. Vittori[37], I. Vivarelli[24a,24b], E. Voevodina[113], F. Vogel[112], J. C. Voigt[52], P. Vokac[136], Yu. Volkotrub[88b], E. Von Toerne[25], B. Vormwald[37], V. Vorobel[137], K. Vorobev[38], M. Vos[168], K. Voss[146], M. Vozak[118], L. Vozdecky[124], N. Vranjes[16], M. Vranjes Milosavljevic[16], M. Vreeswijk[118], N. K. Vu[64c,64d], R. Vuillermet[37], O. Vujinovic[103], I. Vukotic[41], I. K. Vyas[35], S. Wada[161], C. Wagner[148], J. M. Wagner[18a], W. Wagner[176], S. Wahdan[176], H. Wahlberg[93], C. H. Waits[124], J. Walder[138], R. Walker[112], W. Walkowiak[146], A. Wall[132], E. J. Wallin[101], T. Wamorkar[6], A. Z. Wang[140], C. Wang[103], C. Wang[11], H. Wang[18a], J. Wang[66c], P. Wang[104], P. Wang[99], R. Wang[63], R. Wang[6], S. M. Wang[153], S. Wang[14], T. Wang[64a], W. T. Wang[82], W. Wang[14], X. Wang[115a], X. Wang[167], X. Wang[64c], Y. Wang[64d], Y. Wang[115a], Y. Wang[64a], Z. Wang[109], Z. Wang[53,64c,64d], Z. Wang[109], A. Warburton[107], R. J. Ward[21], N. Warrack[61], S. Waterhouse[98], A. T. Watson[21], H. Watson[54], M. F. Watson[21], E. Watton[61,138], G. Watts[143], B. M. Waugh[99], J. M. Webb[56], C. Weber[30], H. A. Weber[19], M. S. Weber[20], S. M. Weber[65a], C. Wei[64a], Y. Wei[56], A. R. Weidberg[130], E. J. Weik[121], J. Weingarten[51], C. Weiser[56], C. J. Wells[50], T. Wenaus[30], B. Wendland[51], T. Wengler[37], N. S. Wenke[113], N. Wermes[25], M. Wessels[65a], A. M. Wharton[94], A. S. White[63], A. White[8], M. J. White[1], D. Whiteson[163], L. Wickremasinghe[128], W. Wiedenmann[175], M. Wielers[138], C. Wiglesworth[44], D. J. Wilbern[124], H. G. Wilkens[37], J. J. H. Wilkinson[33], D. M. Williams[43], H. H. Williams[132], S. Williams[33], S. Willocq[106], B. J. Wilson[104], P. J. Windischhofer[41], F. I. Winkel[31], F. Winklmeier[127], B. T. Winter[56], J. K. Winter[104], M. Wittgen[148], M. Wobisch[100], T. Wojtkowski[62], Z. Wolffs[118], J. Wollrath[37], M. W. Wolter[89], H. Wolters[134a,134c], M. C. Wong[140], E. L. Woodward[43], S. D. Worm[50], B. K. Wosiek[89], K. W. Woźniak[89], S. Wozniewski[57], K. Wraight[61], C. Wu[21], M. Wu[115b], M. Wu[117], S. L. Wu[175], X. Wu[58], Y. Wu[64a], Z. Wu[4], J. Wuerzinger[113,ac], T. R. Wyatt[104], B. M. Wynne[54], S. Xella[44], L. Xia[115a], M. Xia[15], M. Xie[64a], S. Xin[14,115c], A. Xiong[127], J. Xiong[18a], D. Xu[14], H. Xu[64a], L. Xu[64a], R. Xu[132], T. Xu[109], Y. Xu[143], Z. Xu[54], Z. Xu[115a], B. Yabsley[152], S. Yacoob[34a], Y. Yamaguchi[86], E. Yamashita[158], H. Yamauchi[161], T. Yamazaki[18a], Y. Yamazaki[87], S. Yan[61], Z. Yan[106], H. J. Yang[64c,64d], H. T. Yang[64a], S. Yang[64a], T. Yang[66c], X. Yang[37], X. Yang[14], Y. Yang[46], Y. Yang[64a], W.-M. Yao[18a], H. Ye[115a], H. Ye[57], J. Ye[14], S. Ye[30], X. Ye[64a], Y. Yeh[99], I. Yeletskikh[40], B. Yeo[18b], M. R. Yexley[99], T. P. Yildirim[130], P. Yin[43], K. Yorita[173], S. Younas[28b], C. J. S. Young[37], C. Young[148], C. Yu[14,115c], Y. Yu[64a], J. Yuan[14,115c], M. Yuan[109], R. Yuan[64c,64d], L. Yue[99], M. Zaazoua[64a], B. Zabinski[89], I. Zahir[36a], E. Zaid[54], Z. K. Zak[89], T. Zakareishvili[168], S. Zambito[58], J. A. Zamora Saa[141b,141d], J. Zang[158], D. Zanzi[56], R. Zanzottera[73a,73b], O. Zaplatilek[136], C. Zeitnitz[176], H. Zeng[14], J. C. Zeng[167], D. T. Zenger Jr[27], O. Zenin[38], T. Ženiš[29a], S. Zenz[97], S. Zerradi[36a], D. Zerwas[68], M. Zhai[14,115c], D. F. Zhang[144], J. Zhang[64b], J. Zhang[6], K. Zhang[14,115c], L. Zhang[64a], L. Zhang[115a], P. Zhang[14,115c], R. Zhang[175], S. Zhang[109], S. Zhang[92],

T. Zhang[158], X. Zhang[64c], Y. Zhang[143], Y. Zhang[99], Y. Zhang[115a], Z. Zhang[18a], Z. Zhang[64b], Z. Zhang[68], H. Zhao[143], T. Zhao[64b], Y. Zhao[140], Z. Zhao[64a], Z. Zhao[64a], A. Zhemchugov[40], J. Zheng[115a], K. Zheng[167], X. Zheng[64a], Z. Zheng[148], D. Zhong[167], B. Zhou[109], H. Zhou[7], N. Zhou[64c], Y. Zhou[15], Y. Zhou[115a], Y. Zhou[7], C. G. Zhu[64b], J. Zhu[109], X. Zhu[64d], Y. Zhu[64c], Y. Zhu[64a], X. Zhuang[14], K. Zhukov[70], N. I. Zimine[40], J. Zinsser[65b], M. Ziolkowski[146], L. Živković[16], A. Zoccoli[24a,24b], K. Zoch[63], T. G. Zorbas[144], O. Zormpa[48], W. Zou[43], L. Zwalinski[37]

[1] Department of Physics, University of Adelaide, Adelaide, Australia
[2] Department of Physics, University of Alberta, Edmonton, AB, Canada
[3] [(a)]Department of Physics, Ankara University, Ankara, Turkey; [(b)]Division of Physics, TOBB University of Economics and Technology, Ankara, Turkey
[4] LAPP, Université Savoie Mont Blanc, CNRS/IN2P3, Annecy, France
[5] APC, Université Paris Cité, CNRS/IN2P3, Paris, France
[6] High Energy Physics Division, Argonne National Laboratory, Argonne, IL, USA
[7] Department of Physics, University of Arizona, Tucson, AZ, USA
[8] Department of Physics, University of Texas at Arlington, Arlington, TX, USA
[9] Physics Department, National and Kapodistrian University of Athens, Athens, Greece
[10] Physics Department, National Technical University of Athens, Zografou, Greece
[11] Department of Physics, University of Texas at Austin, Austin, TX, USA
[12] Institute of Physics, Azerbaijan Academy of Sciences, Baku, Azerbaijan
[13] Institut de Física d'Altes Energies (IFAE), Barcelona Institute of Science and Technology, Barcelona, Spain
[14] Institute of High Energy Physics, Chinese Academy of Sciences, Beijing, China
[15] Physics Department, Tsinghua University, Beijing, China
[16] Institute of Physics, University of Belgrade, Belgrade, Serbia
[17] Department for Physics and Technology, University of Bergen, Bergen, Norway
[18] [(a)]Physics Division, Lawrence Berkeley National Laboratory, Berkeley, CA, USA; [(b)]University of California, Berkeley, CA, USA
[19] Institut für Physik, Humboldt Universität zu Berlin, Berlin, Germany
[20] Albert Einstein Center for Fundamental Physics and Laboratory for High Energy Physics, University of Bern, Bern, Switzerland
[21] School of Physics and Astronomy, University of Birmingham, Birmingham, UK
[22] [(a)]Department of Physics, Bogazici University, Istanbul, Turkey; [(b)]Department of Physics Engineering, Gaziantep University, Gaziantep, Turkey; [(c)]Department of Physics, Istanbul University, Istanbul, Turkey
[23] [(a)]Facultad de Ciencias y Centro de Investigaciónes, Universidad Antonio Nariño, Bogotá, Colombia; [(b)]Departamento de Física, Universidad Nacional de Colombia, Bogotá, Colombia
[24] [(a)]Dipartimento di Fisica e Astronomia A. Righi, Università di Bologna, Bologna, Italy; [(b)]INFN Sezione di Bologna, Bologna, Italy
[25] Physikalisches Institut, Universität Bonn, Bonn, Germany
[26] Department of Physics, Boston University, Boston, MA, USA
[27] Department of Physics, Brandeis University, Waltham, MA, USA
[28] [(a)]Transilvania University of Brasov, Brasov, Romania; [(b)]Horia Hulubei National Institute of Physics and Nuclear Engineering, Bucharest, Romania; [(c)]Department of Physics, Alexandru Ioan Cuza University of Iasi, Iasi, Romania; [(d)]National Institute for Research and Development of Isotopic and Molecular Technologies, Physics Department, Cluj-Napoca, Romania; [(e)]National University of Science and Technology Politechnica, Bucharest, Romania; [(f)]West University in Timisoara, Timisoara, Romania; [(g)]Faculty of Physics, University of Bucharest, Bucharest, Romania
[29] [(a)]Faculty of Mathematics, Physics and Informatics, Comenius University, Bratislava, Slovakia; [(b)]Department of Subnuclear Physics, Institute of Experimental Physics of the Slovak Academy of Sciences, Kosice, Slovak Republic
[30] Physics Department, Brookhaven National Laboratory, Upton, NY, USA
[31] Universidad de Buenos Aires, Facultad de Ciencias Exactas y Naturales, Departamento de Física, y CONICET, Instituto de Física de Buenos Aires (IFIBA), Buenos Aires, Argentina
[32] California State University, Long Beach, CA, USA
[33] Cavendish Laboratory, University of Cambridge, Cambridge, UK

[34] [(a)]Department of Physics, University of Cape Town, Cape Town, South Africa; [(b)]iThemba Labs, Cape Town, Western Cape, South Africa; [(c)]Department of Mechanical Engineering Science, University of Johannesburg, Johannesburg, South Africa; [(d)]National Institute of Physics, University of the Philippines Diliman (Philippines), Quezon City, Philippines; [(e)]University of South Africa, Department of Physics, Pretoria, South Africa; [(f)]University of Zululand, KwaDlangezwa, South Africa; [(g)]School of Physics, University of the Witwatersrand, Johannesburg, South Africa
[35] Department of Physics, Carleton University, Ottawa, ON, Canada
[36] [(a)]Faculté des Sciences Ain Chock, Université Hassan II de Casablanca, Casablanca, Morocco; [(b)]Faculté des Sciences, Université Ibn-Tofail, Kénitra, Morocco; [(c)]Faculté des Sciences Semlalia, Université Cadi Ayyad, LPHEA-Marrakech, Marrakesh, Morocco; [(d)]LPMR, Faculté des Sciences, Université Mohamed Premier, Oujda, Morocco; [(e)]Faculté des sciences, Université Mohammed V, Rabat, Morocco; [(f)]Institute of Applied Physics, Mohammed VI Polytechnic University, Ben Guerir, Morocco
[37] CERN, Geneva, Switzerland
[38] Affiliated with an Institute Covered by a Cooperation Agreement with CERN, Geneva, Switzerland
[39] Affiliated with an Institute Formerly Covered by a Cooperation Agreement with CERN, Geneva, Switzerland
[40] Affiliated with an International Laboratory Covered by a Cooperation Agreement with CERN, Geneva, Switzerland
[41] Enrico Fermi Institute, University of Chicago, Chicago, IL, USA
[42] LPC, Université Clermont Auvergne, CNRS/IN2P3, Clermont-Ferrand, France
[43] Nevis Laboratory, Columbia University, Irvington, NY, USA
[44] Niels Bohr Institute, University of Copenhagen, Copenhagen, Denmark
[45] [(a)]Dipartimento di Fisica, Università della Calabria, Rende, Italy; [(b)]INFN Gruppo Collegato di Cosenza, Laboratori Nazionali di Frascati, Frascati, Italy
[46] Physics Department, Southern Methodist University, Dallas, TX, USA
[47] Physics Department, University of Texas at Dallas, Richardson, TX, USA
[48] National Centre for Scientific Research "Demokritos", Agia Paraskevi, Greece
[49] [(a)]Department of Physics, Stockholm University, Stockholm, Sweden; [(b)]Oskar Klein Centre, Stockholm, Sweden
[50] Deutsches Elektronen-Synchrotron DESY, Hamburg and Zeuthen, Germany
[51] Fakultät Physik, Technische Universität Dortmund, Dortmund, Germany
[52] Institut für Kern- und Teilchenphysik, Technische Universität Dresden, Dresden, Germany
[53] Department of Physics, Duke University, Durham, NC, USA
[54] SUPA-School of Physics and Astronomy, University of Edinburgh, Edinburgh, UK
[55] INFN e Laboratori Nazionali di Frascati, Frascati, Italy
[56] Physikalisches Institut, Albert-Ludwigs-Universität Freiburg, Freiburg, Germany
[57] II. Physikalisches Institut, Georg-August-Universität Göttingen, Göttingen, Germany
[58] Département de Physique Nucléaire et Corpusculaire, Université de Genève, Geneva, Switzerland
[59] [(a)]Dipartimento di Fisica, Università di Genova, Genoa, Italy; [(b)]INFN Sezione di Genova, Genoa, Italy
[60] II. Physikalisches Institut, Justus-Liebig-Universität Giessen, Giessen, Germany
[61] SUPA-School of Physics and Astronomy, University of Glasgow, Glasgow, UK
[62] LPSC, Université Grenoble Alpes, CNRS/IN2P3, Grenoble INP, Grenoble, France
[63] Laboratory for Particle Physics and Cosmology, Harvard University, Cambridge, MA, USA
[64] [(a)]Department of Modern Physics and State Key Laboratory of Particle Detection and Electronics, University of Science and Technology of China, Hefei, China; [(b)]Institute of Frontier and Interdisciplinary Science and Key Laboratory of Particle Physics and Particle Irradiation (MOE), Shandong University, Qingdao, China; [(c)]School of Physics and Astronomy, Shanghai Jiao Tong University, Key Laboratory for Particle Astrophysics and Cosmology (MOE), SKLPPC, Shanghai, China; [(d)]Tsung-Dao Lee Institute, Shanghai, China; [(e)]School of Physics, Zhengzhou University, Zhengzhou, China
[65] [(a)]Kirchhoff-Institut für Physik, Ruprecht-Karls-Universität Heidelberg, Heidelberg, Germany; [(b)]Physikalisches Institut, Ruprecht-Karls-Universität Heidelberg, Heidelberg, Germany
[66] [(a)]Department of Physics, Chinese University of Hong Kong, Shatin, N.T., Hong Kong; [(b)]Department of Physics, University of Hong Kong, Pok Fu Lam, Hong Kong; [(c)]Department of Physics and Institute for Advanced Study, Hong Kong University of Science and Technology, Clear Water Bay, Kowloon, Hong Kong, China
[67] Department of Physics, National Tsing Hua University, Hsinchu, Taiwan
[68] IJCLab, Université Paris-Saclay, CNRS/IN2P3, 91405 Orsay, France
[69] Centro Nacional de Microelectrónica (IMB-CNM-CSIC), Barcelona, Spain

[70] Department of Physics, Indiana University, Bloomington, IN, USA
[71] [(a)]INFN Gruppo Collegato di Udine, Sezione di Trieste, Udine, Italy; [(b)]ICTP, Trieste, Italy; [(c)]Dipartimento Politecnico di Ingegneria e Architettura, Università di Udine, Udine, Italy
[72] [(a)]INFN Sezione di Lecce, Lecce, Italy; [(b)]Dipartimento di Matematica e Fisica, Università del Salento, Lecce, Italy
[73] [(a)]INFN Sezione di Milano, Milan, Italy; [(b)]Dipartimento di Fisica, Università di Milano, Milan, Italy
[74] [(a)]INFN Sezione di Napoli, Naples, Italy; [(b)]Dipartimento di Fisica, Università di Napoli, Naples, Italy
[75] [(a)]INFN Sezione di Pavia, Pavia, Italy; [(b)]Dipartimento di Fisica, Università di Pavia, Pavia, Italy
[76] [(a)]INFN Sezione di Pisa, Pisa, Italy; [(b)]Dipartimento di Fisica E. Fermi, Università di Pisa, Pisa, Italy
[77] [(a)]INFN Sezione di Roma, Rome, Italy; [(b)]Dipartimento di Fisica, Sapienza Università di Roma, Rome, Italy
[78] [(a)]INFN Sezione di Roma Tor Vergata, Rome, Italy; [(b)]Dipartimento di Fisica, Università di Roma Tor Vergata, Rome, Italy
[79] [(a)]INFN Sezione di Roma Tre, Rome, Italy; [(b)]Dipartimento di Matematica e Fisica, Università Roma Tre, Rome, Italy
[80] [(a)]INFN-TIFPA, Povo, Italy; [(b)]Università degli Studi di Trento, Trento, Italy
[81] Universität Innsbruck, Department of Astro and Particle Physics, Innsbruck, Austria
[82] University of Iowa, Iowa City, IA, USA
[83] Department of Physics and Astronomy, Iowa State University, Ames, IA, USA
[84] Istinye University, Sariyer, Istanbul, Turkey
[85] [(a)]Departamento de Engenharia Elétrica, Universidade Federal de Juiz de Fora (UFJF), Juiz de Fora, Brazil; [(b)]Universidade Federal do Rio de Janeiro COPPE/EE/IF, Rio de Janeiro, Brazil; [(c)]Instituto de Física, Universidade de São Paulo, São Paulo, Brazil; [(d)]Rio de Janeiro State University, Rio de Janeiro, Brazil; [(e)]Federal University of Bahia, Bahia, Brazil
[86] KEK, High Energy Accelerator Research Organization, Tsukuba, Japan
[87] Graduate School of Science, Kobe University, Kobe, Japan
[88] [(a)]Faculty of Physics and Applied Computer Science, AGH University of Krakow, Krakow, Poland; [(b)]Marian Smoluchowski Institute of Physics, Jagiellonian University, Krakow, Poland
[89] Institute of Nuclear Physics Polish Academy of Sciences, Krakow, Poland
[90] Faculty of Science, Kyoto University, Kyoto, Japan
[91] Research Center for Advanced Particle Physics and Department of Physics, Kyushu University, Fukuoka , Japan
[92] L2IT, Université de Toulouse, CNRS/IN2P3, UPS, Toulouse, France
[93] Instituto de Física La Plata, Universidad Nacional de La Plata and CONICET, La Plata, Argentina
[94] Physics Department, Lancaster University, Lancaster, UK
[95] Oliver Lodge Laboratory, University of Liverpool, Liverpool, UK
[96] Department of Experimental Particle Physics, Jožef Stefan Institute and Department of Physics, University of Ljubljana, Ljubljana, Slovenia
[97] Department of Physics and Astronomy, Queen Mary University of London, London, UK
[98] Department of Physics, Royal Holloway University of London, Egham, UK
[99] Department of Physics and Astronomy, University College London, London, UK
[100] Louisiana Tech University, Ruston, LA, USA
[101] Fysiska institutionen, Lunds universitet, Lund, Sweden
[102] Departamento de Física Teorica C-15 and CIAFF, Universidad Autónoma de Madrid, Madrid, Spain
[103] Institut für Physik, Universität Mainz, Mainz, Germany
[104] School of Physics and Astronomy, University of Manchester, Manchester, UK
[105] CPPM, Aix-Marseille Université, CNRS/IN2P3, Marseille, France
[106] Department of Physics, University of Massachusetts, Amherst, MA, USA
[107] Department of Physics, McGill University, Montreal, QC, Canada
[108] School of Physics, University of Melbourne, Melbourne, VIC, Australia
[109] Department of Physics, University of Michigan, Ann Arbor, MI, USA
[110] Department of Physics and Astronomy, Michigan State University, East Lansing, MI, USA
[111] Group of Particle Physics, University of Montreal, Montreal, QC, Canada
[112] Fakultät für Physik, Ludwig-Maximilians-Universität München, Munich, Germany
[113] Max-Planck-Institut für Physik (Werner-Heisenberg-Institut), Munich, Germany
[114] Graduate School of Science and Kobayashi-Maskawa Institute, Nagoya University, Nagoya, Japan

[115] [(a)]Department of Physics, Nanjing University, Nanjing, China; [(b)]School of Science, Shenzhen Campus of Sun Yat-sen University, Guangzhou, China; [(c)]University of Chinese Academy of Science (UCAS), Beijing, China
[116] Department of Physics and Astronomy, University of New Mexico, Albuquerque, NM, USA
[117] Institute for Mathematics, Astrophysics and Particle Physics, Radboud University/Nikhef, Nijmegen, The Netherlands
[118] Nikhef National Institute for Subatomic Physics and University of Amsterdam, Amsterdam, The Netherlands
[119] Department of Physics, Northern Illinois University, DeKalb, IL, USA
[120] [(a)]New York University Abu Dhabi, Abu Dhabi, United Arab Emirates; [(b)]United Arab Emirates University, Al Ain, United Arab Emirates
[121] Department of Physics, New York University, New York, NY, USA
[122] Ochanomizu University, Otsuka, Bunkyo-ku, Tokyo, Japan
[123] Ohio State University, Columbus, OH, USA
[124] Homer L. Dodge Department of Physics and Astronomy, University of Oklahoma, Norman, OK, USA
[125] Department of Physics, Oklahoma State University, Stillwater, OK, USA
[126] Palacký University, Joint Laboratory of Optics, Olomouc, Czech Republic
[127] Institute for Fundamental Science, University of Oregon, Eugene, OR, USA
[128] Graduate School of Science, Osaka University, Osaka, Japan
[129] Department of Physics, University of Oslo, Oslo, Norway
[130] Department of Physics, Oxford University, Oxford, UK
[131] LPNHE, Sorbonne Université, Université Paris Cité, CNRS/IN2P3, Paris, France
[132] Department of Physics, University of Pennsylvania, Philadelphia, PA, USA
[133] Department of Physics and Astronomy, University of Pittsburgh, Pittsburgh, PA, USA
[134] [(a)]Laboratório de Instrumentação e Física Experimental de Partículas-LIP, Lisbon, Portugal; [(b)]Departamento de Física, Faculdade de Ciências, Universidade de Lisboa, Lisbon, Portugal; [(c)]Departamento de Física, Universidade de Coimbra, Coimbra, Portugal; [(d)]Centro de Física Nuclear da Universidade de Lisboa, Lisbon, Portugal; [(e)]Departamento de Física, Escola de Ciências, Universidade do Minho, Braga, Portugal; [(f)]Departamento de Física Teórica y del Cosmos, Universidad de Granada, Granada, Spain; [(g)]Departamento de Física, Instituto Superior Técnico, Universidade de Lisboa, Lisbon, Portugal
[135] Institute of Physics of the Czech Academy of Sciences, Prague, Czech Republic
[136] Czech Technical University in Prague, Prague, Czech Republic
[137] Faculty of Mathematics and Physics, Charles University, Prague, Czech Republic
[138] Particle Physics Department, Rutherford Appleton Laboratory, Didcot, UK
[139] IRFU, CEA, Université Paris-Saclay, Gif-sur-Yvette, France
[140] Santa Cruz Institute for Particle Physics, University of California Santa Cruz, Santa Cruz, CA, USA
[141] [(a)]Departamento de Física, Pontificia Universidad Católica de Chile, Santiago, Chile; [(b)]Millennium Institute for Subatomic Physics at High Energy Frontier (SAPHIR), Santiago, Chile; [(c)]Instituto de Investigación Multidisciplinario en Ciencia y Tecnología y Departamento de Física, Universidad de La Serena, La Serena, Chile; [(d)]Department of Physics, Universidad Andres Bello, Santiago, Chile; [(e)]Instituto de Alta Investigación, Universidad de Tarapacá, Arica, Chile; [(f)]Departamento de Física, Universidad Técnica Federico Santa María, Valparaíso, Chile
[142] Department of Physics, Institute of Science, Tokyo, Japan
[143] Department of Physics, University of Washington, Seattle, WA, USA
[144] Department of Physics and Astronomy, University of Sheffield, Sheffield, UK
[145] Department of Physics, Shinshu University, Nagano, Japan
[146] Department Physik, Universität Siegen, Siegen, Germany
[147] Department of Physics, Simon Fraser University, Burnaby, BC, Canada
[148] SLAC National Accelerator Laboratory, Stanford, CA, USA
[149] Department of Physics, Royal Institute of Technology, Stockholm, Sweden
[150] Departments of Physics and Astronomy, Stony Brook University, Stony Brook, NY, USA
[151] Department of Physics and Astronomy, University of Sussex, Brighton, UK
[152] School of Physics, University of Sydney, Sydney, Australia
[153] Institute of Physics, Academia Sinica, Taipei, Taiwan
[154] [(a)]E. Andronikashvili Institute of Physics, Iv. Javakhishvili Tbilisi State University, Tbilisi, Georgia; [(b)]High Energy Physics Institute, Tbilisi State University, Tbilisi, Georgia; [(c)]University of Georgia, Tbilisi, Georgia
[155] Department of Physics, Technion, Israel Institute of Technology, Haifa, Israel

[156] Raymond and Beverly Sackler School of Physics and Astronomy, Tel Aviv University, Tel Aviv, Israel
[157] Department of Physics, Aristotle University of Thessaloniki, Thessaloniki, Greece
[158] International Center for Elementary Particle Physics and Department of Physics, University of Tokyo, Tokyo, Japan
[159] Department of Physics, University of Toronto, Toronto, ON, Canada
[160] [(a)]TRIUMF, Vancouver, BC, Canada; [(b)]Department of Physics and Astronomy, York University, Toronto, ON, Canada
[161] Division of Physics and Tomonaga Center for the History of the Universe, Faculty of Pure and Applied Sciences, University of Tsukuba, Tsukuba, Japan
[162] Department of Physics and Astronomy, Tufts University, Medford, MA, USA
[163] Department of Physics and Astronomy, University of California Irvine, Irvine, CA, USA
[164] University of West Attica, Athens, Greece
[165] University of Sharjah, Sharjah, United Arab Emirates
[166] Department of Physics and Astronomy, University of Uppsala, Uppsala, Sweden
[167] Department of Physics, University of Illinois, Urbana, IL, USA
[168] Instituto de Física Corpuscular (IFIC), Centro Mixto Universidad de Valencia-CSIC, Valencia, Spain
[169] Department of Physics, University of British Columbia, Vancouver, BC, Canada
[170] Department of Physics and Astronomy, University of Victoria, Victoria, BC, Canada
[171] Fakultät für Physik und Astronomie, Julius-Maximilians-Universität Würzburg, Würzburg, Germany
[172] Department of Physics, University of Warwick, Coventry, UK
[173] Waseda University, Tokyo, Japan
[174] Department of Particle Physics and Astrophysics, Weizmann Institute of Science, Rehovot, Israel
[175] Department of Physics, University of Wisconsin, Madison, WI, USA
[176] Fakultät für Mathematik und Naturwissenschaften, Fachgruppe Physik, Bergische Universität Wuppertal, Wuppertal, Germany
[177] Department of Physics, Yale University, New Haven, CT, USA
[178] Yerevan Physics Institute, Yerevan, Armenia

[a] Also Affiliated with an Institute Covered by a Cooperation Agreement with CERN, Geneva, Switzerland
[b] Also at An-Najah National University, Nablus, Palestine
[c] Also at Borough of Manhattan Community College, City University of New York, New York, NY, USA
[d] Also at Center for High Energy Physics, Peking University, Beijing, China
[e] Also at Center for Interdisciplinary Research and Innovation (CIRI-AUTH), Thessaloniki, Greece
[f] Also at CERN, Geneva, Switzerland
[g] Also at CMD-AC UNEC Research Center, Azerbaijan State University of Economics (UNEC), Baku, Azerbaijan
[h] Also at Département de Physique Nucléaire et Corpusculaire, Université de Genève, Geneva, Switzerland
[i] Also at Departament de Fisica de la Universitat Autonoma de Barcelona, Barcelona, Spain
[j] Also at Department of Financial and Management Engineering, University of the Aegean, Chios, Greece
[k] Also at Department of Physics, California State University, Sacramento, USA
[l] Also at Department of Physics, King's College London, London, UK
[m] Also at Department of Physics, Stanford University, Stanford, CA, USA
[n] Also at Department of Physics, Stellenbosch University, Stellenbosch, South Africa
[o] Also at Department of Physics, University of Fribourg, Fribourg, Switzerland
[p] Also at Department of Physics, University of Thessaly, Volos, Greece
[q] Also at Department of Physics, Westmont College, Santa Barbara, USA
[r] Also at Faculty of Physics, Sofia University, 'St. Kliment Ohridski', Sofia, Bulgaria
[s] Also at Hellenic Open University, Patras, Greece
[t] Also at Imam Mohammad Ibn Saud Islamic University, Riyadh, Saudi Arabia
[u] Also at Institucio Catalana de Recerca i Estudis Avancats, ICREA, Barcelona, Spain
[v] Also at Institut für Experimentalphysik, Universität Hamburg, Hamburg, Germany
[w] Also at Institute for Nuclear Research and Nuclear Energy (INRNE) of the Bulgarian Academy of Sciences, Sofia, Bulgaria
[x] Also at Institute of Applied Physics, Mohammed VI Polytechnic University, Ben Guerir, Morocco
[y] Also at Institute of Particle Physics (IPP), Toronto, Canada
[z] Also at Institute of Physics and Technology, Mongolian Academy of Sciences, Ulaanbaatar, Mongolia

[aa] Also at Institute of Physics, Azerbaijan Academy of Sciences, Baku, Azerbaijan
[ab] Also at National Institute of Physics, University of the Philippines Diliman (Philippines), Philippines
[ac] Also at Technical University of Munich, Munich, Germany
[ad] Also at The Collaborative Innovation Center of Quantum Matter (CICQM), Beijing, China
[ae] Also at TRIUMF, Vancouver, BC, Canada
[af] Also at Università di Napoli Parthenope, Naples, Italy
[ag] Also at University of Colorado Boulder, Department of Physics, Colorado, USA
[ah] Also at Washington College, Chestertown, MD, USA
[ai] Also at Yeditepe University, Physics Department, Istanbul, Turkey
* Deceased